Acta Biomaterialia 9 (2013) 7591–7621

Contents lists available at SciVerse ScienceDirect

Acta Biomaterialia

journal homepage: www.elsevier.com/locate/actabiomat

Review

Synthesis methods for nanosized hydroxyapatite with diverse structures

Mehdi Sadat-Shojai *, Mohammad-Taghi Khorasani, Ehsan Dinpanah-Khoshdargi, Ahmad Jamshidi

Iran Polymer and Petrochemical Institute (IPPI), P.O. Box 14965/115 Tehran, Iran

ARTICLE INFO

Article history:
Received 12 November 2012
Received in revised form 2 April 2013
Accepted 4 April 2013
Available online 11 April 2013

Keywords:
Hydroxyapatite
Calcium phosphate
Nanoparticles
Bioceramics
Bone

ABSTRACT

Hydroxyapatite (HAp) is the major mineral constituent of vertebrate bones and teeth. It has been well documented that HAp nanoparticles can significantly increase the biocompatibility and bioactivity of man-made biomaterials. Over the past decade, HAp nanoparticles have therefore increasingly been in demand, and extensive efforts have been devoted to develop many synthetic routes, involving both scientifically and economically new features. Several investigations have also been made to determine how critical properties of HAp can be effectively controlled by varying the processing parameters. With such a wide variety of methods for the preparation of HAp nanoparticles, choosing a specific procedure to synthesize a well-defined powder can be laborious; accordingly, in the present review, we have summarized all the available information on the preparation methodologies of HAp, and highlighted the inherent advantages and disadvantages involved in each method. This article is focused on nanosized HAp, although recent articles on microsized particles, especially those assembled from nanoparticles and/or nanocrystals, have also been reviewed for comparison. We have also provided several scientific figures and discussed a number of critical issues and challenges which require further research and development.

1. Introduction

Calcium phosphate (CaP) salts are the major mineral constituents of vertebrate bone and tooth [1–4]. As shown in Fig. 1, bone and other calcified tissues can be considered as natural anisotropic composites consisting of biominerals embedded in a protein matrix, other organic materials and water [1,2]. The biomineral phase, which is one or more types of calcium phosphates, comprises 65–70% of bone, water accounts for 5–8% and the organic phase, which is primarily in the form of collagen, accounts for the remaining portion [1–3,5]. The collagen, which gives the bone its elastic resistance, acts as a matrix for the deposition and growth of minerals [1,2,6,7]. Among the CaP salts, hydroxyapatite ($Ca_{10}(PO_4)_6(OH)_2$, HAp), as a thermodynamically most stable crystalline phase of CaP in body fluid, possesses the most similarity to the mineral part of bone [2,3]. In fact, naturally occurring CaP is usually carbonated and calcium-deficient HAp with a Ca/P ratio of less than 1.67 [4,8]. For decades, synthetic HAp has been of interest owing to its excellent biocompatibility [9,10], affinity to biopolymers [11,12] and high osteogenic potential [13,14]. It has been well documented that HAp can promote new bone ingrowth through osteoconduction mechanism without causing any local or systemic toxicity, inflammation or foreign body response [13,15–17]. When a HAp-based ceramic is implanted, a fibrous tissue-free layer containing carbonated apatite forms on its surfaces and contributes to the bonding of the implant to the living bone, resulting in earlier implant stabilization and superior fixation of the implant to the surrounding tissues [15–18]. Furthermore, several studies have shown that HAp or its derivatives can be exploited as a model compound to study biomineralization in the human body [6,7,19–23]. Recent studies have also shown that HAp particles inhibit the growth of many kinds of cancer cells [24,25]. Currently, HAp is commonly the material of choice for various biomedical applications, e.g. as a replacement for bony and periodontal defects [26,27], alveolar ridge [28], middle ear implants [29], tissue engineering systems [30,31], drug delivery agent [32], dental materials [33] and bioactive coating on metallic osseous implants [34]. The general importance of HAp and its derivatives has also led to numerous non-medical industrial and technological applications, e.g. as a catalyst for chemical reactions such as the Michael-type addition and methane oxidation [35,36], host materials for lasers [37], fluorescence materials [38], ion conductors [39] and gas sensors [40]. Synthetic HAp may also be used in column chromatography for simple and rapid fractionation of proteins and nucleic acids [41,42]. Moreover, it has been demonstrated that HAp presents very convenient qualities for water treatment processes [43] and remediation of heavy metal contaminated soils [44].

Among the various HAp structures, nanosized HAp, also known as HAp nanoparticles, with appropriate stoichiometry, morphology and purity, have stimulated great interest in basic scientific research and various biomedical applications [45]. Nanosized HAp,

* Corresponding author. Tel.: +98 21 44580000; fax: +98 21 44580023.
E-mail address: MSadatShojai@gmail.com (M. Sadat-Shojai).

1742-7061/$ - see front matter © 2013 Acta Materialia Inc. Published by Elsevier Ltd. All rights reserved.
http://dx.doi.org/10.1016/j.actbio.2013.04.012

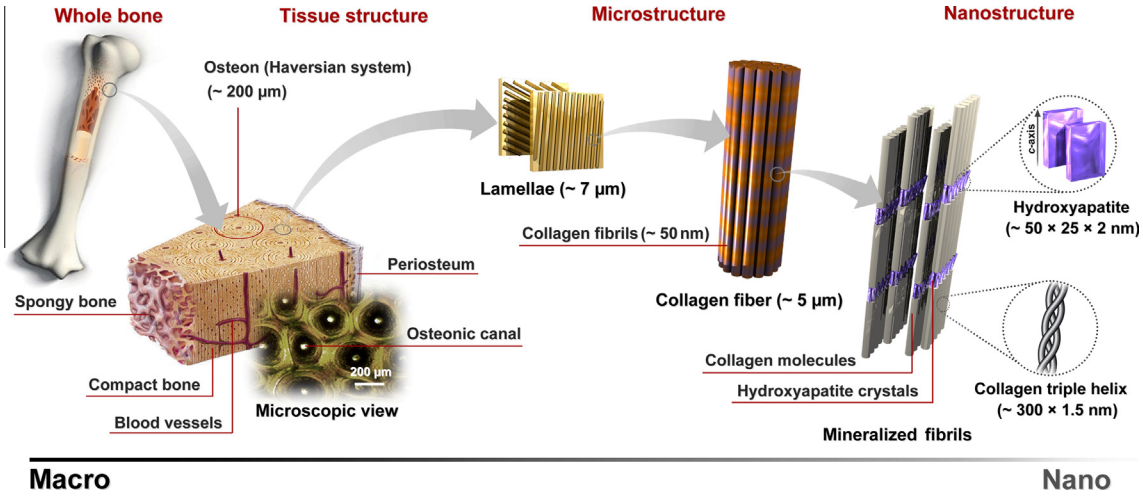

Fig. 1. The hierarchical structure of typical bone at various length scales. The microstructure of cortical or compact bone consists of Haversian systems (circles in cross-section and microscopic view) with osteonic canals and lamellae, and at the nanoscale, the structural framework is collagen fibers composed of bundles of mineralized collagen fibrils.

which has a grain size less than 100 nm in at least one direction, has high surface activity and an ultrafine structure, similar to the mineral found in hard tissues [8]. It is well known that bioceramics that mimic the bone mineral in composition and structure can more readily promote osteointegration and subsequent bone tissue formation. Indeed, as the biological HAps found in physiological hard tissues are nanoscopic plate-like or rod-like crystals that are a few nanometers in thickness and tens of nanometers in length, it is believed that nanosized HAp paralleling natural bone minerals is the best material to use for bone replacement and regeneration [8,46]. Studies have shown that ceramic biomaterials based on nanosized HAp exhibit enhanced resorbability [47,48] and much higher bioactivity [46,49] than micron-sized ceramics. Release of calcium ions from nanosized HAp is also similar to that from biological apatite and significantly faster than that from coarser crystals. In addition, new models for nanoscale enamel and bone demineralization suggest that demineralization reactions may be inhibited when particle sizes fall into certain critical nanoscale levels [50]. Moreover, nanoscale HAp shows improved densification [51,52] and sinterability [52–54] due to its high surface energy and, therefore, problems associated with high-temperature sintering, especially formation of microcracks, can be avoided. Some studies have also reported that nanosized HAp possesses a significant capability of decreasing apoptotic cell death and hence improving cell proliferation and cellular activity related to bone growth [46,55]. The improved cell proliferation and differentiation may be due to superior surface functional properties of nanosized HAp compared to its microphase counterpart; indeed nanosized HAp has higher surface area and surface roughness, resulting in better cell adhesion and cell–matrix interactions [46,47,56]. Therefore, in recent years, bioceramics and biocomposites based on nanosized HAp have been the most promising materials for a variety of biomedical applications [8,47,57,58].

Over the past decade, a number of synthetic routes for producing HAp powders have been developed [45]. To roughly reflect the current interest in HAp synthesis and compare it with the past, we searched the Scopus database for studies reporting the preparation of HAp particles. Criteria for inclusion were English-language articles, peer-reviewed original publications addressing at least one method for synthesis of HAp, and publication year between 1999 and 2011. Fig. 2 shows the results by year of publication. According to the figure, around 67, 65 and 75 articles were published in 2009, 2010 and 2011, respectively, whereas in 1999 the corresponding figure was only 28, indicating increasing interest in HAp fabrication over the recent years. Despite this interest, the preparation of bone-like HAp or HAp having specific characteristics still remains an interesting challenge, especially due to the possibility of formation of intermediary products. Table 1 shows the most important CaP salts, which usually appear as phase impurities during synthesis of HAp particles [8,59–62]. To improve phase composition of HAp, it is therefore important to develop new methods possessing precise control over the crystallographic and chemical structure of powder. In addition to the phase impurities, preparation of nanosized HAp is also connected with a number of additional problems, including difficulties in controlling geometry, size and size distribution, crystallinity, stoichiometry and degree of particle agglomeration. It is well known that in vitro and in vivo biological and mechanical properties of HAp are strongly affected by its structural characteristics; hence, extensive efforts have been made to precisely engineer the HAp crystals, in particular, by developing new routes or modifications of pre-existing methods. As control over the microstructure of HAp matures, demand for a comprehensive review of reported procedures also increases: this is the main motivation for the current paper.

A number of authors have already reviewed the literature on various aspects of HAp. For example, Doremus [63] published a review on processing and mechanical properties of bioceramics. Orlovskii et al. [64] published an early review of three methods

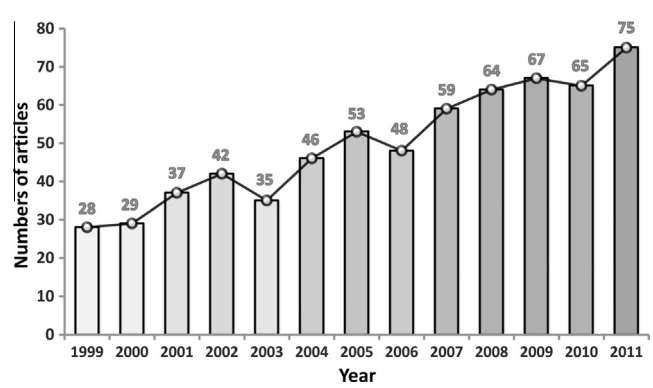

Fig. 2. Annual number of articles on HAp preparation indexed in Scopus over the 1999–2011 period.

Table 1
Main calcium phosphate (CaP) salts.

Name	Symbol(s)	Formula	Ca/P
Monocalcium phosphate monohydrate	(MCPM) and (MCPH)	$Ca(H_2PO_4)_2{\cdot}H_2O$	0.5
Monocalcium phosphate anhydrous	(MCPA) and (MCP)	$Ca(H_2PO_4)_2$	0.5
Dicalcium phosphate dihydrate (Brushite)	(DCPD)	$CaHPO_4{\cdot}2H_2O$	1.0
Dicalcium phosphate anhydrous (Monetite)	(DCPA) and (DCP)	$CaHPO_4$	1.0
Octacalcium phosphate	(OCP)	$Ca_8(HPO_4)_2(PO_4)_4{\cdot}5H_2O$	1.33
α-Tricalcium phosphate	(α-TCP)	$Ca_3(PO_4)_2$	1.5
β-Tricalcium phosphate	(β-TCP)	$Ca_3(PO_4)_2$	1.5
Amorphous calcium phosphate	(ACP)	$Ca_x(PO_4)_y{\cdot}nH_2O$	1.2–2.2
Hydroxyapatite	(HA) and (HAp)	$Ca_{10}(PO_4)_6(OH)_2$	1.67

of HAp synthesis: chemical precipitation, solid-state synthesis and the hydrothermal method. Ferraz et al. [65], Norton et al. [66], and Murugan and Ramakrishna [67] have separately reviewed some of the articles on HAp preparation, mainly those employing wet chemical procedures. Nancollas and Wang [68] discussed some important parameters related to crystal nucleation and the growth/dissolution of various CaP phases. More recently, Dorozhkin [49] and also Zhou and Lee [69] reviewed the preparation of HAp and its application to various biomaterials. Although all of these reviews dealt with HAp or other calcium phosphates, but they were not directed specifically to the topic of the preparation methodologies of HAp. Moreover, most of them concentrated more on the properties, characterization, application and/or surface modification of HAp particles than their synthesis. In addition, we have recently written a book (in Persian), entitled *Hydroxyapatite: Inorganic Nanoparticles of Bone* [45], which gives scientific and practical features of the synthesis, characterization and application of HAp nanoparticles, but still does not exclusively focus on the methods of HAp fabrication reported in the last decade.

In view of the growing interest in the manufacture of HAp, and the increasing need for classification of many new preparation methods, this review article is devoted to the procedures of preparing HAp particles reported in recent years (1999–2011), and especially focuses on a challenging question: how does one choose a specific and cost-effective route from the huge number of methods available to regulate the critical characteristics of HAp? To address this question, the article collates all the available information on the preparation methodologies of HAp particles and shows how the wide variety of new preparation methods can be effectively classified into a few groups. The emphasis of this article will be on nanosized particles, although recent articles on microsized particles, especially those assembled from nanoparticles and/or nanocrystals, are also reviewed for comparison. HAp particles are very prone to various ion substitutions; thus a large number of articles on the preparation of partially ion-substituted HAp, especially carbonated HAp and fluoridated HAp, are included in this review. However, those techniques creating highly chemically modified apatites – especially biomimetic methods based on simulated body fluid – are not the focus of this paper. As mentioned before, this is not the first literature review on HAp, but to the best of our knowledge, it is the first critical review which focuses on the many new methods of preparing HAp, provides several figures for these preparation methods, and systematically compares the inherent advantages and disadvantages of the synthesis procedures.

2. Preparation methods of HAp

During the past decade, many diverse methods have claimed to prepare HAp nanoparticles with precise control over its microstructure. These methods involve various types of known chemical synthesis routes. In each method, processing conditions can be varied across a wide range, resulting in several submethods. With such a great variety, choosing a specific route to synthesize a well-defined powder for a specific application can be laborious; accordingly, in the present review, we have classified the preparation methods into five groups: dry methods (with two subgroups); wet methods (with six subgroups); high-temperature processes (with two subgroups); synthesis methods based on biogenic sources; and combination procedures. Table 2 summarizes this classification, together with the strong and weak points of these methods. In recent years, along with the rapid development of different routes of preparing HAp, there has been a great emphasis on scaling up the suggested procedures; therefore, an individual column of Table 2 is devoted to the comparative cost of each method. By making a comparison of diverse methods, similar to that presented in Table 2, one is able to choose a specific and cost-effective route to regulate the critical properties of the synthetic HAp.

We also searched for the total number of indexed papers relating to each method. The statistical study is presented in Fig. 3. The figure clearly indicates that around 25% of the total 650 papers indexed over the period of 1999–2011 are solely connected to the conventional chemical precipitation method. Following chemical precipitation, combination methods and the hydrothermal process are the next most well-known methods of preparing HAp, accounting for 16 and 14% of papers, respectively. The statistical survey also revealed that the solid-state method has received the least attention in the literature, probably because of its inherent limitations in synthesizing nanosized particles and its lack of clear control over the microstructural characteristics of the powder.

As previously mentioned, the critical characteristics of HAp particles, such as strength, toxicity to cells, osseointegrativity and bioresorbability, depend strongly upon their microstructure – mainly their morphology, stoichiometry, crystallographic structure and phase purity. However, when one considers the nano- or micropowder, the morphology and dimensions of particles seem to be highlighted more than other characteristics [46,55,70]. Indeed, a major challenge in the synthesis of crystalline powders is always the precise control of crystal growth, which directly relates to the size and geometric shape of the final particles. In particular, for HAp crystals, it has been demonstrated that their microscopic shape, size and size distribution can significantly affect their mechanical properties, processing conditions, surface chemistry, biocompatibility and bioactivity [46,55,70–73]. So, by controlling the crystal and/or particle shape, the potential applications of nanoparticles can be expanded. For example, due to poor mechanical reliability, HAp bioceramics having the conventional microstructure cannot be used for load-bearing orthopedic and dental applications [66,74,75]. It has been demonstrated that the mechanical properties can be significantly improved by fabricating HAp particles of complex shapes [8,69,76]. Therefore, it is of great importance to develop new synthesis procedures having precise control over the crystal geometry. According to the literature, shape-tailored HAp can be synthesized through the anisotropic growth of crystal faces induced by organic additives and/or selective operating conditions. In this strategy, initial nucleation first

Table 2
Comparison of different methods for the preparation of HAp nanoparticles.

Method		Processing aspects		Characteristics of powder						Ref.
		Number of chemicals	Cost	Morphology	Crystallinity degree	Phase purity	Ca/P ratio	Size	Size distribution	
Dry methods	Solid-state method	few	low	diverse	very high	usually low	variable	usually micron	wide	[78–82]
	Mechanochemical method	few	low	diverse	very high	low	usually non-stoichiometric	nano	usually wide	[83–97]
Wet methods	Chemical precipitation	frequently few	low	diverse	frequently low	variable	non-stoichiometric	usually nano	variable	[98–193]
	Hydrolysis method	few	usually high	diverse	variable	usually high	stoichiometric	variable	variable	[194–209]
	Sol–gel method	variable	variable	diverse	variable (usually low)	variable	stoichiometric	nano	narrow	[210–238]
	Hydrothermal method	variable	usually high	frequently needle-like	very high	usually high	stoichiometric	nano or micron	usually wide	[239–289]
	Emulsion	many	high	frequently needle-like	frequently low	variable	non-stoichiometric	nano	narrow	[290–314]
	Sonochemical Method	few	usually low	diverse (usually needle-like)	variable	usually high	variable	nano	usually narrow	[315–324]
High Temp. processes	Combustion method	few	usually low	diverse (usually irregular)	variable	usually high	variable	usually nano	wide	[325–337]
	Pyrolysis method	variable	usually low	diverse	high	variable	usually stoichiometric	nano particles embedded in micron aggregates	variable	[338–345]
	Synthesis from biogenic sources	few	usually low	diverse	variable	usually high	variable	variable	variable	[346–387]
	Combination procedures	variable	variable	diverse (frequently needle-like)	frequently high	usually high	usually stoichiometric	usually nano	variable	[388–454]

occurs upon mixing the reactants, and anisotropic growth is then gained by either the face-selective adsorption of additives or a change in the crystallization pathway to, for example, induce Ostwald ripening. Over the past decade, many researchers have tried to fabricate nanometer HAp with one-, two- or three-dimensional geometric shapes. In Table 3, the literature was scanned for HAp particles having different shapes and dimensions. According to the table, the variety of methods by which irregular, rod-like or spherical morphologies can be synthesized is much greater than for others. However, as indicated in the third column of the table, complex shapes are normally constructed from nanoparticles of a simple shape. Furthermore, in almost all cases the dimensions of particles can vary across a very wide range.

From Table 3, it can also be seen that there is a discrepancy in the nomenclature of geometric shapes in the literature. The ambiguity in nomenclature becomes especially serious when one synthesizes an elongated shape (i.e. the geometry indicated in the fourth row of the table). Some authors have suggested that elongated shapes should be named according to their axial dimensions, i.e. their aspect ratio [77]. For example, a fiber has a higher aspect ratio than a needle and a much greater ratio than a rod. Although this nomenclature scheme is somewhat arbitrary, it is important that authors clearly define the meaning of the terms used in any morphological descriptions.

2.1. Dry methods

Dry methods do not use a solvent, unlike wet methods. According to the literature, the characteristics of a powder synthesized by a dry method are not strongly influenced by the processing parameters, hence most dry methods do not require precisely controlled conditions, making them suitable for mass production of powders. A number of researchers have therefore adapted well-known dry methods, including solid-state synthesis and the mechanochemical process, for the preparation of HAp particles.

2.1.1. Solid-state synthesis

Solid-state reaction, as a relatively simple procedure, can be employed in the mass production of HAp powder [78–81]. Supplementary Table S1 shows recent progress in the synthesis of HAp powder using the solid-state method. In a typical procedure, precursors are first milled and then calcined at a very high temperature (e.g. 1000 °C) [78]. The precursors can be calcium- and phosphate-containing chemicals of various types or simply a previously prepared CaP salt. The high temperature of calcination leads to the formation of a well-crystallized structure. The general process is shown in Fig. 4. As a disadvantage, the powder synthesized by a solid-state reaction often exhibits heterogeneity in its phase composition, owing to the small diffusion coefficients of ions within the solid phase [79,80]. Recently, Pramanik et al. [78] claimed to have synthesized HAp particles with a single phase, using powder mixing and cold pressing. For this, samples were prepared by mixing the ingredients, followed by sintering the cold-compacted pellets at various temperatures up to 1250 °C. However, this powder was irregular in shape, with micron-sized grains. Some attempts have also been made to achieve a powder with a regular shape or a nanosized structure, or both. For example, Tas [81] used a modified solid-state reaction called "molten salt synthesis" (MSS) to prepare one-dimensional (1D) HAp. The MSS technique is based on the use of low-melting fluxing agents, e.g. alkali chlorides, sulfates, carbonates or hydroxides, as the medium for the reaction. In this study, a previously synthesized submicron HAp powder was exploited as the starting material and the effects of a specifically chosen alkali salt on the particles' morphology, temperature/time of synthesis and salt to

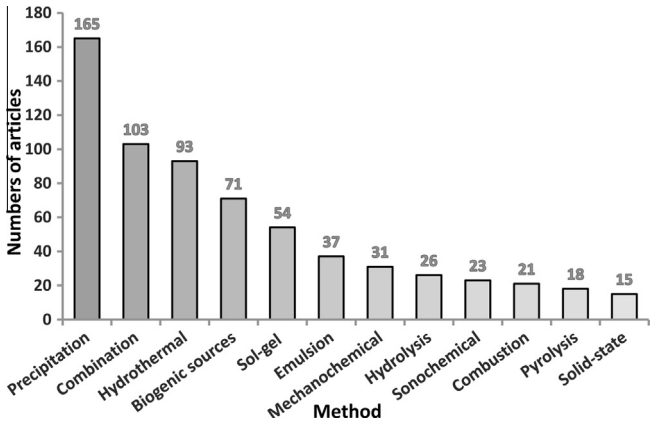

Fig. 3. Total number of articles indexed in Scopus over 1999–2011 by the method of preparation.

HAp ratio were investigated. Tas's results showed that MSS with K_2SO_4 flux is a simple and sturdy technique to fabricate short HAp whiskers in the temperature range of 1080–1200 °C. The study also revealed that other fluxing agents, such as KCl and KBr, produced large single crystals of HAp, rather than whiskers. However, all the samples were reported to have a grain size much larger than 1 μm. Recently, Tseng et al. [82] synthesized HAp nanoparticles through a polyethylene glycol (PEG)-assisted reaction, using calcination of calcium dihydrogenphosphate (MCPM; see Table 1) and calcium hydroxide ($Ca(OH)_2$) at 900 °C in an oxygen atmosphere. They claimed that the process yields a well-crystallized and non-aggregated powder with a nanometer particle size. According to their results, PEG can control the particle size, crystal phase and degree of aggregation, and also decrease the particle size distribution from 80–150 nm to 50–80 nm (as determined by scanning electron microscopy (SEM)). Indeed, HAp(PEG) was well dispersed, while the HAp(non) was seriously aggregated into a single flat piece. Analysis of secondary particle sizes using dynamic light scattering (DLS) showed that the diameter of HAp(-PEG) secondary particles ranges from 150 to 600 nm and that of HAp(non) ranges from 35 to 36 μm, indicating that HAp(PEG) was much less aggregated than HAp(non). The results also suggested that the energy required for formation of HAp nanoparticles in the HAp(PEG) system should be greater than that required for HAp(non), because the crystallization of HAp will proceed after the decomposition of PEG–Ca–P complex in the former system. This effectively delays the phase transition from pure HAp to tricalcium phosphate (TCP).

Regardless of these efforts, and as mentioned before, a solid-state method usually suffers from the small diffusion of ions during the reaction; this is an inherent characteristic, and is why very little work is available on solid-state processing of HAp. To improve the kinetic performance, some researchers have used an alternative approach, known as the mechanochemical method, for the preparation of HAp powder in a dry manner (see the following section). Although the solid-state process, due to its simplicity and low cost, is commonly the method of choice for commercial production of various powders, if one considers the mass production of a biomedical material, such as HAp, for use in drug delivery and cell scaffolds for tissue engineering, a precise control over the characteristics of product becomes much more important than financial considerations. On the other hand, current interest in the synthesis of artificial HAp is to mimic in vivo biomineralization, where the HAp phase is biologically generated with the aid of body fluids. Therefore, the solid-state method definitely cannot be exploited for a biomimetic synthesis. All of these reasons make the solid-state process unattractive, both scientifically and technologically, for the fabrication of HAp particles.

2.1.2. Mechanochemical method

The mechanochemical process, sometimes known as mechanical alloying, is a simple dry method for fabrication various advanced materials, such as nanocrystalline alloys and ceramics [83,84]. Contrary to the solid-state method by which heterogeneous particles with irregular shape are usually produced, powder synthesized using a mechanochemical route usually possesses a well-defined structure. This is due to the perturbation of surface-bonded species as a result of pressure, enhancing the thermodynamic and kinetic reactions between solids [85–89]. Indeed, the mechanochemical process has the advantages of simplicity and reproducibility of a solid-state procedure to perform mass production and the basic characteristics of an ordinary wet reaction to generate a powder with an acceptable microstructure. As shown in Fig. 5, in a typical process, the materials are ground on a planetary mill while the molar ratio between the reagents is kept at the stoichiometric ratio [90,91]. The main processing variables include the type of reagents, the type of milling medium, the type and diameter of the milling balls, the type of atmosphere, the duration of the milling steps and interval pauses, the powder-to-ball mass ratio and the rotational speed [88,90,92–96]. Supplementary Table S2 presents recent progress in the mechanochemical synthesis of HAp powder. Some of relevant (simplified) reactions involved are as follows:

$$6CaHPO_4 \cdot 2H_2O + 4CaO \rightarrow Ca_{10}(PO_4)_6(OH)_2 + 14H_2O \quad (1)$$

$$10CaCO_3 + 6(NH_4)H_2PO_4 \rightarrow Ca_{10}(PO_4)_6(OH)_2 + 8H_2O + 10CO_2 + 6NH_3 \quad (2)$$

$$3Ca_3(PO_4)_2 \cdot xH_2O + Ca(OH)_2 \rightarrow Ca_{10}(PO_4)_6(OH)_2 + xH_2O \quad (3)$$

$$10Ca(OH)_2 + 3P_2O_5 \rightarrow Ca_{10}(PO_4)_6(OH)_2 + 9H_2O \quad (4)$$

$$9CaO + Ca(OH)_2 + 3P_2O_5 \rightarrow Ca_{10}(PO_4)_6(OH)_2 \quad (5)$$

$$6CaHPO_4 \cdot 2H_2O + 3CaO \rightarrow Ca_9(HPO_4)(PO_4)_5OH + 14H_2O \quad (6)$$

Recently, Nasiri-Tabrizi et al. [86] synthesized single-crystal HAp nanorods and nanogranules via a mechanochemical process in polyamide 6 milling medium. They used two distinct experimental procedures, according to the following reactions:

$$6CaHPO_4 + 4Ca(OH)_2 \rightarrow Ca_{10}(PO_4)_6(OH)_2 + 6H_2O \quad (7)$$

$$4CaCO_3 + 6CaHPO_4 \rightarrow Ca_{10}(PO_4)_6(OH)_2 + 2H_2O + 4CO_2 \quad (8)$$

They reported that the average size of particles determined from transmission electron microscopy (TEM) observations was about 13 ± 7 and 15 ± 8 nm for reactions (7) and (8), respectively. Their results indicated that increasing the milling time leads to an increase in lattice strain and a decrease in crystallite size. According to the results, the degree of crystallinity of the product in reaction (7) is higher than that in reaction (8). Moreover, the trend of decreasing crystallinity was found to be related to increasing milling time. Finally, they concluded that the use of polymeric milling medium in the mechanochemical process is an effective way to prepare nanosized HAp particles. In another study, Fathi and Zahrani [97] synthesized fluoridated hydroxyapatite (FHAp) nanopowder with different degrees of fluoridation via mechanical alloying. For this, they mechanically milled a mixture of calcium hydroxide, phosphorous pentoxide and calcium fluoride powders for 6 h at 300 rpm using eight balls of 20 mm diameter and a powder-to-ball mass ratio of 1:35. According to their results, a single-phase FHAp having some carbonated groups and a particle size distribution of 35–65 nm (as determined by TEM) could be prepared after 6 h of mechanical alloying.

2.2. Wet methods

As mentioned before, HAp powder generated from a typical dry method is usually large in size and irregular in shape. Therefore,

Table 3
Various HAp nanostructures with modulated shapes.

Shape	Name(s) in literature	Approx. size range	Method(s) of synthesis*
	irregular, formless, sphere	5 nm–200 μm	ss, mch, cc, hl, sg, hth, em, sch, ht, bs, cp
	sphere, microsphere, nanosphere, ball	10 nm–1000 μm	mch, cc, sg, hth, em, sch, ht, bs, cp
	rod, needle, tube, filament, fiber, wire, whisker, prism, worm, hexagonal prism, platelet, lath, strip	length: 10 nm–150 μm, diameter: 3 nm–50 μm, aspect ratio: 2–1200	ss, mch, cc, hl, sg, hth, em, sch, ht, bs, cp
	plate, flake, sheet	length: 40 nm–50 μm, width: 20 nm–35 μm, thickness: 5 nm–3 μm	cc, hth, bs, cp
	self-assembled nanorods, bundles of nanorods, oriented bundle, oriented raft, enamel prism-like structures, clusters of nanotubes, oriented array of bundled needles, packed nanorods	length: 200 nm–80 μm, width: 100 nm–50 μm (organized nanorods of 10 nm–13 μm diameter and 200 nm–75 μm length)	cc, hl, hth, bs, cp
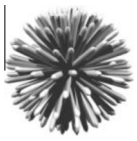	dandelion, chrysanthemum, flower, feathery structure, bundle of fibers, self-assembled nanorods, rosette	1–8 μm (organized nanorods of 80–500 nm diameter and 600 nm–5 μm length)	hth, em, bs, cp
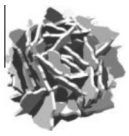	leaf, flake, sheet, plate	800 nm–10 μm (organized nanoplates of 20–100 nm thickness)	cc, hl, cp
	flower	700 nm–60 μm (organized petals of 20 nm–10 μm width and 180 nm–50 μm length)	cc, hth, bs
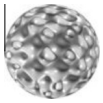	porous microsphere, mesoporous sphere	0.5–7 μm (pores of 20–150 nm)	hth, cp
	bowknot, self-assembled nanorods	1.5–2.5 μm (organized nanorods of 100–150 nm diameter and 1–2 μm length)	cp
	dumbbell	2–3 μm (organized nanoparticles of ~50 nm size)	cc

* ss: solid-state synthesis, mch: mechanochemical method, cc: conventional chemical precipitation, hl: hydrolysis method, sg: sol–gel method, hth: hydrothermal method, em: emulsion method, sch: sonochemical method, ht: high-temperature processes, bs: synthesis from biogenic sources, cp: combination procedures.

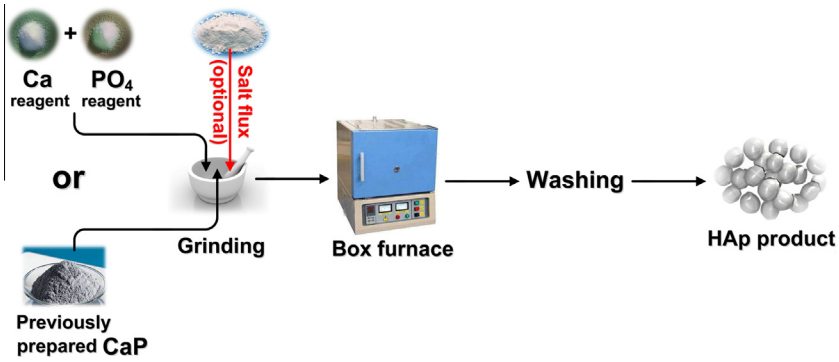

Fig. 4. Preparation of HAp powder via solid-state method.

wet methods have conventionally been applied to the preparation of HAp particles having a nanosized structure with a regular morphology. In addition, from a fundamental perspective aimed at understanding the in vivo biomineralization process, the growth pathways of HAp crystals in solution have been the subject of increasing interest over the past decade [19,98]. Wet chemical reactions have advantages in their ability to control the morphology and the mean size of powder, and, based on many experimental data, they are the most promising techniques for the fabrication of nanosized HAp. The popularity of wet methods is also reflected in Fig. 3, where a simple calculation reveals that wet methods accounts for more than 60% of all articles. Indeed, wet processes are usually easy to conduct and growth conditions can be directly controlled by adjusting the reaction parameters. One of the main potential disadvantages, however, is the low preparation temperature compared to dry methods, resulting in the generation of CaP phases other than HAp (see Table 1) and/or the lowering of the crystallinity of the resultant powder. In addition, various ions in aqueous solution can be incorporated into the crystal structure, leading to trace impurities.

Solution-based reactions, which are accomplished in an organic solvent or, more usually, in water, can be conducted at ambient temperature or elevated temperatures (lower than, close to or higher than boiling point of the solvent). Moreover, reactions can be performed by a number of technical routes involving diverse chemicals and auxiliary additives and apparatus. The following simplified equations show some of the well-known chemical reactions adopted for the wet synthesis of HAp:

$$10Ca(NO_3)_2+6(NH_4)_2HPO_4+8NH_4OH\rightarrow Ca_{10}(PO_4)_6(OH)_2+20NH_4NO_3+6H_2O \quad (9)$$
$$10Ca(NO_3)_2+6(NH_4)_3PO_4+2H_2O\rightarrow Ca_{10}(PO_4)_6(OH)_2+18NH_4NO_3+2HNO_3 \quad (10)$$
$$10Ca(NO_3)_2+6KH_2PO_4+20NH_4OH\rightarrow Ca_{10}(PO_4)_6(OH)_2+6KOH+20NH_4NO_3+12H_2O \quad (11)$$
$$10Ca(NO_3)_2+6H_3PO_4+20NH_4OH\rightarrow Ca_{10}(PO_4)_6(OH)_2+20NH_4NO_3+18H_2O \quad (12)$$
$$10Ca(NO_3)_2+6(NH_4)_2HPO_4+20NaOH\rightarrow Ca_{10}(PO_4)_6(OH)_2+20NaNO_3+12NH_3+18H_2O \quad (13)$$
$$10Ca(NO_3)_2+6(NH_4)_2HPO_4+2H_2O\rightarrow Ca_{10}(PO_4)_6(OH)_2+12NH_4NO_3+8HNO_3 \quad (14)$$
$$10Ca(NO_3)_2+6Na_2HPO_4+2H_2O\rightarrow Ca_{10}(PO_4)_6(OH)_2+12NaNO_3+8HNO_3 \quad (15)$$
$$10Ca(NO_3)_2+6H_3PO_4+2NH_4OH\rightarrow Ca_{10}(PO_4)_6(OH)_2+2NH_4NO_3+18HNO_3 \quad (16)$$
$$10Ca(OH)_2+6(NH_4)_2HPO_4\rightarrow Ca_{10}(PO_4)_6(OH)_2+12NH_3+18H_2O \quad (17)$$
$$10Ca(OH)_2+6H_3PO_4\rightarrow Ca_{10}(PO_4)_6(OH)_2+18H_2O \quad (18)$$
$$10CaCl_2+6(NH_4)_2HPO_4+8NH_4OH\rightarrow Ca_{10}(PO_4)_6(OH)_2+20NH_4Cl+6H_2O \quad (19)$$
$$10CaCl_2+6K_2HPO_4+2H_2O\rightarrow Ca_{10}(PO_4)_6(OH)_2+12KCl+8HCl \quad (20)$$
$$10CaCO_3+6NH_4H_2PO_4+2H_2O\rightarrow Ca_{10}(PO_4)_6(OH)_2+3(NH_4)_2CO_3+7H_2CO_3 \quad (21)$$
$$10CaSO_4\cdot 2H_2O+6(NH_4)_2HPO_4\rightarrow Ca_{10}(PO_4)_6(OH)_2+6(NH_4)_2SO_4+4H_2SO_4+18H_2O \quad (22)$$
$$6CaSO_4\cdot 2H_2O+4Ca(OH)_2+6(NH_4)_2HPO_4\rightarrow Ca_{10}(PO_4)_6(OH)_2+6(NH_4)_2SO_4+18H_2O \quad (23)$$
$$3Ca(H_2PO_4)_2\cdot H_2O+7Ca(OH)_2\rightarrow Ca_{10}(PO_4)_6(OH)_2+15H_2O \quad (24)$$
$$Ca_5(P_3O_{10})_2+5Ca^{2+}+6H_2O\rightarrow Ca_{10}(PO_4)_6(OH)_2+10H^+ \quad (25)$$
$$\frac{10}{n}Ca_nC_{12}H_{22-2n}O_{11}+6(NH_4)_2HPO_4+2H_2O\rightarrow Ca_{10}(PO_4)_6(OH)_2+12NH_3+\frac{10}{n}Ca_{12}H_{22}O_{11} \quad (26)$$

Each reaction can be exploited to create a specific method for preparing HAp. In the following sections, we have classified these methods into six groups and have described the characteristics of the powder obtained from each.

2.2.1. Conventional chemical precipitation

Among the various wet processing methods, conventional chemical precipitation is the simplest route for the synthesis of nanosized HAp. The chemical precipitation is based on the fact that, at room temperature and pH 4.2, HAp is the least soluble and usually the most stable CaP phase in an aqueous solution [8,99–103]. The precipitation reaction is, however, usually conducted at pH values higher than 4.2 and temperatures ranging from room temperature to temperatures close to (though not at) the boiling point of water [104–113]. Fig. 6 shows a schematic diagram of the steps involved in the chemical precipitation of HAp, along with the parameters proposed to affect the characteristics of the powder. To produce HAp nanoparticles, chemical precipitation can be accomplished using various calcium- and phosphate-containing reagents, e.g. calcium hydroxide or calcium nitrate as the Ca^{2+} source and orthophosphoric acid or diammonium hydrogen phosphate as the PO_4^{3-} source. A typical procedure involves the dropwise addition of one reagent to another under continuous and gentle stirring, while the molar ratio of elements (Ca/P) is kept at stoichiometry according to its ratio in HAp (1.67) [114–119]. As the last step, the resultant suspension may be aged under atmospheric pressure [99,115,119] or immediately washed, filtered, dried and crushed into a powder [116,118]. Recently, Paz et al. [120] reported the use of supersaturated calcium solutions as a biomimetic process to prepare HAp nanoparticles. They showed that the morphology, crystallinity and size distribution of the resulting nanoparticles are strongly dependent on the synthesis method and ripening time. For example, while normal chemical precipitation resulted in nanoparticles with a needle-like morphology of ~23 nm in width and ~62 nm in length, with a particle size distribution of 27–118 nm (determined by TEM and a particle size analyzer), biomimetic synthesis based on a supersaturated solution led to a spherical powder of ~23 nm in size, with a narrower size distribution of 15–41 nm.

A powder prepared by simple precipitation is, however, usually non-stoichiometric and poorly crystallized without any regular shape [121–123]. Many factors are claimed to cause these drawbacks, including the high chemical affinity of HAp to some ions, the complex nature of the CaP crystals, hydrogen-bonded interactions among the HAp particles and the role of the kinetic parameters, which, depending on the experimental conditions, prevail over the thermodynamic parameters [59,124]. For example, the non-stoichiometric feature may occur as a result of vacancies in the crystal lattice [125,126], the substitution of diverse ions such as carbonate, potassium and chloride [59,127] or the presence of additional phases [59,128], etc. Therefore, a precise control over the processing conditions is always advised for the preparation of a powder with minimal defects. Supplementary Table S3 presents recent attempts to synthesize HAp using precipitation methods. As the table indicates, the pH value and temperature employed during the precipitation reaction and/or the aging step are the most challenging factors. Indeed, to obtain a single-crystal HAp with high phase purity, the precipitation reaction is usually conducted at a high pH or a high temperature, or both. Whenever the pH value must be lowered (e.g. to achieve a specific morphology), the temperature should be raised and vice versa [104,129–134]. This leads to a dramatic decrease in the generation of phase impurities (e.g. dicalcium phosphate anhydrous (DCPA) and octacalcium phosphate (OCP)), resulting in HAp as a dominant phase [104,113,133–135].

More recent approaches, according to Supplementary Table S3, propose alternative routes based on various additives and/or modification of the main procedure. A well-known example is based on the biomimetic templating systems, in which the characteristics of powder, especially morphology and crystallinity, can be controlled at significantly lower temperatures and pHs. In this strategy, various macromolecules act as a soft temporary template or nucleation centers to modulate the morphology and increase the crystallinity, according to Fig. 7 [136–147]. Indeed, macromolecules adsorb on the crystal surface and influence the crystal growth of seeds [143–150]. The first major examples of macromolecular templating of HAp took place in the 1990s, when researchers tried to synthesize HAp particles of complex shapes. For instance, Antonietti et al. [151] employed a double-hydrophilic block copolymer consisting of a long poly(ethylene oxide) block and a short poly(methacrylic acid) block, modified by partial alkylation with dodecylamine as a dispersed template for controlled precipitation of calcium phosphate from aqueous solution at different pH values. In recent years, however, attention has usually been directed towards simpler templating systems – not just because of their simplicity, but also because the use of medically harmful substances should be kept to a minimum.

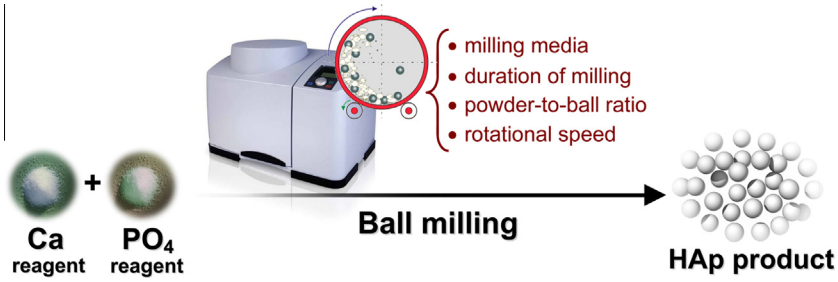

Fig. 5. Preparation of HAp nanoparticles via mechanochemical method.

More recent macromolecules used for soft templating of HAp are popular surfactants, including cetyl trimethyl ammonium bromide (CTAB), PEGs having different molecular weights, and various Tweens. Surfactants, as amphiphilic molecules with a hydrophobic tail and a hydrophilic head, can self-assemble to form micelles as soon as their concentration exceeds the critical micelle concentration. At a certain concentration and pH, micelles with a specific shape are formed and act as nucleation centers for crystal growth [152–154]. Regarding CTAB, the most popular surfactant in the synthesis of HAp, the molecules are ionized to create cations of a tetrahedral structure, followed by the formation of a layer through the cationic parts [136,152–155]. Surrounding this ionic mantle, the PO_4^{3-} counter-ions with oriented water molecules may form an outer diffuse layer, starting the nucleation process. Liu et al. [154] synthesized HAp nanorods of 50–80 nm in diameter and 0.5–1.2 μm in length (determined by TEM) using surfactants of CTAB and PEG 400. Zhang and Zhu [124] controlled the morphology of fluoride-substituted HAp nanoparticles by adding Tween-80. They claimed that morphological changes can occur as a result of difference between the growth rates of crystal faces resulting from the adsorption of Tween. Indeed, without the addition of any surfactant, the resultant FHAp showed a spheroidal shape with a relatively broad size distribution of 80–300 nm (determined by field emission scanning electron microscopy (FESEM)). In contrast, FHAp synthesized in the presence of Tween-80 has a relatively uniform rod-like shape, with an average diameter of about 50 nm.

Several attempts have also been made to determine the effect of PEG on the chemical precipitation of HAp nanoparticles [154–157]. According to the studies, PEG molecules modify the surface of nanocrystals and act as a dispersing agent during the process of synthesis. Recently, Qiu et al. [157] synthesized spherical HAp of 30–50 nm in diameter in the presence of PEG, by a reaction pathway described in Fig. 8. Their results show that the crystallinity of resultant powder was higher in the presence of PEG. To explain the morphological and structural effects of PEG, they investigated the interaction between Ca^{2+} and PEG by the electrical conductivity. Their results reveal that PEG reduces the transfer rate of Ca^{2+} in the process of HAp crystallization, indicating the interaction between PEG and HAp. According to Fig. 8, when PEG is dissolved in aqueous solution, a PEG–OH bond is first formed and then chelated with Ca^{2+} released from $Ca(NO_3)_2$ to form a PEG–O–Ca^{2+}–O–PEG bond. This then reacts with the PO_4^{3-} from $(NH_4)_3PO_4$ to produce the HAp crystal nucleus. It was found that a large deposit is generated in a short time when there is no or little PEG, indicating the rapid generation of HAp. With increasing concentration of PEG, the initial deposits gradually decrease and longer times are required to produce large quantities of particles, indicating that PEG reduces the release rate of Ca^{2+} and hence restrains the formation of HAp crystals. When the rate of calcium release and the deposit rate of the crystal nucleus achieve a dynamical equilibrium, HAp nucleus is deposited isotropically, and spherical particles are finally obtained. More recently, Shkilnyy et al. [158] showed that poly(ethylene oxide)-b-poly(L-lysine) block copolymers lead to an interesting morphology of calcium phosphate; electron microscopy showed that a porous material with channel-like features forms. They indicated that this morphology is the result of the aggregation of nanosized rod-like primary particles, which changes upon drying to exhibit the observed channel-like features. Comparison experiments conducted in the absence of the copolymers showed that this morphology only forms in the presence of the copolymer blocks, suggesting a distinct interaction of the polymeric additive with either the crystal or the phosphate ions prior to mineralization.

Besides macromolecules, attempts have also been made to control the characteristics of HAp using small organic compounds [159–171]. Li and Meng [172], for example, prepared nanosized HAp using titration of a supersaturated solution of lime chelated with citric acid, using orthophosphoric acid. They suggested that the chelating agent inhibits crystal growth and results in the shortening of the *a*-axis and lengthening of the *c*-axis in the crystal cells. Recently, Martins et al. [173] described a precipitation method by which dumbbell-shaped and needle-like particles were precipitated at physiological temperature (i.e. 37 °C). According to their results, in the presence of citrate molecules, a small variation in the starting pH of the solution switches the morphology from micrometric bundles to nanometric needles. They explained the role of the citrate species in terms of supersaturation of solution and the development of particles' surface charge. In fact, the anisotropy of surface charge distribution arising from the adsorption of citrate species onto preferential crystal facets was found to affect the formation of specific shapes by the oriented aggregation of the primary particles. By contrast, when the pH value is increased, the adsorption of more negatively charged species increases the negative charge of the particle shell and promotes particle repulsion, resulting in the prevention of particle agglomeration and hence maintaining the nanometric size of the particles. Many researchers have also used the addition of urea, in place of NH_4OH or NaOH, to adjust the pH value, and claim that it gives more homogeneous precipitation and further phase transformation to HAp [98,174–181]. According to the literature, CO_3^{2-} ions released from the urea during hydrolysis can incorporate into the HAp crystals, leading to a carbonated structure paralleling human bone apatite. Recently, Zhang et al. [182] investigated the effect of urea concentration on the phase composition and morphology of the precipitated powder. According to their results, the slow adjustment on pH by hydrolysis of 0.5 M urea leads to a mixture of OCP and HAp with a ribbon-like morphology, whereas a single-phase HAp can be obtained upon hydrolysis of 0.03 M urea. More recently, our group [183] demonstrated that the aspect ratio of fibrous precipitated HAp decreases slightly in the presence of urea, while the crystalline fraction increases. Our results also indicated that the Ca/P ratio of HAp nanoparticles increases slightly in the presence of urea.

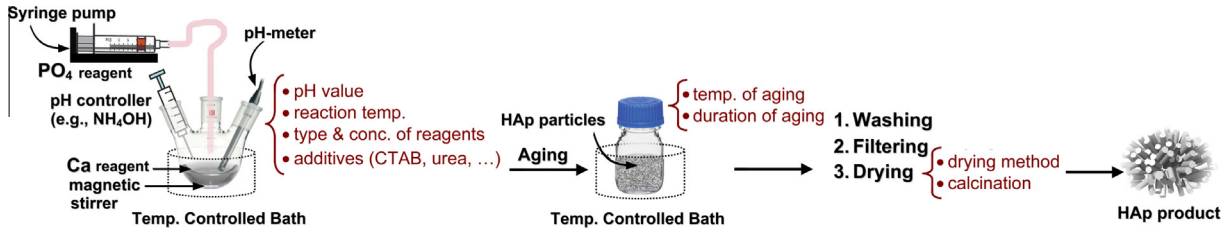

Fig. 6. Preparation of HAp nanoparticles via conventional chemical precipitation.

Besides other parameters, the mixing rate of the reactants, the calcination temperature (if applicable), the drying method, the solvent system and the concentration of the reactants have all been reported to affect the characteristics of the final powder [184–192]. For example, the mixing rate determines the rate of the reaction and hence the chemical structure of the powder. Usually, a slow titration is advised to improve the chemical homogeneity and stoichiometry of the final product. Moreover, the addition rate is strongly linked to the pH obtained at the end of the synthesis and to the stability of the suspension [65,192]. Recently, Wang et al. [193] investigated the effects of the solvent system (pure water and a water/ethanol mixture) and the type of drying method (atmospheric drying, vacuum drying and freeze-drying) on the characteristics of the resulting powder. They concluded that, by increasing the proportion of ethanol in the solvent system, the size of the particles increases and the dispersibility decreases, owing to higher supersaturation. According to TEM observations, the diameter of their nanoparticles synthesized in water was about 20–30 nm, while in ethanol it was about 100–150 nm. Indeed, HAp, as an alkalescent salt, has a low solubility in water and even lower solubility in ethanol, leading to an increase in supersaturation and thus in the growth of particles with an increasing amount of ethanol. The method of drying was also found to be important in determining both the morphology and the dispersibility. The size of the particles dried by means of atmospheric drying was slightly smaller than those dried by freeze-drying. Moreover, particles dried under vacuum conditions were nearly spherical, with a few rods, and their dispersibility was poorer. Wang et al. concluded that the powder dried using freeze-drying had an ultrafine structure with the best dispersibility.

2.2.2. Hydrolysis method

HAp nanoparticles can be prepared by the hydrolysis of other CaP phases, including DCPA, dicalcium phosphate dihydrate (DCPD) and TCP, according to the following (simplified) equations:

$$10CaHPO_4 + 2H_2O \rightarrow Ca_{10}(PO_4)_6(OH)_2 + 4H_3PO_4 \quad (27)$$

$$10CaHPO_4 + 12OH^- \rightarrow Ca_{10}(PO_4)_6(OH)_2 + 4PO_4^{3-} + 10H_2O \quad (28)$$

$$6CaHPO_4 + 4Ca(OH)_2 \rightarrow Ca_{10}(PO_4)_6(OH)_2 + 6H_2O \quad (29)$$

$$6CaHPO_4 + 4CaCO_3 + 2H_2O \rightarrow Ca_{10}(PO_4)_6(OH)_2 + 4H_2CO_3 \quad (30)$$

$$10CaHPO_4 \cdot 2H_2O \rightarrow Ca_{10}(PO_4)_6(OH)_2 + 18H_2O + 12H^+ + 4PO_4^{3-} \quad (31)$$

$$6CaHPO_4 \cdot 2H_2O + 4Ca(OH)_2 \rightarrow Ca_{10}(PO_4)_6(OH)_2 + 18H_2O \quad (32)$$

$$10Ca_3(PO_4)_2 + 6H_2O \rightarrow 3Ca_{10}(PO_4)_6(OH)_2 + 2PO_4^{3-} + 6H^+ \quad (33)$$

$$10Ca_3(PO_4)_2 + 6OH^- \rightarrow 3Ca_{10}(PO_4)_6(OH)_2 + 2PO_4^{3-} \quad (34)$$

During the 1990s, some attention had also been given to the hydrolysis of OCP [194,195]. However, in the last decade, this type of conversion has not been of great interest for the preparation of HAp particles, probably because of the slow rate of OCP hydrolysis and/or the ability of OCP to incorporate impurity species, including additives and foreign ions used for its transformation to HAp.

Aqueous hydrolysis of CaP phases into HAp usually proceeds by dissolution and precipitation processes [196–200]. Indeed, formation of HAp crystals through many other wet methods also proceeds via one or more intermediate phases having a transitory existence [59,134]. The hydrolysis method is, however, considered as a distinct method when one intends to convert a preprepared or a commercially available CaP into HAp. Supplementary Table S4 presents various attempts to synthesize HAp using this approach. Among the CaP salts, acidic phases such as DCPA and DCPD are thermodynamically less stable under pH values higher than 6–7 and undergo transformation into a more stable CaP, e.g. HAp, through the pathways illustrated in Fig. 9 [201–207]. These phase transformations depend strongly on the pH value, temperature and presence of other ions besides excess calcium and phosphate. Stulajterova and Medvecky [205] studied the conversion of DCPD into HAp by the hydrolysis of DCPD in alkaline solutions at a temperature of 39 °C with or without additional

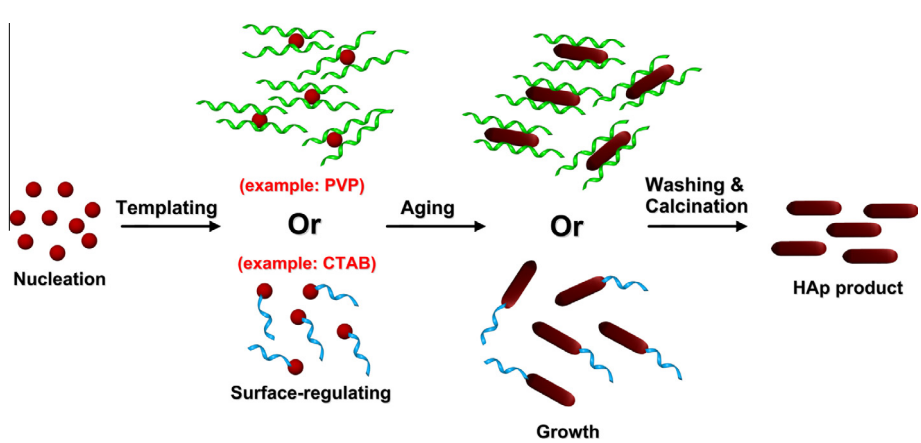

Fig. 7. Formation mechanism of rod-like HAp nanoparticles based on different templating systems.

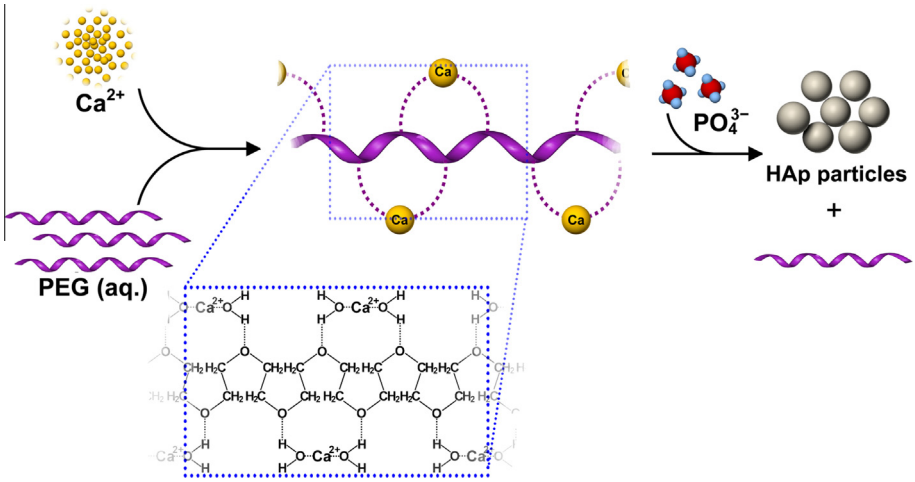

Fig. 8. Proposed reaction pathway for the preparation of HAp nanoparticles in the presence of PEG molecules.

calcium ions. According to the results, calcium-deficient HAp is formed by the phase transformation of DCPD in an aqueous solution having an initial pH of 10.8 at a temperature of 39 °C, whereas stoichiometric HAp, the thermodynamically most stable form of CaP, is obtained in a solution without excess Ca^{2+} only after a long hydrolysis time. Indeed, the presence of Ca^{2+} ions can accelerate the conversion of DCPD into calcium-deficient HAp. Stulajterova and Medvecky's results also confirmed the surface nucleation of HAp and the gradual transformation of DCPD by a dissolution–precipitation mechanism. The hydrolysis method is also considered to be an interesting way to modify the characteristics of a preprepared HAp powder. Seo and Lee [208] synthesized HAp whiskers by refluxing the aqueous slurry of commercial-grade HAp at 80 or 100 °C for 24 h in the presence of ethylenediamine tetraacetic acid (EDTA). They adjusted the pH of the solution to 7 or 9 and used hydrogen peroxide to promote the precipitation of HAp crystals. According to their results, the higher the H_2O_2 concentration, the pH value and the refluxing temperature, the longer and thinner the whiskers formed. Indeed, HAp powder is converted into HAp whiskers by a simple dissolution–reprecipitation process, in which amorphous reprecipitates initially form in the $Ca(EDTA)^{2-}$–PO_4^{3-} mixed solution and then grow continuously into long, thin HAp whiskers. FESEM micrographs showed that whiskers produced at 100 °C with 6% H_2O_2 at pH 9 had the highest aspect ratio of about 50–60 (a length of ~3 μm and a width of ~50 nm).

As mentioned at the beginning of this subsection, HAp can also be obtained by the hydrolysis of TCP under certain conditions. Ten-Huisen and Brown [209] presented an investigation of factors affecting the kinetics of calcium-deficient HAp formation from α-TCP. For this, they investigated the relationships between the rates of hydrolysis, the reaction temperature and microstructural development by isothermal calorimetry under different hydrolysis conditions. They showed that the hydrolysis of TCP to HAp occurs by a nucleation and growth mechanism. Moreover, according to the results, there is a linear relationship between hydrolysis temperature and HAp surface area, and the crystallites become more regular as the reaction temperature is increased. In the last decade, a number of attempts have been made to synthesis HAp of different shapes by hydrolysis of TCP under different experimental conditions (Supplementary Table S4). For example, Park et al. [197] synthesized HAp whiskers of different aspect ratios by the hydrolysis of α-TCP. They showed that aspect ratio, stoichiometry and thermal stability of obtained HAp are all strongly dependent on the pH of the hydrolysis.

2.2.3. Sol–gel method

The sol–gel method was one of the first methods proposed for the wet synthesis of HAp. However, coating of different substrates seems to have a major contribution to the sol–gel processing of HAp, and only a few studies have directly focused on the sol–gel synthesis of HAp nanoparticles (Supplementary Table S5). Sol–gel offers advantage of molecular-level mixing of reactants, improving the chemical homogeneity of the resulting powder [210–215]. Low-temperature formation and fusion of the prepared crystals are other notable advantages of the sol–gel process. In fact, temperatures higher than 1000 °C are usually advised to sinter HAp crystals prepared from other wet methods, whereas temperatures several hundred degrees lower are required for calcination and sintering of sol–gel HAp, leading to a decrease in degradation during the sintering. Additionally, a powder obtained by a typical sol–gel method usually exhibits a stoichiometric structure with a large surface area and a small cluster size (ranging from 50 nm to about 1 μm, depending on the processing parameters) [216–220]. In vitro studies have reported that the bioresorbability of the sol–gel HAp is higher than conventional powder and is close to biological apatite [221]. Major disadvantages include the generation of secondary phase (usually calcium oxide, CaO) and the high cost of some of the starting materials, especially alkoxide-based precursors. Secondary CaO phase has been demonstrated to be harmful to the biocompatibility of HAp and therefore attempts have been made to remove the coexisting CaO, either through washing of the calcined powder using a dilute acid solution (mainly HCl) or modification of the main procedure, e.g. through increasing the aging time [222–224].

The conventional sol–gel process involves the preparation of a 3D inorganic network by mixing alkoxides (or other suitable precursors) in either an aqueous or an organic phase, followed by aging at room temperature, gelation, drying on a hot plate and finally removing of organic residues from the resulting dried gel using post-heat treatment (calcination) [225–229]. The overall procedure is illustrated in Fig. 10. In the solution phase, reaction between the calcium and phosphorus precursors occurs slowly; this is why a long period of aging is usually required for the apatitic phase to form. Moreover, the thermal treatment step has been found to be critical in the generation of pure HAp and the expulsion of residual organic parts, gaseous products and water molecules from the porous gel [211–214,227]. Indeed, insufficient aging and/or uncontrolled gelation and heat treatment may cause the generation of various impurities, mainly CaO, $Ca_2P_2O_7$, $Ca_3(PO_4)_2$ and $CaCO_3$ [222,223]. Further, the rate of gelation, the nature of the solvent, and the temperature and pH employed during the

process strongly depend on the chemical nature of the reagents used in the sol–gel synthesis.

As in other wet methods, a number of precursors can be exploited in a typical sol–gel process (see also Fig. 10). In the majority of cases, calcium diethoxide or calcium nitrate is reacted with triethylphosphite or triethylphosphate, either in an aqueous or organic solution [228–233]. A general reaction may be shown as follows:

$$6Ca(NO_3)_2 + 6(C_2H_5O)_3P(O) \rightarrow Ca_{10}(PO_4)_6(OH)_2 + \text{byproducts} \quad (35)$$

Hsieh et al. [223] prepared nanocrystalline HAp according to the above reaction and studied the effect of gelation rate on the apatite formation. They reported that fast gelation leads to a high CaO generation, whereas slow gelation results in a minor CaO, which can be easily washed out by distilled water. Recently, nonalkoxide sol–gel processing of HAp without any need for adjusting pH has also been developed [221,234–238]. For this, a Ca precursor, usually $Ca(NO_3)_2$, and phosphoric pentoxide are first mixed in ethanol, resulting in a stable sol, followed by aging (usually at room temperature), drying (~100–150 °C) and finally heat treatment at elevated temperatures (~300–900 °C). The as-prepared powder was indicated to have a nanocrystalline structure, the crystallite size and crystallinity of which can increase with increasing the calcination temperature. Fathi et al. [221] reported that HAp powder synthesized by this process exhibits a nanoscaled (25 nm) and carbonated apatitic structure paralleling human bone apatite. Fathi et al.'s results also indicated that the morphology, crystallinity and crystallite size of the sol–gel HAp nanoparticles depend on the calcination temperature. In another study, Feng et al. [235] investigated the effect of aging time on the particle size. TEM observations showed that HAp nanopowders with different sizes of 10–15, 15–25 and 50–80 nm can be obtained after 4, 48 and 72 h of aging, respectively. This suggests that aging can contribute to powder growth and agglomeration.

2.2.4. Hydrothermal method

Hydrothermal process, as one of the most common methods for preparation of HAp, is usually identified by the reaction of chemicals in an aqueous solution at elevated temperature and pressure. Hydrothermal synthesis can also simply be considered as a chemical precipitation in which the aging step is conducted at a high temperature – typically above the boiling point of water – inside an autoclave or pressure vessel [239–247]. Supplementary Table S6 presents recent progress in the hydrothermal synthesis of HAp powder. As indicated in the table and also shown in Table 3, hydrothermal method has usually been exploited to prepare 1D nanosized HAp (i.e. nanorods), owing to its capability to induce 1D growth, though synthesis of specific and often unusual morphologies by using specific conditions and/or additives has also been reported. Furthermore, as demonstrated in Fig. 3, hydrothermal process is ranked as the third most popular method after the conventional precipitation and combination methods. It has been demonstrated that HAp nanoparticles obtained from the hydrothermal conditions is relatively stoichiometric and highly crystalline [248–253]. Moreover, phase purity and Ca/P ratio of HAp precipitate significantly improve with increasing the hydrothermal temperature [254–258]. However, elevated temperature and pressure need expensive equipments, making the hydrothermal process more expensive than some of the other wet methods.

So far, an abundance of data regarding the hydrothermal synthesis of HAp has been published, leading to some discrepancies in the optimum experimental conditions. A well-known example is the conditions by which elongated structures can be obtained; some studies show that the rod-like HAp is synthesized in acidic [251,259,260] or approximately neutral conditions [261,262], and others show that the nanorods are synthesized in alkaline conditions [249,263,264]. Recently, we [265] have reported that HAp nanorods having high crystallinity and high aspect ratio could simply be prepared through precipitation at approximately neutral conditions followed by a hydrothermal treatment at 200 °C for 60 h. In this case, the nanoparticles show high dispersion stability, indicating their high surface charge and low tendency for agglomeration. Fig. 11 shows the SEM and TEM photomicrographs of a typical rod-like HAp nanopowder synthesized under typical hydrothermal conditions [183]. It is usually suggested that the formation of rod-like crystals through the hydrothermal crystallization comprises two main stages, including nucleation step in which tiny crystalline nuclei in a supersaturated medium are formed (reaction of ions), and growth step in which nuclei continuously grow into the final shape and size (hydrothermal treatment) [183,266]. Fig. 12 schematically illustrates these two steps. Very recently, we [183,267] used different experimental design approaches to evaluate various processing parameters involved in these two steps. We demonstrated that temperature and pH are the most significant factors affecting the structural and morphological characteristics of HAp nanoparticles. According to our results, aspect ratio of the fibrous nanoparticles (determined from SEM analysis) steeply decreases with increasing the pH value. We also showed that different morphologies ranging from rod-like to spherical nanoparticles with various characteristics can be obtained by controlling the driving force of the chemical reaction. In Fig. 13, we summarized our recent results on the preparation of HAp nanoparticles under different hydrothermal conditions [267]. According to the figure, the high pH value results in an isotropic or weak-anisotropic growth; that is, the crystallites can grow to form spherical nanoparticles or at most very short nanorods. However, with a decrease in pH value of suspension, an anisotropic growth occur; that is, crystallites will grow into one-dimensional nanorods or two-dimensional nanoplates. Additionally, more complicated shapes, including three-dimensional feathery structure, three-dimensional microcubes, and three-dimensional microfibers are only obtained if the pH value decreases to 4, a pH which other CaP phases (i.e. DCPA, DCPD, and OCP) become dominant (Fig. 13). Recently, hydrothermal conditions by which a well-defined plate-shaped structure can be obtained have also been reported [268,269].

The most notable disadvantage of hydrothermal method is the poor capability of the process to control the morphology and size distribution of nanoparticles. Indeed, the morphology of particles

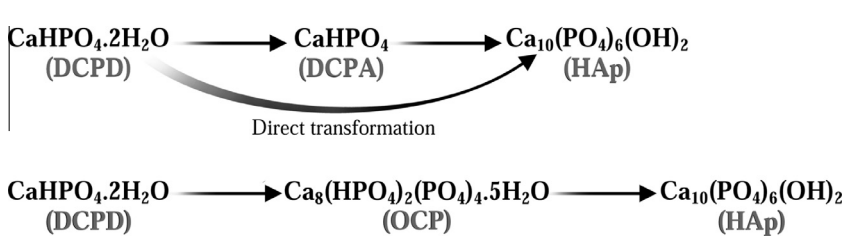

Fig. 9. Possible routes for phase transformation of DCPD and DCPA to HAp. Reprinted from Ref. [267] with permission.

obtained by a normal hydrothermal method is usually irregular, spherical, or at most rod-like, with a very broad size distribution (determined usually by analysis of TEM, FESEM, or SEM photomicrographs), e.g. 0.7–3.0 μm [250], 10–80 nm [254], or 9–152 nm [270]. Same as other chemical precipitations, to improve the procedure, a number of organic modifiers can be used, of which two types, including calcium chelating agents and various organic surfactants are more usual. EDTA as the most well-known calcium chelating agent acts as a hexadentate unit by wrapping itself around the Ca^{2+} ion with four oxygens and two nitrogens to form several five-member chelate rings [271–275]. Following the chelating process, the resultant complex can be decomposed by a controlled hydrothermal treatment. It has been found that in the presence of EDTA, longer crystals under milder hydrothermal temperatures can be obtained [264,271,272,275]. This can be explained by the fact that EDTA can strongly chelate the free calcium ions, and subsequently control the crystal growth of HAp nucleus. In fact, as a result of complexation, concentration of free calcium ions dramatically decreases, leading to the HAp nuclei with smaller size and quantity. During the hydrothermal treatment, calcium ions are released and each individual nucleus will grow to the distinct single needle-like particles and finally to well-separated long fibers. Zhu et al. [264], recently, reported that hydrothermal temperature of around 160 °C and a low pH value, with the molar ratio of EDTA/Ca = 1 can lead to a large HAp prism. Fabrication of dandelion-like HAp nanostructures through EDTA at the very high pH value of 12 has recently been reported by Lak et al. [273]. According to the results, the obtained 3D dandelion-like nanostructures were composed of radially oriented nanorods with an average diameter of ~200 nm. They showed that all the nanorods were grown individually from a central spherical core and no considerable aggregation occurred between them. Indeed, all the nanorods were densely aligned perpendicular to the surface of the core. Because no additional templates were used in the synthesis process, the dandelion-like nanostructures were thought to be self-assembled. In other words, EDTA affected the self-assembly of the initially formed precipitates and culminated in the formation of 3D dandelion-like nanostructures during the hydrothermal treatment. Fig. 14 schematically illustrates the steps involved in this process. According to the figure, EDTA wraps itself around the calcium ion to form Ca–EDTA molecular complexes. It is well-known that pH value has a considerable effect on Ca–EDTA complex stability, and increasing the pH value enhances the complex stability. Lak et al. indicated that pH value plays a key role in the synthesis of dandelion-like structures in the presence of EDTA. Indeed, the strong absorption of OH^- ions on the planes of initial clusters with high specific surface energy occurs due to high concentration of OH^- (pH = 12). In other words, growth rate of the facets of the primary clusters can be controlled by absorption of OH^- on the facets. Because of ionic interactions, the surface hydroxyl groups act as the active sites for adsorption of Ca–EDTA complexes. Subsequently, the Ca–EDTA complexes were integrated into the active sites of obtained crystallite. The space inhibitions of Ca-complex molecules with each other prevent the Ca atoms to be ordered according to the intrinsic crystal structure of HAp; therefore, adsorbed Ca–EDTA molecules on the surface dictate a 3D pattern structure for further growth in hydrothermal conditions (Fig. 14). During the subsequent hydrothermal treatment, Ca-complexes decompose and HAp crystals are grown on the previously formed pattern according to anisotropic growth along the c-axis, and a dandelion-like HAp is finally obtained.

HAp powders of desired characteristics can also be fabricated with the aid of organic modifiers, such as PEG, Tween-20, and d-sorbitol, by different hydrothermal temperatures [260,276–283] (for details, see Supplementary Table S6). For example, PEG is beneficial to the formation of HAp nanorods with a larger aspect ratio at high synthesis temperature; Tween-20 favors the formation of small-sized nanorods; and D-sorbitol helps the formation of nanorods with long length at low synthesis temperatures [270]. Recently, a novel hydrothermal method based on the liquid–solid–solution strategy has been developed by Wang et al. to synthesize surface-modified HAp nanorods of various aspect ratios [284]. According to this strategy, controlled growth of HAp nanorods with tunable morphology can be achieved by properly tuning the interfaces between surfactants and the central atoms of HAp. For this, linoleic acid and its corresponding sodium salts were chosen as anionic surfactants to complex with Ca^{2+} on the surface of HAp. Moreover, octadecylamine, which reacts with linoleic acid to form cationic surfactants because of its basicity, was adopted because of its possible interaction with the anion group of PO_4^{3-}. In the reported procedure, octadecylamine (or sodium linoleate), linoleic acid, and ethanol were mixed together under agitation, followed by adding $Ca(NO_3)_2$ to form the liquid (ethanol/ linoleic acid), solid (sodium linoleate), and solution ($Ca(NO_3)_2$ aqueous solution) phases. After the ion-exchange of Ca^{2+} and Na^+, a solution of Na_3PO_4 was added to react with the calcium linoleate. The mixture was finally agitated and hydrothermally treated at a controlled temperature. Wang et al. suggested that along with the reaction process, the linoleic acid absorbs on the surface of the in situ generated HAp nanorods, with the alkyl chains left outside and then, a spontaneous phase-separation process occurs because HAp nanocrystals settle and because of the incompatibility between the

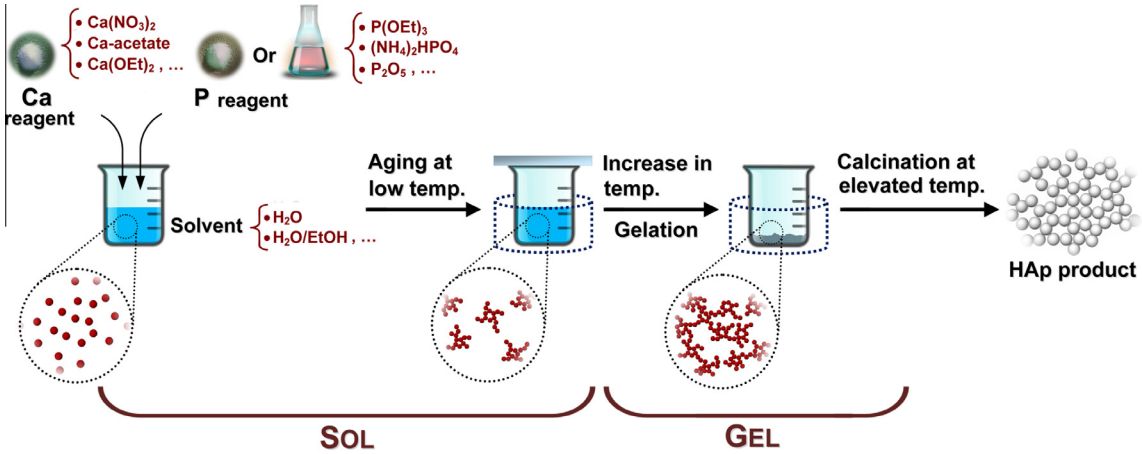

Fig. 10. Preparation of HAp nanoparticles via sol–gel process.

hydrophobic alkyl chains and their hydrophilic surrounding. Synthesis of HAp nanoparticles based on using CTAB under hydrothermal conditions has also been reported [268,272,285,286]. For example, rod-like and dandelion-like HAp nanoparticles have recently been synthesized through CTAB and CTAB/PEG systems, respectively (see Supplementary Table S6) [287]. In addition to the conventional organic modifiers, some attempts have also been made to exploit the more recently developed organic materials in controlling the crystal growth of HAp. Zhang et al. [288], for instance, synthesized HAp nanorods (80 nm by 10 nm, with aspect ratio of about 8) with narrow particle size distribution in the presence of anionic starburst dendrimers. Very recently, Zhu et al. [289] synthesized rod-like HAp nanoparticles of various aspect ratios (e.g. 8.0 ± 0.9 and 4.0 ± 0.8) by means of low-temperature hydrothermal method in the presence of N-[(2-hydroxy-3-trimethylammonium) propyl] chitosan chloride (HTCC) as a cationic polymer template. Fig. 15 shows the schematic description of the reaction. According to the figure, HTCC molecules are first incorporated into PO_4^{3-} and OH^- anions by charge and stereochemical complementarily, and the rigid chains of polymer molecules are then converted to extended chains as a result of the subsequent decrease in surface energy. The resultant extended chains are connected through the ion bonds of PO_4^{3-} to form a 2D structure, followed by formation of a 3D rod-like morphology through self-assembling of 2D layers via hydrogen bond interactions. Finally, nucleation and subsequent crystal growth can occur upon adding the Ca precursor and hydrothermal treatment, respectively. Zhu et al. also suggested that the size and morphology of nanoparticles can be tailored by varying the synthesis conditions, including pH, hydrothermal temperature, and ratio of phosphate ions to the quaternary ammonium in the template.

2.2.5. Emulsion method

The precise control over morphology, size, and size distribution of grains or particles is extremely important and certainly difficult; especially when one intends to produce nanoscopic material with minimal agglomeration and aggregation. Emulsion processing of HAp particles was initially introduced to refine the clustering and to restrict the formation of hard agglomerates [290]; however, this technique is now a subject of great interest not only to prepare an agglomerate-free ceramic powder, but also to control the microstructure and morphology of resulting particles. Indeed, among many different wet processes developed for HAp synthesis, emulsion method is suggested to be more efficient to reduce the particle size, to control the morphology, and to limit the agglomeration of HAp particles [291–298]. Moreover, simplicity and mild synthesis condition without any high-temperature requirement during the main procedure make the emulsion technique to be an appropriate method.

A microemulsion is a thermodynamically stable, isotropic transparent dispersion of two immiscible liquids, such as water and organic, stabilized by the presence of surface active agents (i.e. surfactants). Surfactants as amphiphilic molecules with a hydrophilic head connected to a hydrophobic tail can reduce the surface tension of the immiscible liquids, resulting in a dispersed phase confined in nanometer regimes; the generated emulsion is thus capable of delivering nanosized particles when the reaction is confined in the nanosized domains. Emulsion process depends strongly on the type of surfactant(s) used and concentration of the surfactant(s) present in the liquid medium [290,291,299]. For example, various organized assemblies of surfactants, such as micelles and vesicles, can be obtained depending on chemical structure of the surfactant, especially its molecular weight and relative size of the hydrophobic tail with respect to the hydrophilic head. These assemblies have been shown to provide a suitable environment for the controlled growth of nanoparticles. The hydrophobic monolayer (i.e. surfactants) can subsequently be removed easily by calcination, during which the resulting powder may also undergo little growth in crystallite and particle sizes [294,299,300].

Up to now, three main categories of surfactants have been employed in the microemulsion synthesis of HAp, including ionic (cationic and anionic) surfactants, nonionic surfactants, and block-copolymers with different molecular weights. The different chemical nature and molecular weights of these surfactants makes it possible to produce various organized assemblies (spheres, rods, discs, bicontinuous, etc.) and therefore specific HAp particles' geometries. Supplementary Table S7 shows recent progress in the emulsion synthesis of HAp. As indicated in the table, emulsion process can be accomplished by three main routes, including water-in-oil emulsion, oil-in-water emulsion, and water-in-oil-in-water double emulsion. The mechanism of these emulsification systems have been schematically illustrated in Fig. 16. Our estimation, however, shows that the synthesis of HAp is usually conducted through the water-in-oil system accounted for about 70% of all papers related to the emulsion synthesis of HAp. The water-in-oil emulsion is based on a transparent inverse microemulsion system containing reverse micelles dispersing in a continuous oil phase [301–304]. Each micelle consists of solution droplets surrounded by certain surfactant molecular groups, forming a "water pool" suspended in the oil phase. Following the addition of the second microemulsion containing another reagent, fusion–fission between the reverse micelles causes the reaction between calcium and phosphate ions and finally formation of HAp crystals, as illustrated in Fig. 17 [304–306].

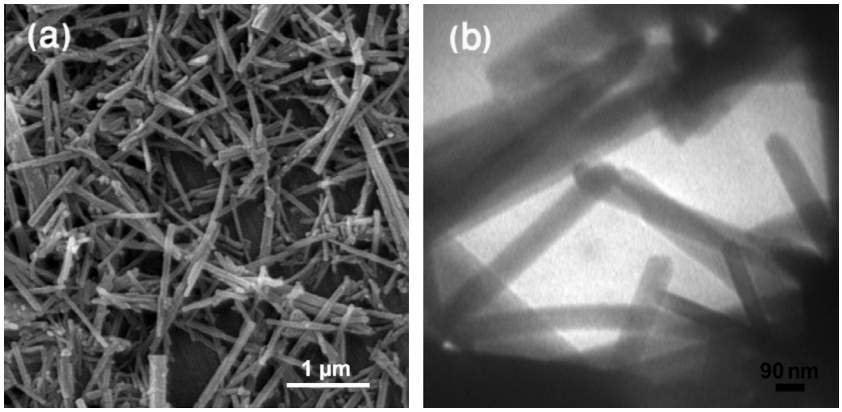

Fig. 11. (a) SEM and (b) TEM images of rod-like HAp nanoparticles. Reprinted from Ref. [183] with permission.

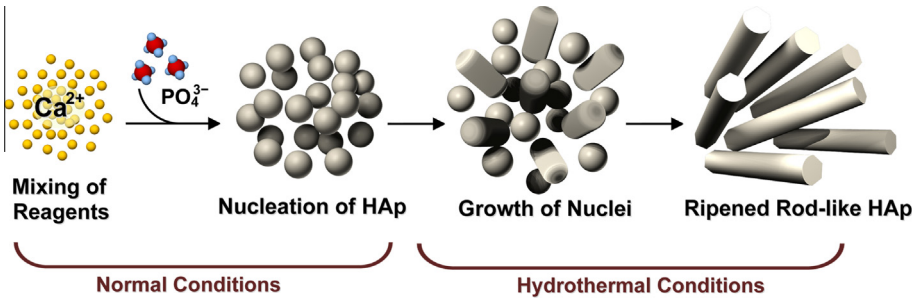

Fig. 12. Two-step process of preparation of rod-like HAp nanoparticles under hydrothermal conditions.

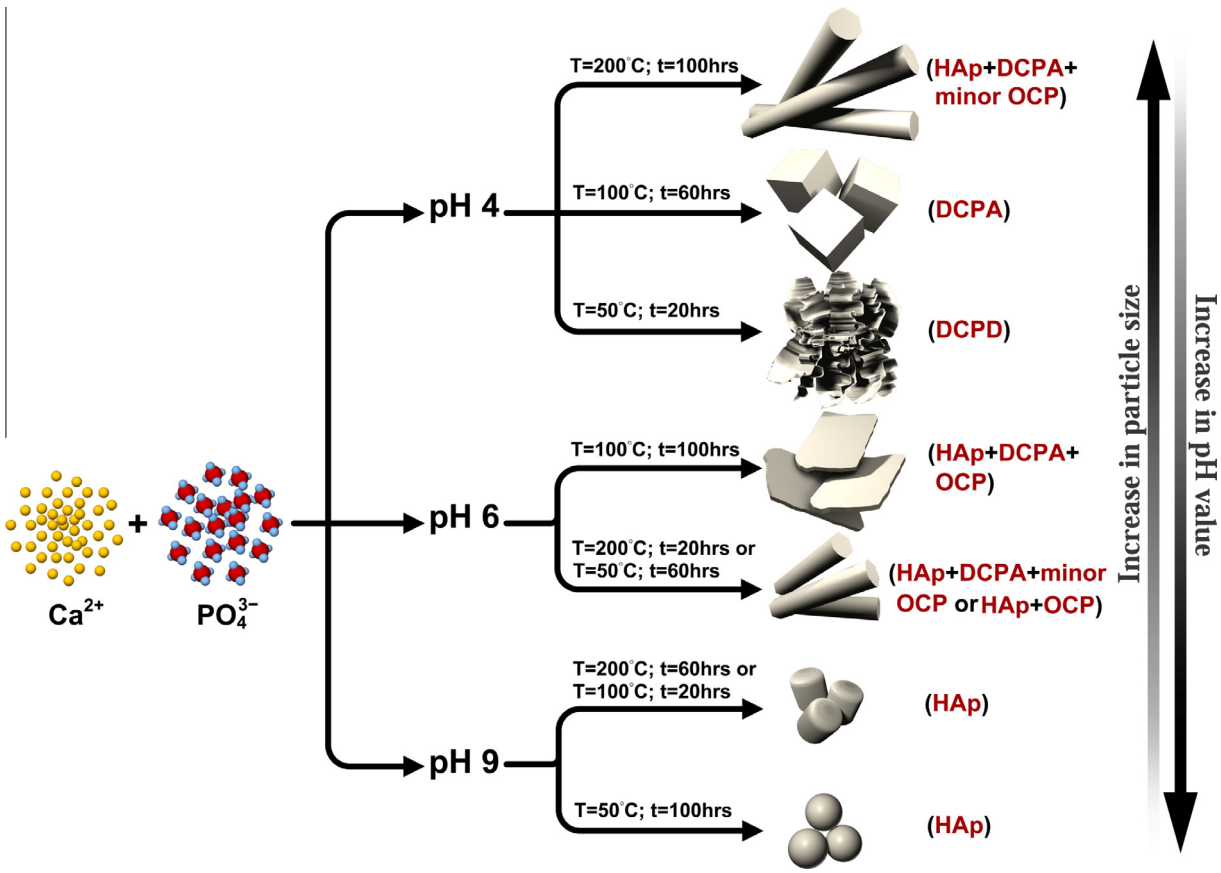

Fig. 13. Effect of pH, temperature, and duration of hydrothermal treatment on phase, morphology, and particle size of the CaP powder. Reprinted from Ref. [267] with permission.

Taking into account the templating role of each micelle as an independent micro- or nano-reactor, final morphology and particle size of HAp particles (for example, spherical and rod-like morphologies in Fig. 17) will be same as the shape and size of the micelles, respectively. Furthermore, morphology and crystallinity of the resulting powder can be adjusted through electrostatic interactions between head group of ionic surfactants and oppositely charged groups on HAp seeds, as shown in Fig. 18 [299,307,308]. Indeed, by choosing a specific surfactant(s) and therefore a specific templating system, the electrostatic field is changed, allowing the characteristics of resulting powder to be controlled. Especially in the case of nanowires, formation of amorphous nuclear/surfactant complex and the electrostatic field inside the reverse micelles maintain the unidirectional and irreversible fusion of the reverse micelles, resulting in one-dimensional growth of crystals [300,309–314].

As mentioned before, depending on the nature of surfactant(s), HAp nanoparticles of different characteristics (size, shape, crustallinity, etc.) can be produced. Sun et al. [307], for example, synthesized the single-crystal HAp nanorods of 8–15 nm in diameter and 25–50 nm in length using polyoxyethylene (TX-100) and CTAB. They indicated that homogeneity in size and shape of HAp particles observed by TEM can be attributed to the different stabilization functions of different kinds of surfactant on the interfacial layer; while TX-100 was suggested to act as a tridimensional stabilizer, function of CTAB as an ionic surfactant is the electrostatic stabilization of the microemulsion system. Additionally, they demonstrated that incorporating alcohols (n-butanol and n-hexanol) as co-surfactant can improve the interfacial properties of the microemulsion from a microstructural standpoint; the alcohol modifies the surfactant packing parameters by absorbing to the interfacial film and thus

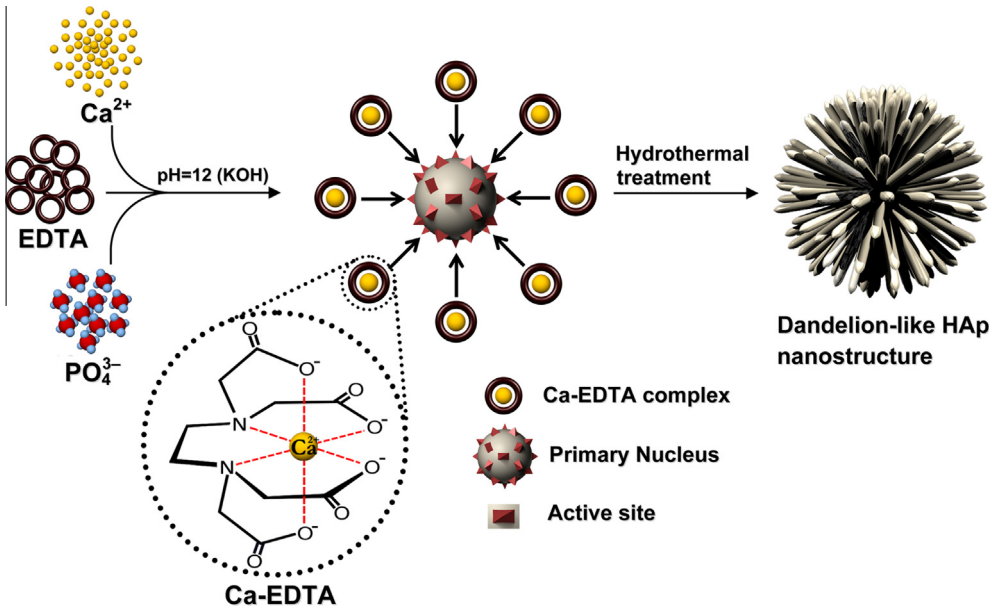

Fig. 14. Hydrothermal synthesis of dandelion-like HAp nanostructures in the presence of EDTA.

influencing the radius of curvature of microemulsion droplets. In a similar study, Guo et al. [311] synthesized HAp nanoparticles by a reverse microemulsion with a mixed surfactant system of TX-100 and Tween-80. They reported that microemulsion route leads to a significant improvement in particle size and degree of particle agglomeration compared to the conventional direct precipitation method. Moreover, TEM observations showed that different particle size and size distribution (e.g. 21–57 or 28–64 nm) can be obtained depending on the weight ratio of TX-100 and Tween 80. Lai et al. [312] investigated the nucleation kinetics of CaP nanoparicles in the reverse micelle solution. Their reaction system consisted of CTAB, cyclohexane, and n-pentanol. They found that the initial amorphous nuclei in reverse micelles were mainly composed of DCPA rather than HAp because of the kinetic favor of DCPA. Moreover, results showed that nucleation rates in reverse micelle solution are lower than those conducted in aqueous solution. They suggested that reverse micelles might condense reaction solution thus increasing its concentration. An increase in ion strength makes reverse micelles invulnerable which might disfavor the effective coalescence and the nucleation process as well. From our study, we [308] prepared HAp nanoparticles of 75–98 nm in size using a mixed surfactant system comprising CTAB, n-pentanol, and Span-60. According to the results, Span-60 as a nonionic surfactant can effectively deter the formation of rod-like morphology by decreasing the electrostatic field inside the reverse micelles. In this case, the CTAB molecules didn't have any significant role in controlling the morphology, and are only used to control particle size. Li et al. [300] synthesized nanocrystalline HAp particles of spherical (25–35 nm) and rod-like (10–80 nm × 140–180 nm) morphologies using reverse microemulsion at room temperature. They reported that no obvious other's phase occurred after as-prepared particles calcined under different temperatures up to 700 °C. Recently, Saha et al. [299] have investigated the effect of processing parameters, including type of surfactant, aqueous to organic ratio (A/O), Ca^{2+} concentration, pH, and aging time on the characteristics of final powder. They used isooctane, hexane, and cyclohexane as organic solvents, and dioctyl sulfosuccinate sodium salt (AOT), dodecyl phosphate (DP), poly (oxyethylene)$_5$ nonylphenol ether (NP5), and poly(oxyethylene)$_{12}$ nonylphenol ether (NP12) as surfactants to make the emulsion. According to the results, HAp nanoparticle of different morphologies such as spherical, needle shape or rod-like can be obtained simply by adjusting the conditions of the emulsion system. Their study revealed that increasing the A/O ratio increases specific surface area of synthesized powder, and according to the BET data, the highest surface area can be obtained with NP5 at A/O ratio of 1:5 and pH 7 after calcinations at 450 °C. It was also observed that increase in pH decreased the aspect ratio of the powder and nearly spherical nanopowder was obtained with NP12 at pH 9. According to the results, hydrophilic head groups of NP5 or NP12 act as a coordination site for Ca^{2+}, providing the necessary confinement in two dimensional spaces to direct the mineral growth and form the elongated crystals. In the system with lower water content (A/O = 1:15), i.e. higher organic phase and higher surfactant ratio, the stability of the micelle was found to be affected due to lower hydrogen bonding available with the aqueous core. As a result, the surfactant-micelle equilibrium is shifted and dynamic exchange with other micelles and isolated surfactant molecules in the organic phase would be significantly faster, forming micelles with larger size. In this case, the nucleation and mineral growth of HAp crystals take place in the micelle of roughly spherical shape leading to the formation of nanopowder with a lower aspect ratio.

2.2.6. Sonochemical method

Sonochemical methods, which always yield nanosized products, are based on the chemical reactions activated by powerful ultrasound radiation. Supplementary Table S8 presents recent progress in the sonochemical synthesis of HAp nanoparticles. The physical mechanism behind the sonochemical synthesis is acoustic cavitation in an aqueous phase where the formation, growth and collapse of microbubbles occur according to Fig. 19 [315,316]. Indeed, reactivity of chemicals is stimulated to accelerate the heterogeneous reactions between liquid and solid reactants [317]. It has recently been demonstrated that sonication increases the rate of HAp crystal growth up to 5.5 times [318]. It has also been reported that HAp nanoparticles synthesized by a sonochemical process possess more uniform, smaller, and purer crystals with minimal agglomeration [318–321]. These nanoparticles can significantly enhance the sintering kinetics, due to the higher surface area, and therefore the mechanical properties of final product. Cao et al. [322] prepared needle-like nanocrystalline HAp by the ultrasonic precipitation

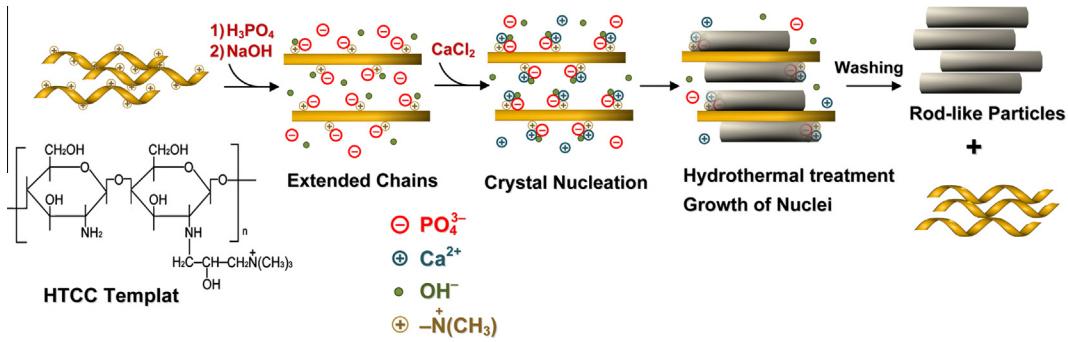

Fig. 15. Preparation of rod-like HAp nanoparticles using low-temperature hydrothermal treatment in the presence of HTCC as a cationic polymer template.

using urea as organic modifier. They showed that addition of urea favors the formation of HAp nanoparticles. They also found an Arrhenius relationship between the rate of HAp formation and the reaction temperature. According to the Arrhenius-derived equation, activation energy of the formation of HAp nanoparticles under ultrasonic irradiation was calculated to be 59.9 kJ/mol. They finally concluded that HAp content should increase with increasing the preparation temperature and/or time. In another study, Kim and Saito [317] used an aqueous suspension containing phosphoric acid and calcium hydroxide and applied the ultrasonic irradiation to investigate the sonochemical effects on the preparation of HAp. They concluded that single phase HAp could be synthesized after 60 min sonication. Similarly, their results showed that the HAp formation can be significantly promoted under sonochemical conditions. Recently, Han et al. [323] synthesized stable HAp nanoparticles from $Ca(H_2PO_4)_2$ and $Ca(OH)_2$ aqueous solutions by using the ultrasound irradiation and adding glycosaminoglycans (GAGs) as regulation additive. According to their study, an increase in the irradiation time will increase the particle size a little and improve the crystallinity degree. They reported that the size distribution and surface charge of nanoparticles are also affected by concentration of GAGs. Based on DLS analysis, with the GAG concentration of 0.35 g/L, optimized HAp powder was reported to be obtained with number-average particle size of 22 nm in 85% area and 55 nm in 15% area between 18 nm and 117 nm. Indeed, GAGs interact strongly with HAp through electrostatic interactions between the anionic domains on the GAG macromolecule (carboxyl and sulphate) and the cationic sites on HAp mineral (calcium), leading to the control of HAp nucleation and growth. Han et al. [324] also investigated the change of phase composition and morphology of sonochemically synthesized HAp nanoparticles during thermal treatment. More recently, Rouhani et al. [318] proposed a rapid method to prepare ball-like HAp nanoparticles by sonication of a pseudo-body solution (PBS) containing inorganic ions. According to the results, the sonication time is an important factor affecting the formation of crystalline phase of nanoparticles; so that a 15 min sonication (28–34 kHz, 100 W) at 37 °C resulted in a pure HAp. Their results clearly showed that the particles generated by sonication were generally smaller and more spherical than those obtained without sonication. Comparison of the particle size demonstrated that sonication decreased the particle size from 30 nm (corresponding to specific surface area of 63 m^2/g) to 18 nm (corresponding to specific surface area of 107 m^2/g).

2.3. High-temperature processes

High-temperature processes can be identified by their elevated temperatures used to burn or partially burn the precursors. According to the literature (see Supplementary Table S9), high-temperature processes can be performed by two techniques, including combustion and pyrolysis.

2.3.1. Combustion

Combustion method or solution combustion method, a conventional process to prepare various oxide ceramics, is being considered to be a promising method for preparation of CaP nanocrystals [325–327]. The basis of combustion technique comes from thermochemical concepts used in the field of propellants and explosives chemistry. The key feature of the combustion synthesis of HAp is its ability to quickly produce powder with high purity in a single step operation. Moreover, the approach has advantages of inexpensive raw materials, relatively simple preparation process, and well chemical homogeneity of synthesized powder as a result of intimate blending of constituents [328–331]. As illustrated in Fig. 20, solution combustion processing of HAp involves a very rapid exothermic and self-sustaining redox reaction between oxidants (calcium nitrate and HNO_3) and a suitable organic fuel (e.g. glycine, urea, sucrose, citric acid, and succinic acid) in an aqueous phase [332–334]. For this, the aqueous stock solutions of $Ca(NO_3)_2$ and $(NH_4)_2HPO_4$ are first mixed, followed by adding the concentrated HNO_3 to dissolve the resulting white precipitate; a single or a mixture of two or more fuels are subsequently incorporated into the resulting solution. The reaction can be initiated by heating the mixture in a furnace at a fairly low temperature (e.g. 300 °C); this is then followed by a sudden increase in temperature, as a result of the combustion, to a maximum value. The final step is the fast cooling of mixture to induce maximum nucleation and to prevent any further particle growth. Exothermicity of the combustion reaction supplies the heat required to maintain the temperature of the system, and once initiated, no external heating is needed anymore [328,329]. The resulting product is usually soft agglomerates of very fine particles. Several processing parameters, including fuel to oxidizer ratio [328,335], initial furnace temperature [328,335], nature of the fuel [329,333,336], and quantity of the initial precursor [335] have been reported to affect the maximum reaction temperature (i.e. flame temperature), and accordingly the characteristics of the final powder (see also Supplementary Table S9). In particular, different fuels have proved to be capable of delivering different flame temperatures ranging from 100 to 900 °C (e.g. citric acid: ~150 °C; succinic acid: ~425 °C; urea: ~800 °C; glycine: ~890 °C). Ghosh et al. have recently published several papers on the preparation of nanosized HAp using combustion method [328,335,337]. According to their study [337], different combinations of urea and glycine and occasional addition of small amounts of highly water-soluble glucose, a fuel with a lower decomposition temperature (~180 °C), lead to different flame temperatures, and therefore different HAp products. Indeed, thermochemistry of combustion reaction can be controlled by tailoring the fuel composition. For example, a very small quantity of glucose added to either urea or glycine, significantly reduced the

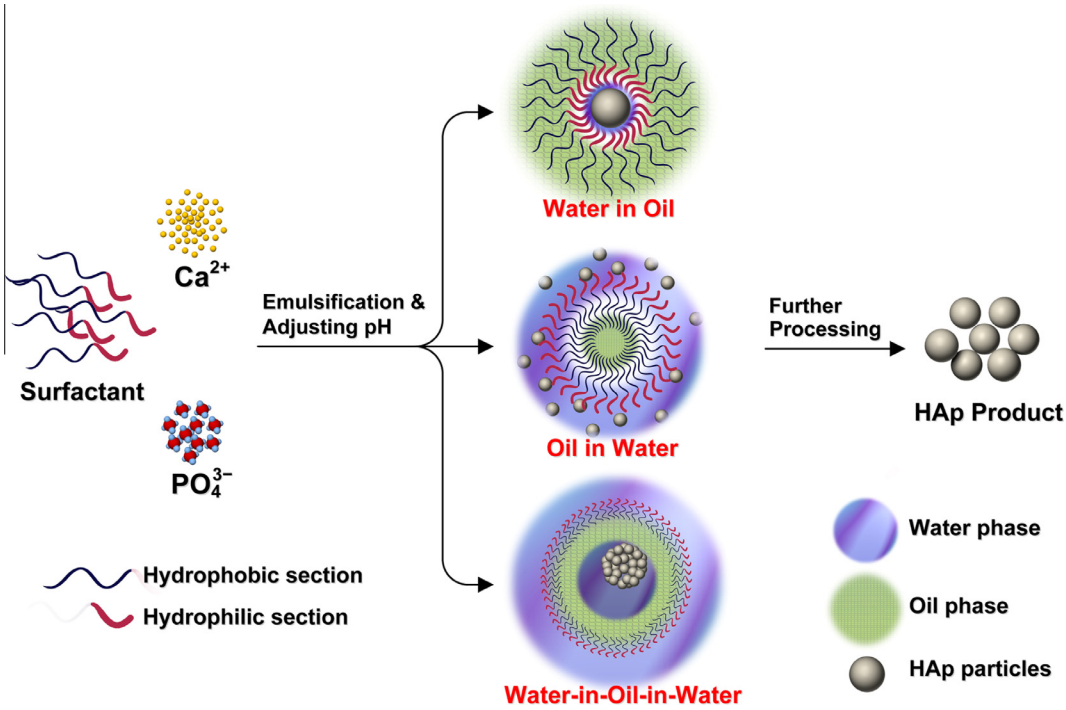

Fig. 16. Three main routes of emulsification in the emulsion synthesis of HAp nanoparticles.

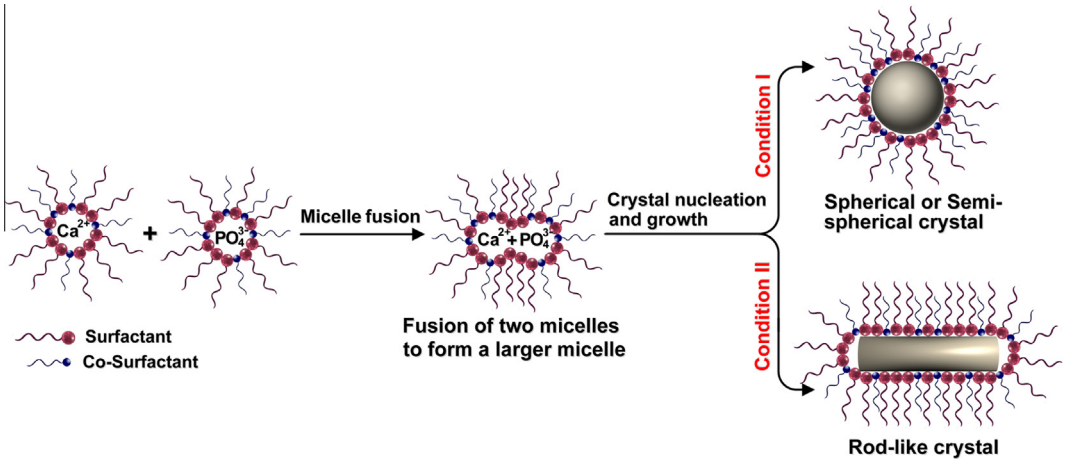

Fig. 17. Fusion process of the reverse micelles containing different ions to form HAp nanoparticles of spherical morphology (condition I) or rod-like morphology (condition II).

flame temperature. On the other hand, with increasing the percentage of glucose, the vigorous mode of self-propagating combustion reaction becomes smouldering in nature. BET results showed that specific surface area of powder obtained from glucose–stoichiometric urea/glycine mixed fuel was higher than that obtained from urea–glycine composition. Additionally, based on DLS analysis, particle size distribution of as-prepared powder was found to decrease with increase in urea content. Ghosh et al. [335] also demonstrated that a decrease in both batch size and initial furnace temperature and/or an increase in fuel to oxidizer ratio result in a decrease in crystallite size. Very recently, they [328] showed that stoichiometric glycine–calcium nitrate leads to the higher flame temperature compared to stoichiometric urea–calcium nitrate system, resulting in a powder with lower specific surface area. Moreover, in both cases of glycine and urea, combustion with excess fuel produced particles with higher surface area. They also indicated that well crystalline and weekly agglomerated nanosized powder having diameters ranging from 20 nm to 120 nm (determined by FESEM) could be prepared simply by an optimized reaction. Similarly, Sasikumar and Vijayaraghavan [329] have synthesized HAp nanoparticles by the combustion synthesis route, using citric acid and succinic acid as fuels. According to the results, carbonated HAp can be obtained either through citric acid or succinic acid, whereas β-TCP is only formed when a mixture of them is used. However, by adding the citric acid to the succinic acid, the auto ignition temperature of succinic acid was found to decrease to lower temperatures.

2.3.2. Pyrolysis

To produce a stoichiometric single-crystal HAp, processing conditions involved in various wet and dry methods usually need to be strictly controlled. Some post treatments and/or long-term aging under elevated temperatures may also be required to achieve a high crystalline product. By contrast, HAp particles fabricated directly by a rapid pyrolysis-based method have been reported to

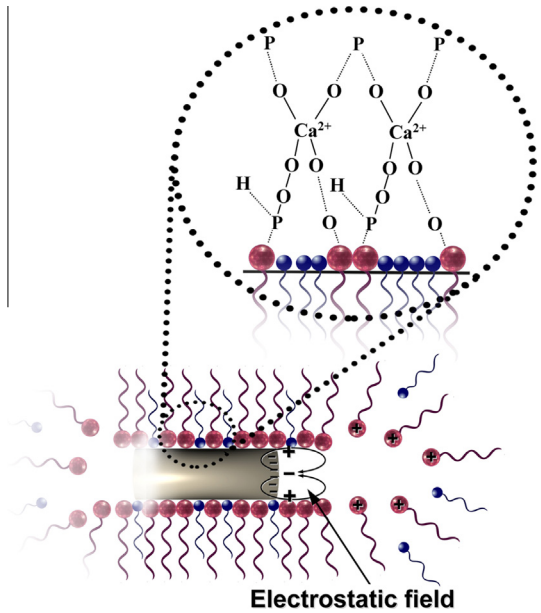

Fig. 18. Electrostatic field proposed to be generated inside the reverse micelles; enlarged illustration shows the interaction between the HAp crystal and a cationic surfactant.

be stoichiometric, homogeneous, and highly crystalline [338–340]. In a typical pyrolysis, particles can form from reactants in a gas phase generated by physical evaporation of liquid precursors. In comparison with the combustion method, no fuel mixed with the reactants is needed in the pyrolysis synthesis and the process can be easily scaled up for continuous production of HAp particles. It should be mentioned that the pyrolysis method can also be classified under a broad category generally known as aerosol methods (or gas-phase methods), in which gas-to-particle or liquid-to-particle conversions occure in an aerosol decomposition process.

Pyrolysis method, sometimes known as "spray pyrolysis", involves spraying the precursor solutions into a flame or a hot zone of an electric furnace using an ultrasonic generator. This is then followed by reaction of the generated vapors and gases at high temperatures to produce final powder, typically in an aggregated and agglomerated form [340–342]. In fact, the high temperature leads to the complete evaporation of precursor droplets followed by nucleation and growth of nanoparticles in the gas phase. Fig. 21 shows the schematic illustration of the equipment. According to the figure, size of the particles is strongly dependent upon size of the droplets generated during the process; thus, some attempts have been made to reduce particle size by formation of fine droplets [338,342].

So far, few studies have investigated the pyrolysis synthesis of HAp powder (Supplementary Table S9). Vallet-Regi et al. [343] published an early study on the pyrolysis synthesis of HAp. They produced an aerosol with ultrafine droplets (2–4 μm) by ultrasonic frequency of a precursor solution containing $CaCl_2$ and $(NH_4)H_2PO_4$. The aerosol flow was then passed through a long tubular furnace at temperature of 500 °C, leading to submicronic HAp particles. Following this study, Aizawa et al. [344] examined effect of urea as a foaming agent on the formation of HAp through the spray-pyrolysis technique. They found that crystalline phases of the powders prepared from the spraying solution without urea were HAp and a small amount of β-TCP; however, only carbonate-containing HAp was formed from the solutions with urea. The SEM observations showed that the particle size of the as-prepared powder decreased with increasing urea concentration in the spraying solution. This reduction of particle size may be due to the foaming action of CO_2 generated by decomposition of urea. In another study, Aizawa et al. [339] investigated the effect of pyrolysis temperature and concentration of the starting solutions on the pyrolysis synthesis of HAp. For this, they used HNO_3 solutions containing different concentrations of $Ca(NO_3)_2$ and $(NH_4)_2HPO_4$ with the Ca/P ratio of 1.67. These solutions were sprayed into a heating zone composed of two electric furnaces; the lower furnace for evaporation of solvent from the droplets (300–500 °C) and the upper furnace for pyrolysis of the precipitated salts (750–900 °C). They reported that a pure and easily sinterable HAp powder can be obtained when the spray-pyrolysis temperature was 850 °C for the upper furnace and 400 °C for the lower one. The resulting powder was composed of spherical particles in a submicron-size range. Moreover, specific surface area of the prepared particles was reported to significantly decrease with increasing the concentration of starting solution. Very recently, Itatani et al. [340] prepared submicronic HAp powder by spray pyrolysis of precursor solution containing $Ca(NO_3)_2$, $(NH_4)_2HPO_4$ and concentrated HNO_3 at 600 °C using an ultrasonic vibrator. They reported that the resulting powders were composed of spherical agglomerates; the agglomerate diameter decreased with decreasing concentration of spraying solution. For example, mean diameter of agglomerates obtained by the spray pyrolysis of a solution with very low concentration of reactants was as small as 0.34 μm (determined by TEM).

As mentioned before, pyrolysis synthesis of HAp particles can also be performed in the flame, where the reactions of vapor-phase precursors take place at a significantly higher temperature compared to the furnace. Indeed, a flame can provide a sufficiently high temperature to form a uniform and dense HAp structure. Although furnace temperature is more accurate and controllable, but the flame temperature can also be easily adjusted by varying fuel and oxidizer flow rates. As a disadvantage, small decomposition of HAp into the α-TCP has been reported [338], because of high temperature of flame (usually above 2000 °C). Recently, Cho and Kang [338] prepared nanosized HAp with high crystallinity and appropriate stoichiometry (~1.69) by high-temperature flame spray pyrolysis followed by a post-treatment at temperatures between 400 and 1000 °C. They also investigated the effect of PEG added to the spray solution on morphology, mean size, and crystallinity of resulting powder. They reported that the mean sizes of HAp powders were changed from several tens to several hundreds nanometers depending on the concentration of PEG added to the spray solutions. For example, pyrolysis of a solution with low concentration of 0.1 M PEG led to a powder with mean size less than 100 nm.

As a disadvantage of pyrolysis process, secondary aggregations are usually formed during the pyrolysis, resulting in a decrease in specific surface area. To address this problem, An et al. [345] employed a salt-assisted decomposition approach; a process by which nanosized particles without any significant agglomeration can be prepared by addition of a specific salt to the precursor solution. For this, a solution mists containing $Ca(NO_3)_2$, H_3PO_4, and $NaNO_3$ were generated by an ultrasonic atomizer and carried into a furnace which was preheated to a given temperature (either 500 or 700 °C). In this procedure, $NaNO_3$ acts as a matrix to interrupt agglomerate formation of the primary nanoparticles. The nanosized particles are subsequently obtained by removing the salts from the secondary particles comprising salts and HAp using a simple washing step. It was reported that the synthesized nanoparticles were rod-like and single phase with high crystallinity and good stoichiometry. In addition, the particle size (determined by TEM) and aspect ratio was demonstrated to be affected by the salt quantity and synthesis temperature.

Finally, we should mention that there are some other densification methods which are similar to the spray pyrolysis, except for

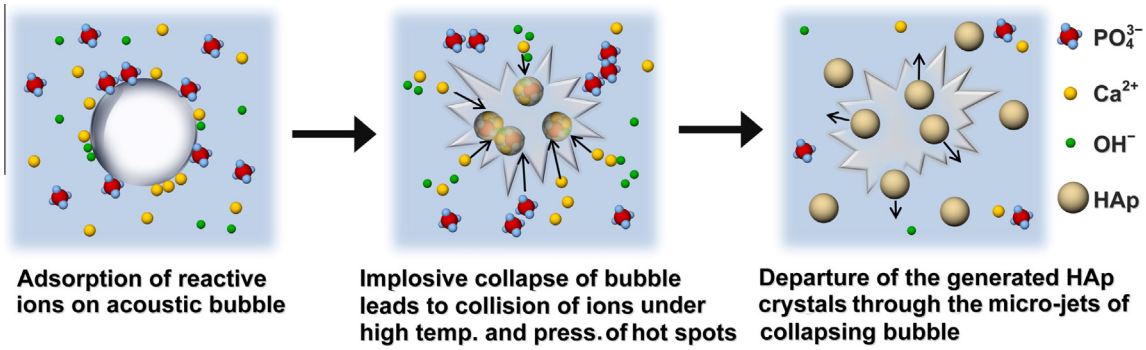

Fig. 19. Mechanism proposed to be involved in the sonochemical synthesis of HAp nanoparticles.

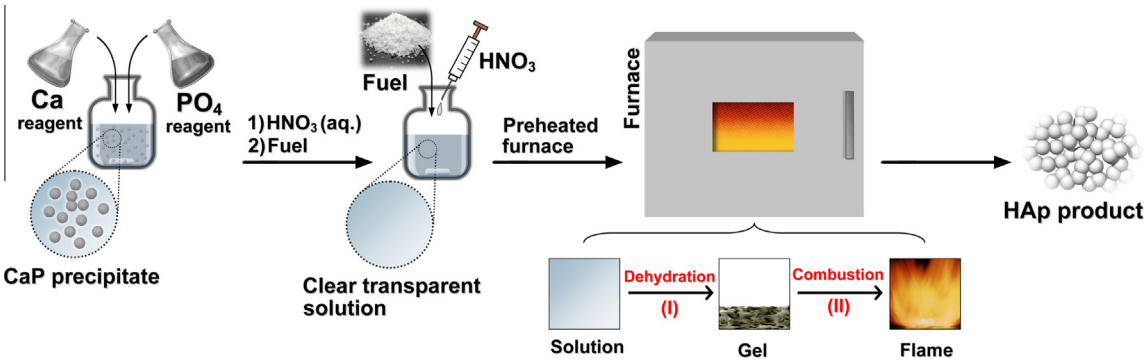

Fig. 20. Preparation of HAp nanoparticles via solution combustion method.

the type of precursor and some technical details. The most well-known example is spray drying method that typically uses colloidal HAp particles (i.e. HAp sols) as precursor to produce particulate materials. A typical spray drying process involves three steps: feeding suspended HAp slurry to a nozzle; atomizing of suspension into a stream of heated air flowing through an evaporation chamber; and finally trapping of the resulting particles by an electrostatic precipitator [71,72]. Accordingly, there is always a preliminary chemical step to synthesize the phase of HAp; thus, the spray drying and other similar methods (such as thermal spraying) should be considered as a complement of other methods. Additionally, spray drying usually results in spherical granules or large micrometer-sized particles having a hollow structure [61,62,73] which have not been discussed here, as they are outside the scope of this article.

2.4. Synthesis from biogenic sources

HAp ceramic generated partially or entirely from biogenic sources is proposed to be accepted better by the living organs, because of its physicochemical similarity to the human bone apatite. Supplementary Table S10 shows recent studies on the production of HAp using various biogenic sources. A careful look at the table reveals five different groups, including extraction of minerals from biowastes, synthesis from eggshells, synthesis from exoskeleton of marine organisms, synthesis with the aid of natural biomolecules, and synthesis using biomembranes. This can schematically be summarized in Fig. 22.

According to Supplementary Table S10, extraction of biominerals from biowastes (mainly bovine bones, fish-scales, and fish bones) is the most well-known method for the preparation of HAp using biogenic sources. This is an interesting process, in particular, not only because of some superior characteristics of the extracted material, but also due to the economical and environmental benefits of waste recovery [346–350]. Preparation of HAp using biowastes usually involves a few hours annealing during which the organic materials in the bone get removed, leaving pure HAp as the residue (Fig. 22(a)) [351–357]. According to Fig. 22(a), beside the simple thermal annealing (i.e. calcination), some other extraction processes, including enzymatic hydrolysis, plasma processing, subcritical water processing, and alkaline hydrothermal hydrolysis can also be used [348,358,359]. Moreover, some attempts have been made to reduce the particle size of powder to the nanometric scale [360,361]. For example, Ruksudjarit et al. [361] synthesized nanocrystalline HAp from bovine bone by a vibro-milling technique. They demonstrated that vibro-milling method can separate and disperse the HAp nanocrystals from its parent bone structure. For this, the bovine bone was deproteinized using hot water, calcined at 800 °C, crushed into small pieces, and finally milled in a ball mill pot for at least 24 h. The resulting powder was then ground by vibro-milling apparatus for various milling times. According to the results, HAp powder with diameter less than 100 nm can be obtained when the milling duration is 2, 4, or 8 h. Recently, Barakat et al. [348] used conventional thermal decomposition, subcritical water process (hot liquid water under pressure), and alkaline hydrothermal method to, respectively, decompose, dissolve, and hydrolyze the organic compounds of bovine bone. Their results showed that all these methods have the ability to remove organic matters of bone and to produce pure HAp with an average yield of 65%. Moreover, thermal processing resulted in nanorod HAp of about 300 nm in length, whereas subcritical water and alkaline hydrothermal processes led to HAp nanoparticles possessing small nanoflakes. More recently, a rapid plasma processing has been used to extract HAp from bovine bone [359]. According to the results, only 90 s plasma processing using transferred arc plasma results in an organic free bovine HAp.

Besides the hard tissues of animals, some attempts have also been made to produce HAp, especially carbonated HAp, using eggshell waste [362–365]. As indicated in Fig. 22(b), eggshells are composed mainly of calcium carbonate (~95–97%), and thus, can be adapted as a calcium precursor in the synthesis of HAp [366]. Typically, the eggshells are first heated at ~900 °C in a furnace to decompose organic matter and to convert calcium carbonate to calcium oxide which in turn on exposure to atmosphere forms calcium hydroxide ($Ca(OH)_2$); the as-prepared $Ca(OH)_2$ is subsequently reacted with a suitable phosphorus precursor to produce HAp crystals [366–368]. Some researchers have also tried to replace the heating step by a chemical treatment; for example, eggshells can be treated by HNO_3 or HCl to produce $Ca(NO_3)_2$ and $CaCl_2$, respectively [364,369]. Recently, Boonyang et al. [370] conducted a hydrothermal reaction at 250 °C between crocodile eggshells and three different phosphate precursors, including $(NH_4)_2HPO_4$, $Ca_3(PO_4)_2$, and H_3PO_4. They reported that only $(NH_4)_2HPO_4$ and $Ca_3(PO_4)_2$ gave monophase HAp within 25 and 8 h of treatment, respectively. Moreover, microstructure of the as-prepared HAps was reported to be clusters of agglomerated plate-like crystals.

According to Fig. 22(c), calcium carbonates present in skeleton of various marine species are other natural raw materials exploited in the synthesis of HAp. A typical procedure involves ion exchanging under hydrothermal conditions, for example, according to the following reaction [371–376]:

$$10CaCO_3 + 6(NH_4)_2HPO_4 + 2H_2O \rightarrow Ca_{10}(PO_4)_6(OH)_2 + 6(NH_4)_2CO_3 + 4H_2O + 4CO_2 \quad (36)$$

Calcium carbonate originated from marine species usually exhibits characteristic porosity and interconnectivity similar to that found in human bone [375–379]. To maintain this unique internal morphology, phytogenic calcium carbonates are usually used in the original form, e.g. in fragments in the case of algae and in shaped blocks in the case of corals [375,377,380]. Indeed, the inherent differences between vegetative structures of different marine species lead to the HAp blocks having different internal morphologies and pore sizes. For example, HAp prepared using corals typically has a pore size of several hundreds of microns, whereas pore size of that synthesized using the marine algae rarely exceeds a few micrometers [375–378]. The larger and higher macroporosity of the structure, similar to the natural cancellous bone, has been reported to result in earlier bone mineralization during the implantation; and hence corals-generated HAps are claimed to be more beneficial to bone repair applications.

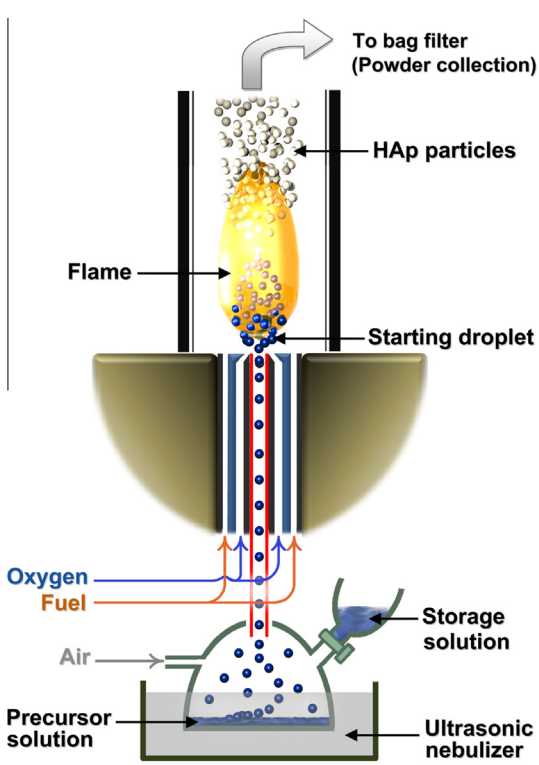

Fig. 21. Schematic diagram illustrating the equipment setup for the preparation of HAp nanoparticles via flame spray pyrolysis.

Synthesis of nanosized particles in the presence of various biomolecules extracted from diverse natural materials, as indicated in Fig. 22(d), is the fourth approach for the preparation of HAp using natural sources [364,381–384]. For example, Zhao et al. [364] have reported that ovalbumin (a natural biosurfactant) extracted from egg white affects the morphology and surface charge of the HAp powder. Indeed, interactions between ovalbumin and HAp crystals were found to have a great effect on the surface charges of particles. According to the results, large HAp spindle-like particles aggregated from needle-like nanocrystals of 20–50 nm in length and 2–6 nm in thickness can be obtained in the presence of ovalbumin. Recently, various biomolecules originated from orange peel, potato peel, egg shell, papaya leaf, and calendula flower were reported to affect the characteristics of HAp powder [384]. According to the studies, the extracted biomolecules (amino acids, carotene, papain, carotenoids, vitamins, etc.), as the medicinally important materials, can exert a significant control on the synthesis of nanosized HAp. Indeed, only small quantities of the biomolecules led to a significant change in both size and morphology of resulting powder.

As indicated in Fig. 22(e) and Supplementary Table S10, a few studies have recently reported on the utilization of natural membrane to produce HAp nanostructures using a diffusion-controlled nucleation mechanism. For example, eggshell membrane – a structure constructed from interwoven fibers of collagen with nanometer-sized pores in between them – can be exploited to control the diffusion of phosphate ions towards calcium ions during the HAp nucleation [385,386]. As a result of slow and controlled movement of ions across the membrane, HAp structures with a specific morphology can be obtained. Recently, Zhang et al. [385,387] fabricated the flower-like structures of HAp (see Table 3) either using eggshell membrane or bamboo membrane. They reported that flower-like HAp agglomerates with high crystallinity can be produced on the upper or lower side of the both membranes (see Fig. 22(e)). Moreover, as a result of intrinsic differences between bamboo membrane (mainly composed of cellulose) and eggshell membrane (mainly composed of proteins), the as-prepared structures were different in terms of morphology and other characteristics. Additionally, both the morphology and the crystal structure of agglomerates were indicated to be influenced by temperature, pH value, and holding time. For example, based on TEM analysis, flower-like structures composed of nanosheets with a length of 20–80 nm and a width of 20–40 nm can be obtained on the upper side of the eggshell membrane at temperature of 37.5 °C, pH value of 7.4, and holding time of 12 days. Very recently, Neelakandeswari et al. [386] prepared needle-like HAp nanoparticles using eggshell membranes. Again, both the structure and morphology of powder were reported to be affected by pH of the reaction.

2.5. Combination procedures

To improve the properties of final product, two or more distinct methods can be combined to create a synergistic strategy [388–390]. As indicated in Supplementary Table S11, many hybrid tech-

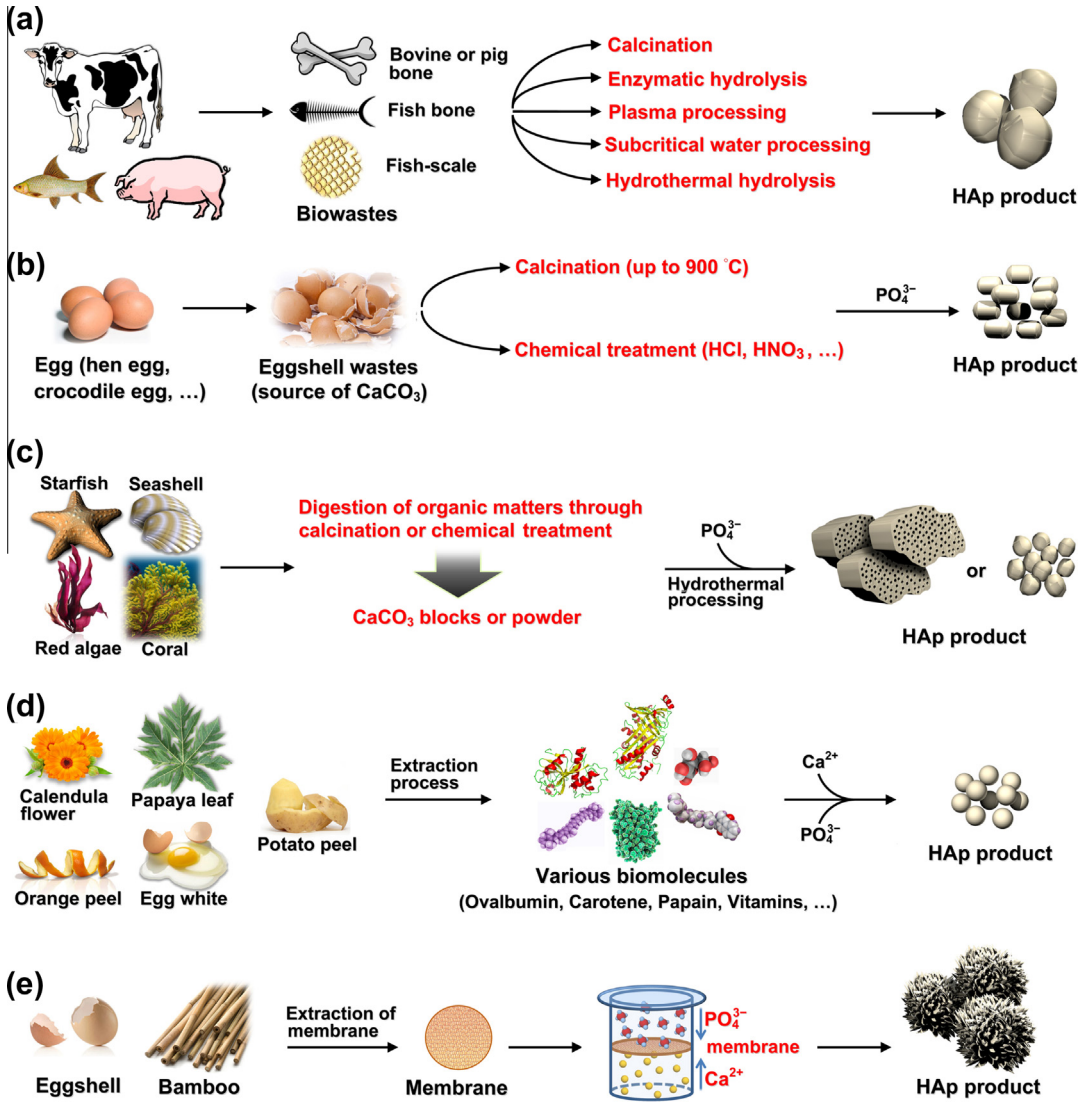

Fig. 22. Preparation of HAp via biogenic sources: (a) extraction of minerals from biowaste; (b) synthesis from eggshells; (c) synthesis from exoskeleton of marine organisms; (d) synthesis with the aid of naturally derived biomolecules; and (e) synthesis using biomembranes.

niques mainly hydrothermal–mechanochemical [391–401], hydrothermal–hydrolysis [402–410], and hydrothermal–microemulsion combinations [411–416] have been developed over the past decade. However, the most well-known approach is to combine the mechanochemical method with the hydrothermal procedure through incorporation of an aqueous phase into the system. The resulting mechanochemical–hydrothermal hybrid, sometimes known as wet mechanochemical, can accelerate those kinetic processes that usually limit the rate of reaction in a conventional mechanochemical method (i.e. dissolution, diffusion, and adsorption) [393–396,400]. Suchanek et al. [398] used this method to prepare crystalline carbonated HAp at room temperature by milling a slurry at the rotation speed of 1500 rpm for 1 h and then at 800 rpm for 4 h. According to the study, the resulting powder consisted of equiaxed nanocrystals of about 20 nm in diameter (determined by TEM), which formed larger aggregates with 0.35–1.63 μm in size (determined by DLS). Compared to the hydrothermal process where a lot of energy is usually required to generate elevated temperatures, high energy consumption can be avoided in the combined method. In fact, while the activation of slurry results in local zones of high temperatures, up to 700 °C, due to the friction effects and adiabatic heating of gas bubbles, the overall temperature of reaction remains close to the room temperature; and that is why any external heating or pressure vessel is not required in a normal wet mechanochemical process [395,397,399,401]. Recently, Abdel-Aal et al. [392] used statistical design approach to determine the optimum experimental conditions. Their results revealed that milling time is the most significant factor affecting the particle size; the longer the milling time, the smaller the crystallite size. According to the results, nanosized particles with a narrow size distribution of 10 to 20 nm (determined by TEM) can be obtained at optimized conditions.

Hydrothermal–hydrolysis and hydrothermal–microemulsion hybrids are other well-known combinations, according to Supplementary Table S11. Hydrothermal–hydrolysis process, which is used to accelerate the kinetic of hydrolysis, can be simply conducted by hydrolysis of a CaP phase, usually DCPD or TCP, under elevated temperatures and pressures. For example, Liu et al. [402] have converted α-TCP to HAp using this combination method in the presence of excess calcium ions. They showed that well HAp crystals with different morphologies (microflowers, microplates, packed nanorods, and microrods) can be obtained by adjusting the reaction temperature and concentration of extra ions. Hydrothermal–microemulsion hybrid, also known as solvothermal, can

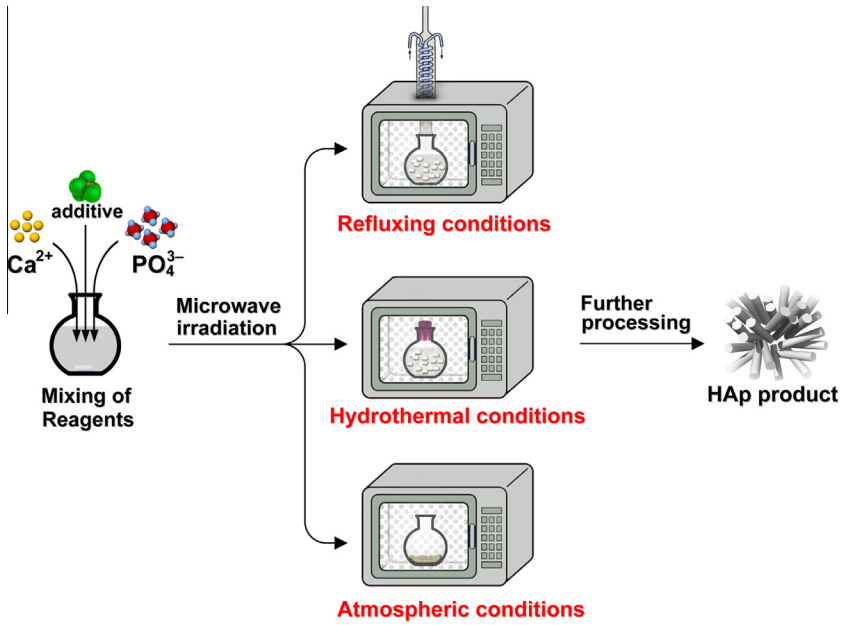

Fig. 23. Three main routes for preparation of HAp nanoparticles via microwave-assisted synthesis.

offer some further benefits. It is known that rod-like nanoparticles with narrow particle size distribution can be obtained through microemulsion technique, although the resulting nanorods exhibits low crystallinity with low aspect ratio (see Section 2.2.5). On the other hand, the hydrothermal synthesis usually leads to highly crystalline particles of elongated shape, but usually in an agglomerated form with a wide particle size distribution. The solvothermal synthesis, which brings together these two different approaches, can therefore provide a unique method to prepare the crystalline rod-like nanoparticles with minimal agglomeration and narrow size distribution. For example, stoichiometric HAp nanorods with 25–40 nm in diameter and 55–350 nm in length have been reported to be obtained by a solvothermal system comprising CTAB, n-pentanol, n-hexane, and water [412]. For this, the nucleation of HAp first occurs at room temperature within the reverse micelles and then generated nuclei start to grow under high temperature and pressure. Sometimes, some procedures without having the templating system are also named as solvothermal, owing to the fact that a mixture of water and a water-miscible organic solvent is employed during the synthesis [417,418]. For example, Ma et al. [419] prepared HAp microtubes using $CaCl_2$ and NaH_2PO_4 in a solvent mixture of water/N,N-dimethylformamide (DMF) at 160 °C. However, according to our classification, these procedures cannot be considered as a real hybrid due to the absence of the microemulsion system.

All mentioned methods in Supplementary Table S11 are substantially based on combination of two distinct methods described in Sections 2.1–2.4. However, there are also several contributions to the combination of previously described methods with a new procedure, so that one may consider them as a hybrid process. The most well-known example is microwave-assisted methods, in which microwave irradiation is used to activate the reaction. In contrast to the conventional procedures, where the material is externally heated through conduction, microwave heating involves in situ conversion of microwave energy into heat using the inherent properties of reaction mixture [420–422]. Microwave processing of HAp particles was initially employed for sintering of HAp ceramics to produce a dense material with improved physical and mechanical properties [423,424]; however, this technique is now a subject of interest to synthesize HAp nanoparticles in a less energy-consuming and more reproducible manner. In actual practice, microwave treatment results in rapid and uniform heating of entire bulk of the substance to the temperature of treatment without any significant thermal stress or temperature gradient [425–428]. This can increase the reaction kinetics and effectively reduce duration of the process [428–432]. As a result of fast homogenous nucleation, microwave synthesis of HAp nanoparticles is usually accomplished in less than 30 min. It is believed that microwave irradiation may also lead to a powder having some improved characteristics, including smaller size, higher purity, and narrower size distribution. Supplementary Table S12 presents recent progress in the microwave synthesis of HAp nanoparticles. A careful look at the table reveals that the microwave processing of HAp can be conducted under either refluxing or hydrothermal conditions or even at atmospheric conditions with short time or long time irradiation, as also schematically illustrated in Fig. 23. Moreover, several attempts have also been made to combine the microwave irradiation with solid-state [433–435], hydrolysis [436,437], sonochemical [438], and solution combustion [439,440] methods.

There are several examples for microwave synthesis of HAp under refluxing system [425,431,441,442]. Kumar et al. [425] recently described the synthesis of HAp nanostrips of 50–70 nm in diameter and 50–100 nm in length by refluxing an aqueous solution under microwave irradiation in the presence of EDTA. They demonstrated that EDTA plays an important role in controlling the morphology of the powder. In a similar study, Kalita and Verma [431] synthesized highly crystalline HAp nanopowder of 5–30 nm in size having a mixed (elliptical and rod-shape) morphology with the aid of EDTA and microwave irradiation. Liu et al. [441,442] synthesized bow-knot-like and flower-like HAp nanostructures (see Table 3) using microwave assisted reactions. They suggested that shape of crystals can be easily controlled by adjusting the stability of Ca–EDTA complex and the hindrance effect of OH^- on the crystallite facets. Microwave-assisted reactions can also simply be conducted at atmospheric conditions without refluxing system, either through a short time or long time irradiation [428,443–448]. Arami et al. [449] synthesized HAp nanostrips of 10 nm in width and 55 nm in length, via 5 min microwave irradiation of a precursor

(pH = 12) comprising $Ca(NO_3)_2$, Na_2HPO_4, NaOH, and CTAB. Siddharthan et al. [450] synthesized HAp nanoparticles by microwave irradiation to a precursor of $Ca(NO_3)_2$ and H_3PO_4 until drying the precipitate. According to the results, the power of irradiation was found to affect both the particle size and the particle shape. As just mentioned, microwave reactions can also be accomplished under hydrothermal conditions. While in the conventional hydrothermal procedures, a stainless steel vessel is usually used, a typical microwave–hydrothermal technique employs a polymeric reactor which is transparent to microwaves. The procedure involves a few minutes microwave irradiation to result in rapid formation of HAp precipitate [432,451–453]. Katsuki and Furuta [430] synthesized HAp nanorods with 5–50 nm in diameter and 30–300 nm in length from gypsum ($CaSO_4.2H_2O$) powder reacted with $(NH_4)_2HPO_4$ solution, using 5 min microwave–hydrothermal treatment at 100 °C. They showed that the introduction of microwaves into the hydrothermal process leads to an increase in HAp formation by approximately two orders of magnitude. Recently, Han et al. [454] synthesized nanosized HAp powder by a microwave–hydrothermal treatment at 600 psi and 300 °C for up to 30 min. They reported that applied microwave power and mole ratio of Ca/P are among the important factors affecting the characteristics of HAp. According to the results, low microwave power of 450 W and Ca/P ratio of 1.57 lead to a mixed CaP compound including $Ca(OH)_2$, $CaHPO_4$ and HAp, whereas running the reaction at 550 W power and Ca/P 1.67 results in monophase HAp.

3. Conclusion and outlook

In the review article presented here, the preparation methods of HAp nanoparticles were classified as follows:

(a) Dry methods. Dry methods, which can be identified in contrast to wet methods where a solvent is always used, can be performed in two main ways: solid-state synthesis and mechanochemical process. These methods have the convenience of producing highly crystalline HAp from relatively inexpensive raw materials. The main disadvantage is the large size of particles in the case of solid-state synthesis and the low phase purity of HAp in the case of mechanochemical process. In recent years, progress in preparing HAp using dry methods, especially solid-state method, has been very slow.

(b) Wet methods. Aqueous solutions of various sources for phosphate and calcium ions are employed and HAp crystals are normally produced by precipitation. Wet processes can be performed by a number of technical routes classified into six groups: conventional chemical precipitation, hydrolysis method, sol–gel method, hydrothermal method, emulsion method, and sonochemical method. Wet chemical methods have the advantages in precise control over the morphology and size of particles, and based on the statistical analysis, they are the most promising methods for the synthesis of nanosized HAp. However, difficulties in controlling the crystallinity and phase purity of nanoparticles, and some technically intricate and time-consuming details make some wet procedures unsuitable for scaling up to produce large quantities of HAp.

(c) High-temperature processes. These methods, which have the convenience of avoiding undesirable CaP phases, are used to produce HAp with high crystallinity and good chemical homogeneity. Two possible routes for high-temperature synthesis of HAp are combustion method and pyrolysis process, of which the former has received more attention. Poor control over the processing variables and generation of the secondary aggregates, especially during the pyrolysis, are the main disadvantages.

(d) Synthesis from biogenic sources. To produce HAp ceramics various natural materials, mainly bone waste, eggshells, exoskeleton of marine organisms, naturally derived biomolecules, and biomembranes, have been employed over the past decade. This field is expected to attract more attention in the near future, owing to the better physicochemical properties of the HAp generated from biogenic sources. However, some of these materials can be exclusively used to produce HAp blocks or at most HAp particles of large size. This stresses the need for further work in the area.

(e) Combination procedures. These methods, as relatively new strategies, employ two or more distinct procedures to synthesize HAp nanoparticles. Among several possibilities, combinations of hydrothermal–mechanochemical, hydrothermal–hydrolysis, and hydrothermal–microemulsion have received more attention. Reports on various hybrids employed microwave method have also been published recently. In general, combination procedures open exciting possibilities to improve the characteristics of HAp nanoparticles.

Despite the great variety of methods for preparation of HAp nanoparticles, only a few of them are satisfactory in terms of economics or performance, mainly due to the diverse materials needed in the synthesis, complicated and expensive processes, serious aggregation and agglomeration, wide particle size distribution, and various phase impurities which usually occur in the crystal structure. For example, in a typical wet method, production of HAp requires a precise control over the reaction conditions along with a long-term aging in the final step. On the other hand, there seems to be little effort on scaling up the introduced methods; and unfortunately little work has been reported to evaluate the biological interactions of the prepared nanoparticles, at least in the open literature. To address these issues, new synthesis routes which can practically be put to use in the biomaterials industries have to be established. Future studies must also consider all aspects of an effective and feasible synthetic route and examine the biological characteristics of the prepared powder. An alternative approach may be to develop innovative and practical combinations, e.g. mechanochemical–solvothermal method or microwave–assisted sol–gel process. Moreover, synthesis of nanoparticles with new characteristics, e.g. novel 3D morphologies, can also be another interesting challenge for future research.

Appendix A. Figures with essential colour discrimination

Certain figures in this article, particularly Figures 1, 4–7, 12–23 are difficult to interpret in black and white. The full colour images can be found in the on-line version, at http://dx.doi.org/10.1016/j.actbio.2013.04.012.

Appendix B. Supplementary Tables

Supplementary data associated with this article can be found, in the online version, at http://dx.doi.org/10.1016/j.actbio.2013.04.012.

References

[1] Sato K. Mechanism of hydroxyapatite mineralization in biological systems. J Ceram Soc Japan 2007;115:124–30.
[2] Malmberg P, Nygren H. Methods for the analysis of the composition of bone tissue, with a focus on imaging mass spectrometry (TOF-SIMS). Proteomics 2008;8:3755–62.
[3] Batchelar DL, Davidson MTM, Dabrowski W, Cunningham IA. Bone-composition imaging using coherent-scatter computed tomography: assessing bone health beyond bone mineral density. Med Phys 2006;33:904–15.

[4] Märten A, Fratzl P, Paris O, Zaslansky P. On the mineral in collagen of human crown dentine. Biomaterials 2010;31:5479–90.
[5] Hu YY, Rawal A, Schmidt-Rohr K. Strongly bound citrate stabilizes the apatite nanocrystals in bone. Proc Natl Acad Sci USA 2010;107:22425–9.
[6] Jee SS, Kasinath RK, DiMasi E, Kim YY, Gower L. Oriented hydroxyapatite in turkey tendon mineralized via the polymer-induced liquid-precursor (PILP) process. CrystEngComm 2011;13:2077–83.
[7] Iijima M, Moriwaki Y, Yamaguchi R, Kuboki Y. Effect of solution pH on the calcium phosphates formation and ionic diffusion on and through the collagenous matrix. Connect Tissue Res 1997;36:73–83.
[8] Vallet-Regí M, González-Calbet JM. Calcium phosphates as substitution of bone tissues. Prog Solid State Chem 2004;32:1–31.
[9] Rabiei A, Blalock T, Thomas B, Cuomo J, Yang Y, Ong J. Microstructure, mechanical properties, and biological response to functionally graded HA coatings. Mater Sci Eng C 2007;27:529–33.
[10] Chen L, Mccrate JM, Lee JCM, Li H. The role of surface charge on the uptake and biocompatibility of hydroxyapatite nanoparticles with osteoblast cells. Nanotechnology 2011;22:105708.
[11] Chen D, Tang C, Chan K, Tsui C, Yu PHF, Leung MCP, et al. Dynamic mechanical properties and in vitro bioactivity of PHBHV/HA nanocomposite. Compos Sci Technol 2007;67:1617–26.
[12] Pelin IM, Maier SS, Chitanu GC, Bulacovschi V. Preparation and characterization of a hydroxyapatite–collagen composite as component for injectable bone substitute. Mater Sci Eng C 2009;29:2188–94.
[13] O'Hare P, Meenan BJ, Burke GA, Byrne G, Dowling D, Hunt JA. Biological responses to hydroxyapatite surfaces deposited via a co-incident microblasting technique. Biomaterials 2010;31:515–22.
[14] Gu Y, Khor K, Cheang P. Bone-like apatite layer formation on hydroxyapatite prepared by spark plasma sintering (SPS). Biomaterials 2004;25:4127–34.
[15] Habibovic P, Kruyt MC, Juhl MV, Clyens S, Martinetti R, Dolcini L, et al. Comparative in vivo study of six hydroxyapatite-based bone graft substitutes. J Orthop Res 2008;26:1363–70.
[16] Marini E, Ballanti P, Silvestrini G, Valdinucci F, Bonucci E. The presence of different growth factors does not influence bone response to hydroxyapatite: preliminary results. J Orthopaed Traumatol 2004;5:34–43.
[17] Kokubo T, Takadama H. How useful is SBF in predicting in vivo bone bioactivity? Biomaterials 2006;27:2907–15.
[18] Rabiee S, Moztarzadeh F, Solati-Hashjin M. Synthesis and characterization of hydroxyapatite cement. J Mol Struct 2010;969:172–5.
[19] Eiden-Assmann S, Viertelhaus M, Heiss A, Hoetzer K, Felsche J. The influence of amino acids on the biomineralization of hydroxyapatite in gelatin. J Inorg Biochem 2002;91:481–6.
[20] Kniep R, Simon P. Fluorapatite–gelatine-nanocomposites: Self-organized morphogenesis, real structure and relations to natural hard materials. Top Curr Chem 2007;270:73–125.
[21] Gower LB. Biomimetic model systems for investigating the amorphous precursor pathway and its role in biomineralization. Chem Rev 2008;108:4551–627.
[22] Bigi A, Marchetti F, Ripamonti A, Roveri N, Foresti E. Magnesium and strontium interaction with carbonate-containing hydroxyapatite in aqueous medium. J Inorg Biochem 1981;15:317–27.
[23] Iijima M, Du C, Abbott C, Doi Y, Moradian-Oldak J. Control of apatite crystal growth by the co-operative effect of a recombinant porcine amelogenin and fluoride. Eur J Oral Sci 2006;114:304–7.
[24] Hou CH, Hou SM, Hsueh YS, Lin J, Wu HC, Lin FH. The in vivo performance of biomagnetic hydroxyapatite nanoparticles in cancer hyperthermia therapy. Biomaterials 2009;30:3956–60.
[25] Li J, Yin Y, Yao F, Zhang L, Yao K. Effect of nano-and micro-hydroxyapatite/chitosan–gelatin network film on human gastric cancer cells. Mater Lett 2008;62:3220–3.
[26] Furukawa T, Matsusue Y, Yasunaga T, Nakagawa Y, Okada Y, Shikinami Y, et al. Histomorphometric study on high-strength hydroxyapatite/poly(L-lactide) composite rods for internal fixation of bone fractures. J Biomed Mater Res 2000;50:410–9.
[27] Trombelli L, Simonelli A, Pramstraller M, Wikesjö UME, Farina R. Single flap approach with and without guided tissue regeneration and a hydroxyapatite biomaterial in the management of intraosseous periodontal defects. J Periodontol 2010;81:1256–63.
[28] Strietzel FP, Reichart PA, Graf HL. Lateral alveolar ridge augmentation using a synthetic nano-crystalline hydroxyapatite bone substitution material (Ostim®). Clin Oral Implants Res 2007;18:743–51.
[29] Ye Q, Ohsaki K, Li K, Li DJ, Zhu CS, Ogawa T, et al. Histological reaction to hydroxyapatite in the middle ear of rats. Auris Nasus Larynx 2001;28:131–6.
[30] Seol YJ, Kim JY, Park EK, Kim SY, Cho DW. Fabrication of a hydroxyapatite scaffold for bone tissue regeneration using microstereolithography and molding technology. Microelectron Eng 2009;86:1443–6.
[31] Lv Q, Nair L, Laurencin CT. Fabrication, characterization, and in vitro evaluation of poly(lactic acid glycolic acid)/nano-hydroxyapatite composite microsphere-based scaffolds for bone tissue engineering in rotating bioreactors. J Biomed Mater Res 2009;91:679–91.
[32] Itokazu M, Yang W, Aoki T, Ohara A, Kato N. Synthesis of antibiotic-loaded interporous hydroxyapatite blocks by vacuum method and in vitro drug release testing. Biomaterials 1998;19:817–9.
[33] Sadat-Shojai M, Atai M, Nodehi A. Method for production of biocompatible nanoparticles containing dental adhesive. US Patent 8,357,732; 2013 http://www.uspto.gov/web/patents/patog/week04/OG/html/1386-4/US08357732-20130122.html.
[34] Blackwood D, Seah K. Electrochemical cathodic deposition of hydroxyapatite: improvements in adhesion and crystallinity. Mater Sci Eng C 2009;29:1233–8.
[35] Zahouily M, Abrouki Y, Bahlaouan B, Rayadh A, Sebti S. Hydroxyapatite: new efficient catalyst for the Michael addition. Catal Commun 2003;4:521–4.
[36] Sugiyama S, Minami T, Hayashi H, Tanaka M, Shigemoto N, Moffat JB. Partial oxidation of methane to carbon oxides and hydrogen on hydroxyapatite: enhanced selectivity to carbon monoxide with tetrachloromethane. Energ Fuel 1996;10:828–30.
[37] DeLoach LD, Payne SA, Chase L, Smith LK, Kway WL, Krupke WF. Evaluation of absorption and emission properties of Yb^{3+} doped crystals for laser applications. IEEE J Quantum Elect 1993;29:1179–91.
[38] Li L, Liu Y, Tao J, Zhang M, Pan H, Xu X, et al. Surface modification of hydroxyapatite nanocrystallite by a small amount of terbium provides a biocompatible fluorescent probe. J Phys Chem C 2008;112:12219–24.
[39] Bouhaouss A, Bensaoud A, Laghzizil A, Ferhat M. Effect of chemical treatments on the ionic conductivity of carbonate apatite. Int J Inorg Mater 2001;3:437–41.
[40] Mahabole M, Aiyer R, Ramakrishna C, Sreedhar B, Khairnar R. Synthesis, characterization and gas sensing property of hydroxyapatite ceramic. Bull Mater Sci 2005;28:535–45.
[41] Jungbauer A, Hahn R, Deinhofer K, Luo P. Performance and characterization of a nanophased porous hydroxyapatite for protein chromatography. Biotechnol Bioeng 2004;87:364–75.
[42] Purdy K, Embley T, Takii S, Nedwell D. Rapid extraction of DNA and rRNA from sediments by a novel hydroxyapatite spin-column method. Appl Environ Microbiol 1996;62:3905–7.
[43] Lin K, Pan J, Chen Y, Cheng R, Xu X. Study the adsorption of phenol from aqueous solution on hydroxyapatite nanopowders. J Hazard Mater 2009;161:231–40.
[44] Hashimoto Y, Taki T, Sato T. Sorption of dissolved lead from shooting range soils using hydroxyapatite amendments synthesized from industrial byproducts as affected by varying pH conditions. J Environ Manag 2009;90:1782–9.
[45] Sadat-Shojai M. Hydroxyapatite: inorganic nanoparticles of bone (properties, applications, and preparation methodologies). Tehran: Iranian Students Book Agency (ISBA); 2010 (in Persian).
[46] Cai Y, Liu Y, Yan W, Hu Q, Tao J, Zhang M, et al. Role of hydroxyapatite nanoparticle size in bone cell proliferation. J Mater Chem 2007;17:3780–7.
[47] Wang Y, Liu L, Guo S. Characterization of biodegradable and cytocompatible nano-hydroxyapatite/polycaprolactone porous scaffolds in degradation in vitro. Polym Degrad Stab 2010;95:207–13.
[48] Dong Z, Li Y, Zou Q. Degradation and biocompatibility of porous nano-hydroxyapatite/polyurethane composite scaffold for bone tissue engineering. Appl Surf Sci 2009;255:6087–91.
[49] Dorozhkin SV. Nanosized and nanocrystalline calcium orthophosphates. Acta Biomater 2010;6:715–34.
[50] Wang L, Nancollas GH. Pathways to biomineralization and biodemineralization of calcium phosphates: the thermodynamic and kinetic controls. Dalton Trans 2009:2665–72.
[51] Eriksson M, Liu Y, Hu J, Gao L, Nygren M, Shen Z. Transparent hydroxyapatite ceramics with nanograin structure prepared by high pressure spark plasma sintering at the minimized sintering temperature. J Eur Ceram Soc 2011;31:1533–40.
[52] Bose S, Banerjee A, Dasgupta S, Bandyopadhyay A. Synthesis, processing, mechanical, and biological property. Characterization of hydroxyapatite whisker-reinforced hydroxyapatite composites. J Am Ceram Soc 2009;92:323–30.
[53] Bose S, Dasgupta S, Tarafder S, Bandyopadhyay A. Microwave-processed nanocrystalline hydroxyapatite: simultaneous enhancement of mechanical and biological properties. Acta Biomater 2010;6:3782–90.
[54] Bianco A, Cacciotti I, Lombardi M, Montanaro L. Si-substituted hydroxyapatite nanopowders: synthesis, thermal stability and sinterability. Mater Res Bull 2009;44:345–54.
[55] Li B, Guo B, Fan H, Zhang X. Preparation of nano-hydroxyapatite particles with different morphology and their response to highly malignant melanoma cells in vitro. Appl Surf Sci 2008;255:357–60.
[56] Webster TJ, Ergun C, Doremus RH, Siegel RW, Bizios R. Enhanced osteoclast-like cell functions on nanophase ceramics. Biomaterials 2001;22:1327–33.
[57] Rusu VM, Ng CH, Wilke M, Tiersch B, Fratzl P, Peter MG. Size-controlled hydroxyapatite nanoparticles as self-organized organic–inorganic composite materials. Biomaterials 2005;26:5414–26.
[58] Song J, Saiz E, Bertozzi CR. A new approach to mineralization of biocompatible hydrogel scaffolds: an efficient process toward 3-dimensional bonelike composites. J Am Chem Soc 2003;125:1236–43.
[59] Koutsopoulos S. Synthesis and characterization of hydroxyapatite crystals: a review study on the analytical methods. J Biomed Mater Res 2002;62:600–12.
[60] Carrodeguas R, De Aza S. α-Tricalcium phosphate: synthesis, properties and biomedical applications. Acta Biomater 2011;7:3536–46.
[61] Kweh S, Khor K, Cheang P. The production and characterization of hydroxyapatite (HA) powders. J Mater Proc Technol 1999;89:373–7.
[62] Itatani K, Iwafune K, Howell FS, Aizawa M. Preparation of various calcium-phosphate powders by ultrasonic spray freeze-drying technique. Mater Res Bull 2000;35:575–85.

[63] Doremus R. Bioceramics. J Mater Sci 1992;27:285–97.
[64] Orlovskii V, Komlev V, Barinov S. Hydroxyapatite and hydroxyapatite-based ceramics. Inorg Mater 2002;38:973–84.
[65] Ferraz M, Monteiro F, Manuel C. Hydroxyapatite nanoparticles: a review of preparation methodologies. J Appl Biomater Biomech 2004;2:74–80.
[66] Norton J, Malik K, Darr J, Rehman I. Recent developments in processing and surface modification of hydroxyapatite. Adv Appl Ceram 2006;105:113–39.
[67] Murugan R, Ramakrishna S. Development of cell-responsive nanophase hydroxyapatite for tissue engineering. Am J Biochem Biotechnol 2007;3:118–24.
[68] Wang L, Nancollas GH. Calcium orthophosphates: crystallization and dissolution. Chem Rev 2008;108:4628–69.
[69] Zhou H, Lee J. Nanoscale hydroxyapatite particles for bone tissue engineering. Acta Biomater 2011;7:2769–81.
[70] Xu J, Khor KA, Sui J, Zhang J, Chen W. Protein expression profiles in osteoblasts in response to differentially shaped hydroxyapatite nanoparticles. Biomaterials 2009;30:5385–91.
[71] Lugscheider E, Knepper M, Gross K. Production of spherical apatite powders – the first step for optimized thermal-sprayed apatite coatings. J Therm Spray Technol 1992;1:215–21.
[72] Wang A, Lu Y, Zhu R, Li S, Ma X. Effect of process parameters on the performance of spray dried hydroxyapatite microspheres. Powder Technol 2009;191:1–6.
[73] Sun R, Lu Y, Chen K. Preparation and characterization of hollow hydroxyapatite microspheres by spray drying method. Mater Sci Eng C 2009;29:1088–92.
[74] Cheang P, Khor K. Effect of particulate morphology on the tensile behaviour of polymer–hydroxyapatite composites. Mater Sci Eng A 2003;345:47–54.
[75] Bakar A, Cheng M, Tang S, Yu S, Liao K, Tan C, et al. Tensile properties, tension–tension fatigue and biological response of polyetheretherketone hydroxyapatite composites for load-bearing orthopedic implants. Biomaterials 2003;24:2245–50.
[76] Dorozhkin SV. Calcium orthophosphate-based biocomposites and hybrid biomaterials. J Mater Sci 2009;44:2343–87.
[77] Aldrich DS, Smith MA. Pharmaceutical applications of infrared microspectroscopy. In: Humeki HJ, editor. Practical guide to infrared microspectroscopy. New York: Marcel Dekker, Inc.; 1995.
[78] Pramanik S, Agarwal AK, Rai K, Garg A. Development of high strength hydroxyapatite by solid-state-sintering process. Ceram Int 2007;33:419–26.
[79] Zhang HG, Zhu Q. Preparation of fluoride-substituted hydroxyapatite by a molten salt synthesis route. J Mater Sci: Mater Med 2006;17:691–5.
[80] Teshima K, Lee SH, Sakurai M, Kameno Y, Yubuta K, Suzuki T, et al. Well-formed one-dimensional hydroxyapatite crystals grown by an environmentally friendly flux method. Cryst Growth Des 2009;9:2937–40.
[81] Taş AC. Molten salt synthesis of calcium hydroxyapatite whiskers. J Am Ceram Soc 2001;84:295–300.
[82] Tseng YH, Kuo CS, Li YY, Huang CP. Polymer-assisted synthesis of hydroxyapatite nanoparticle. Mater Sci Eng C 2009;29:819–22.
[83] Silva C, Graça MPF, Valente M, Sombra ASB. Crystallite size study of nanocrystalline hydroxyapatite and ceramic system with titanium oxide obtained by dry ball milling. J Mater Sci 2007;42:3851–5.
[84] Fahami A, Ebrahimi-Kahrizsangi R, Nasiri-Tabrizi B. Mechanochemical synthesis of hydroxyapatite/titanium nanocomposite. Solid State Sci 2011;13:135–41.
[85] Mochales C, Wilson RM, Dowker SEP, Ginebra MP. Dry mechanosynthesis of nanocrystalline calcium deficient hydroxyapatite: structural characterisation. J Alloys Compd 2011;509:7389–94.
[86] Nasiri-Tabrizi B, Honarmandi P, Ebrahimi-Kahrizsangi R. Synthesis of nanosize single-crystal hydroxyapatite via mechanochemical method. Mater Lett 2009;63:543–6.
[87] Fathi M, Zahrani EM. Mechanochemical synthesis of fluoridated hydroxyapatite nanopowder. Int J Mod Phys B 2008;22:3099–106.
[88] Silva C, Pinheiro A, De Oliveira R, Goes J, Aranha N, De Oliveira L, et al. Properties and in vivo investigation of nanocrystalline hydroxyapatite obtained by mechanical alloying. Mater Sci Eng C 2004;24:549–54.
[89] El Briak-BenAbdeslam H, Ginebra M, Vert M, Boudeville P. Wet or dry mechanochemical synthesis of calcium phosphates? Influence of the water content on DCPD–CaO reaction kinetics. Acta Biomater 2008;4:378–86.
[90] Fathi M, Mohammadi Zahrani E. Mechanical alloying synthesis and bioactivity evaluation of nanocrystalline fluoridated hydroxyapatite. J Cryst Growth 2009;311:1392–403.
[91] Yeong B, Junmin X, Wang J. Mechanochemical synthesis of hydroxyapatite from calcium oxide and brushite. J Am Ceram Soc 2004;84:465–7.
[92] Honarmandi P, Shokuhfar A, Nasiri-Tabrizi B, Ebrahimi-Kahrizsangi R. Milling media effects on synthesis, morphology and structural characteristics of single crystal hydroxyapatite nanoparticles. Adv Appl Ceram 2010;109:117–22.
[93] Kim W, Zhang Q, Saito F. Mechanochemical synthesis of hydroxyapatite from $Ca(OH)_2$–P_2O_5 and CaO–$Ca(OH)_2$–P_2O_5 mixtures. J Mater Sci 2000;35:5401–5.
[94] Silva C, Pinheiro A, Miranda M, Góes J, Sombra A. Structural properties of hydroxyapatite obtained by mechanosynthesis. Solid State Sci 2003;5:553–8.
[95] Yeong K, Wang J, Ng S. Mechanochemical synthesis of nanocrystalline hydroxyapatite from CaO and $CaHPO_4$. Biomaterials 2001;22:2705–12.
[96] Krajewski A, Celotti G, Ravaglioli A, Toriyama M. Spectrometric study of the thermal evolution of mechanochemically prepared hydroxyapatite-based powders. Cryst Res Technol 1996;31:637–46.
[97] Fathi M, Zahrani EM. Fabrication and characterization of fluoridated hydroxyapatite nanopowders via mechanical alloying. J Alloys Compd 2009;475:408–14.
[98] Zhan J, Tseng YH, Chan JCC, Mou CY. Biomimetic formation of hydroxyapatite nanorods by a single-crystal-to-single-crystal transformation. Adv Funct Mater 2005;15:2005–10.
[99] Kim DW, Cho IS, Kim JY, Jang HL, Han GS, Ryu HS, et al. Simple large-scale synthesis of hydroxyapatite nanoparticles: in situ observation of crystallization process. Langmuir 2009;26:384–8.
[100] Koutsopoulos S, Barlos K, Gatos D, Dalas E. The effect of various Prothymosin α fragments on the crystal growth of hydroxyapatite in aqueous solution. J Cryst Growth 2004;267:306–11.
[101] Zhang Y, Zhou L, Li D, Xue N, Xu X, Li J. Oriented nano-structured hydroxyapatite from the template. Chem Phys Lett 2003;376:493–7.
[102] Hongquan Z, Yuhua Y, Youfa W, Shipu L. Morphology and formation mechanism of hydroxyapatite whiskers from moderately acid solution. Mater Res 2003;6:111–5.
[103] Ikoma T, Yamazaki A, Nakamura S, Akao M. Preparation and structure refinement of monoclinic hydroxyapatite. J Solid State Chem 1999;144:272–6.
[104] Catros S, Guillemot F, Lebraud E, Chanseau C, Perez S, Bareille R, et al. Physico-chemical and biological properties of a nano-hydroxyapatite powder synthesized at room temperature. IRBM 2010;31:226–33.
[105] Zhang Y, Lu J. A mild and efficient biomimetic synthesis of rodlike hydroxyapatite particles with a high aspect ratio using polyvinylpyrrolidone as capping agent. Cryst Growth Des 2008;8:2101–7.
[106] Zhang Y, Lu J. The transformation of single-crystal calcium phosphate ribbon-like fibres to hydroxyapatite spheres assembled from nanorods. Nanotechnology 2008;19:155608.
[107] Tao J, Jiang W, Pan H, Xu X, Tang R. Preparation of large-sized hydroxyapatite single crystals using homogeneous releasing controls. J Cryst Growth 2007;308:151–8.
[108] Pang Y, Bao X. Influence of temperature, ripening time and calcination on the morphology and crystallinity of hydroxyapatite nanoparticles. J Eur Ceram Soc 2003;23:1697–704.
[109] Lazić S, Zec S, Miljević N, Milonjić S. The effect of temperature on the properties of hydroxyapatite precipitated from calcium hydroxide and phosphoric acid. Thermochim Acta 2001;374:13–22.
[110] Huang YT, Imura M, Nemoto Y, Cheng CH, Yamauchi Y. Block-copolymer-assisted synthesis of hydroxyapatite nanoparticles with high surface area and uniform size. Sci Technol Adv Mater 2011;12:045005 (6pp).
[111] Wang F, Li MS, Lu YP, Qi YX, Liu YX. Synthesis and microstructure of hydroxyapatite nanofibers synthesized at 37 °C. Mater Chem Phys 2006;95:145–9.
[112] Feng W, Mu-Sen L, Yu-Peng L, Sheng-Song G. Synthesis of nanocrystalline hydroxyapatite powders in stimulated body fluid. J Mater Sci 2005;40:2073–6.
[113] Ebrahimpour A, Johnsson M, Richardson CF, Nancollas GH. The characterization of hydroxyapatite preparations. J Colloid Interface Sci 1993;159:158–63.
[114] Swain S, Sarkar D. A comparative study: hydroxyapatite spherical nanopowders and elongated nanorods. Ceram Int 2011;37:2927–30.
[115] Afshar A, Ghorbani M, Ehsani N, Saeri M, Sorrell C. Some important factors in the wet precipitation process of hydroxyapatite. Mater Design 2003;24:197–202.
[116] Kong L, Ma J, Boey F. Nanosized hydroxyapatite powders derived from coprecipitation process. J Mater Sci 2002;37:1131–4.
[117] Sadat-Shojai M, Khorasani MT, Jamshidi A, Irani S. Nano-hydroxyapatite reinforced polyhydroxybutyrate composites: a comprehensive study on the structural and in vitro biological properties. Mater Sci Eng C 2013;33:2776–87.
[118] Gomez-Morales J, Torrent-Burgues J, Boix T, Fraile J, Rodriguez-Clemente R. Precipitation of stoichiometric hydroxyapatite by a continuous method. Cryst Res Technol 2001;36:15–26.
[119] Fomin A, Barinov S, Ievlev V, Smirnov V, Mikhailov B, Kutsev S, et al. Nanocrystalline hydroxyapatite ceramics. Inorg Mater 2009;45:1193–6.
[120] Paz A, Guadarrama D, López M, González JE, Brizuela N, Aragón J. A comparative study of hydroxyapatite nanoparticles synthesized by different routes. Quím Nova 2012;35:1724–7.
[121] Gibson IR, Bonfield W. Novel synthesis and characterization of an AB-type carbonate-substituted hydroxyapatite. J Biomed Mater Res 2001;59:697–708.
[122] Verwilghen C, Chkir M, Rio S, Nzihou A, Sharrock P, Depelsenaire G. Convenient conversion of calcium carbonate to hydroxyapatite at ambient pressure. Mater Sci Eng C 2009;29:771–3.
[123] Kumta PN, Sfeir C, Lee DH, Olton D, Choi D. Nanostructured calcium phosphates for biomedical applications: novel synthesis and characterization. Acta Biomater 2005;1:65–83.
[124] Zhang HG, Zhu Q. Surfactant-assisted preparation of fluoride-substituted hydroxyapatite nanorods. Mater Lett 2005;59:3054–8.
[125] Palazzo B, Walsh D, Iafisco M, Foresti E, Bertinetti L, Martra G, et al. Amino acid synergetic effect on structure, morphology and surface properties of biomimetic apatite nanocrystals. Acta Biomater 2009;5:1241–52.
[126] Liou SC, Chen SY, Lee HY, Bow JS. Structural characterization of nano-sized calcium deficient apatite powders. Biomaterials 2004;25:189–96.

[127] Iafisco M, Delgado-López J, Gómez-Morales J, Hernández-Hernández M, Rodríguez-Ruiz I, Roveri N. Formation of calcium phosphates by vapour diffusion in highly concentrated ionic micro-droplets. Cryst Res Technol 2011;46:841–6.
[128] Liu C, Huang Y, Shen W, Cui J. Kinetics of hydroxyapatite precipitation at pH 10 to 11. Biomaterials 2001;22:301–6.
[129] Zhang Y, Lu J. A simple method to tailor spherical nanocrystal hydroxyapatite at low temperature. J Nanopart Res 2007;9:589–94.
[130] Okada M, Furuzono T. Calcination of rod-like hydroxyapatite nanocrystals with an anti-sintering agent surrounding the crystals. J Nanopart Res 2007;9:807–15.
[131] Koumoulidis GC, Vaimakis TC, Sdoukos AT, Boukos NK, Trapalis CC. Preparation of hydroxyapatite lathlike particles using high-speed dispersing equipment. J Am Ceram Soc 2004;84:1203–8.
[132] Chen H, Clarkson BH, Sun K, Mansfield JF. Self-assembly of synthetic hydroxyapatite nanorods into an enamel prism-like structure. J Colloid Interface Sci 2005;288:97–103.
[133] Wang J, Shaw LL. Morphology-enhanced low-temperature sintering of nanocrystalline hydroxyapatite. Adv Mater 2007;19:2364–9.
[134] Zhang H, Yan Y, Wang Y, Li S. Thermal stability of hydroxyapatite whiskers prepared by homogenous precipitation. Adv Eng Mater 2002;4:916–9.
[135] Liu Y, Nancollas GH. Crystallization and colloidal stability of calcium phosphate phases. J Phys Chem B 1997;101:3464–8.
[136] Song J, Liu Y, Zhang Y, Jiao L. Mechanical properties of hydroxyapatite ceramics sintered from powders with different morphologies. Mater Sci Eng A 2011;528:5421–7.
[137] Cai Y, Mei D, Jiang T, Yao J. Synthesis of oriented hydroxyapatite crystals: effect of reaction conditions in the presence or absence of silk sericin. Mater Lett 2010;64:2676–8.
[138] Shanthi P, Mangalaraja R, Uthirakumar A, Velmathi S, Balasubramanian T, Ashok M. Synthesis and characterization of porous shell-like nano hydroxyapatite using Cetrimide as template. J Colloid Interface Sci 2010;350:39–43.
[139] Ye F, Guo H, Zhang H, He X. Polymeric micelle-templated synthesis of hydroxyapatite hollow nanoparticles for a drug delivery system. Acta Biomater 2010;6:2212–8.
[140] Ye F, Guo H, Zhang H. Biomimetic synthesis of oriented hydroxyapatite mediated by nonionic surfactants. Nanotechnology 2008;19:245605 [7pp].
[141] Qiu C, Xiao X, Liu R, She H. Biomimetic synthesis of spherical nano-hydroxyapatite with polyvinylpyrrolidone as template. Mater Sci Technol 2008;24:612–7.
[142] He D, Xiao X, Liu F, Liu R. Hydroxyapatite nanospindles by biomimetic synthesis with chitosan as template. Mater Sci Technol 2007;23:1228–32.
[143] Liu C, Ji X, Cheng G. Template synthesis and characterization of highly ordered lamellar hydroxyapatite. Appl Surf Sci 2007;253:6840–3.
[144] Uota M, Arakawa H, Kitamura N, Yoshimura T, Tanaka J, Kijima T. Synthesis of high surface area hydroxyapatite nanoparticles by mixed surfactant-mediated approach. Langmuir 2005;21:4724–8.
[145] Wu Y, Bose S. Nanocrystalline hydroxyapatite: micelle templated synthesis and characterization. Langmuir 2005;21:3232–4.
[146] Rhee SH, Tanaka J. Effect of chondroitin sulfate on the crystal growth of hydroxyapatite. J Am Ceram Soc 2000;83:2100–2.
[147] Wei G, Reichert J, Bossert J, Jandt KD. Novel biopolymeric template for the nucleation and growth of hydroxyapatite crystals based on self-assembled fibrinogen fibrils. Biomacromolecules 2008;9:3258–67.
[148] Song RQ, Cölfen H. Additive controlled crystallization. CrystEngComm 2011;13:1249–76.
[149] Peytcheva A, Cölfen H, Schnablegger H, Antonietti M. Calcium phosphate colloids with hierarchical structure controlled by polyaspartates. Colloid Polym Sci 2002;280:218–27.
[150] Schweizer S, Taubert A. Polymer-controlled, bio-inspired calcium phosphate mineralization from aqueous solution. Macromol Biosci 2007;7:1085–99.
[151] Antonietti M, Breulmann M, Göltner CG, Cölfen H, Wong KKW, Walsh D, et al. Inorganic/organic mesostructures with complex architectures: precipitation of calcium phosphate in the presence of double-hydrophilic block copolymers. Chem Eur J 1999;4:2493–500.
[152] Sl Shanthi PM, Ashok M, Balasubramanian T, Riyasdeen A, Akbarsha M. Synthesis and characterization of nano-hydroxyapatite at ambient temperature using cationic surfactant. Mater Lett 2009;63:2123–5.
[153] Yao J, Tjandra W, Chen YZ, Tam KC, Ma J, Soh B. Hydroxyapatite nanostructure material derived using cationic surfactant as a template. J Mater Chem 2003;13:3053–7.
[154] Liu Y, Hou D, Wang G. A simple wet chemical synthesis and characterization of hydroxyapatite nanorods. Mater Chem Phys 2004;86:69–73.
[155] Liu Y, Wang W, Zhan Y, Zheng C, Wang G. A simple route to hydroxyapatite nanofibers. Mater Lett 2002;56:496–501.
[156] Xiao F, Ye J, Wang Y, Rao P. Deagglomeration of HA during the precipitation synthesis. J Mater Sci 2005;40:5439–42.
[157] Qiu C, Xiao X, Liu R. Biomimetic synthesis of spherical nano-hydroxyapatite in the presence of polyethylene glycol. Ceram Int 2008;34:1747–51.
[158] Shkilnyy A, Brandt J, Mantion A, Paris O, Schlaad H, Taubert A. Calcium phosphate with a channel-like morphology by polymer templating. Chem Mater 2009;21:1572–8.
[159] Li C, Zhao L, Han J, Wang R, Xiong C, Xie X. Synthesis of citrate-stabilized hydrocolloids of hydroxyapatite through a novel two-stage method: a possible aggregates-breakdown mechanism of colloid formation. J Colloid Interface Sci 2011;360:341–9.
[160] Safronova T, Putlyaev V, Sergeeva A, Kunenkov E, Tret'yakov YD. Synthesis of nanocrystalline calcium hydroxyapatite from calcium saccharates and ammonium hydrogen phosphate. Dokl Chem 2009;426:118–23.
[161] Tan J, Chen M, Xia J. Water-dispersible hydroxyapatite nanorods synthesized by a facile method. Appl Surf Sci 2009;255:8774–9.
[162] Li C. Crystalline behaviors of hydroxyapatite in the neutralized reaction with different citrate additions. Powder Technol 2009;192:1–5.
[163] Lee SC, Choi HW, Lee HJ, Kim KJ, Chang JH, Kim SY, et al. In-situ synthesis of reactive hydroxyapatite nano-crystals for a novel approach of surface grafting polymerization. J Mater Chem 2007;17:174–80.
[164] Gonzalez-McQuire R, Chane-Ching JY, Vignaud E, Lebugle A, Mann S. Synthesis and characterization of amino acid-functionalized hydroxyapatite nanorods. J Mater Chem 2004;14:2277–81.
[165] Pena J, Vallet-Regı M. Hydroxyapatite, tricalcium phosphate and biphasic materials prepared by a liquid mix technique. J Eur Ceram Soc 2003;23:1687–96.
[166] Koutsopoulos S, Dalas E. The crystallization of hydroxyapatite in the presence of lysine. J Colloid Interface Sci 2000;231:207–12.
[167] Koutsopoulos S, Dalas E, Klouras N. Inhibition of hydroxyapatite crystal growth by substituted titanocenes. Langmuir 2000;16:6745–9.
[168] Koutsopoulos S, Dalas E. The effect of acidic amino acids on hydroxyapatite crystallization. J Cryst Growth 2000;217:410–5.
[169] Koutsopoulos S, Dalas E. Inhibition of hydroxyapatite formation in aqueous solutions by amino acids with hydrophobic side groups. Langmuir 2000;16:6739–44.
[170] Rosseeva E, Golovanova O, Frank-Kamenetskaya O. The influence of amino acids on the formation of nanocrystalline hydroxyapatite. Glass Phys Chem 2007;33:283–6.
[171] Hu YY, Liu X, Ma X, Rawal A, Prozorov T, Akinc M, et al. Biomimetic self-assembling copolymer–hydroxyapatite nanocomposites with the nanocrystal size controlled by citrate. Chem Mater 2011;23:2481–90.
[172] Li C, Meng F. Nano-crystallinite hydroxyapatite synthesized by neutralization with the assist of citric acid. Mater Lett 2008;62:932–4.
[173] Martins MA, Santos C, Almeida MM, Costa MEV. Hydroxyapatite micro-and nanoparticles: nucleation and growth mechanisms in the presence of citrate species. J Colloid Interface Sci 2008;318:210–6.
[174] Chen C, Li J, Huang Z, Cheng X, Yu J, Wang H, et al. Phase transformation process and step growth mechanism of hydroxyapatite whiskers under constant impulsion system. J Cryst Growth 2011;327:154–60.
[175] Cheng X, Huang Z, Li J, Liu Y, Chen C, Chi R, et al. Self-assembled growth and pore size control of the bubble-template porous carbonated hydroxyapatite microsphere. Cryst Growth Des 2010;10:1180–8.
[176] He QJ, Huang ZL. Template-directed growth and characterization of flowerlike porous carbonated hydroxyapatite spheres. Cryst Res Technol 2007;42:460–5.
[177] Jokic B, Tanaskovic D, Jankovic-Castvan I, Drmanic S, Petrovic R, Janackovic D. Synthesis of nanosized calcium hydroxyapatite particles by the catalytic decomposition of urea with urease. J Mater Res 2007;22:1156–61.
[178] Wang Y, Yan Y, Li M, Jiang X. Nfluential factors on morphology of hydroxyapatite crystals. J Wuhan Univ Technol 2003;18:33–6.
[179] Wang YF, Yan YH, Dai HL, Li MJ. Preparation of hydroxyapatite fibers by the homogeneous precipitation method. J Wuhan Univ Technol 2002;17:39–41.
[180] Bayraktar D, Tas A. Formation of hydroxyapatite precursors at 37 °C in urea- and enzyme urease-containing body fluids. J Mater Sci Lett 2001;20:401–3.
[181] Bayraktar D, Tas AC. Chemical preparation of carbonated calcium hydroxyapatite powders at 37 °C in urea-containing synthetic body fluids. J Eur Ceram Soc 1999;19:2573–9.
[182] Zhang Y, Lu J, Wang J, Yang S, Chen Y. Synthesis of nanorod and needle-like hydroxyapatite crystal and role of pH adjustment. J Cryst Growth 2009;311:4740–6.
[183] Sadat-Shojai M, Atai M, Nodehi A. Design of experiments (DOE) for the optimization of hydrothermal synthesis of hydroxyapatite nanoparticles. J Braz Chem Soc 2011;22:571–82.
[184] Kandori K, Kuroda T, Togashi S, Katayama E. Preparation of calcium hydroxyapatite nanoparticles using microreactor and their characteristics of protein adsorption. J Phys Chem B 2010;115:653–9.
[185] Gopi D, Bhalaji P, Prakash V, Ramasamy A, Kavitha L, Ferreira J. An effective and facile synthesis of hydroxyapatite powders using oxalic acid–ethylene glycol mixture. Curr Appl Phys 2011;11:590–3.
[186] El Hammari L, Merroun H, Coradin T, Cassaignon S, Laghzizil A, Saoiabi A. Mesoporous hydroxyapatites prepared in ethanol–water media: structure and surface properties. Mater Chem Phys 2007;104:448–53.
[187] Mobasherpour I, Heshajin MS, Kazemzadeh A, Zakeri M. Synthesis of nanocrystalline hydroxyapatite by using precipitation method. J Alloys Compd 2007;430:330–3.
[188] Koumoulidis G, Trapalis C, Vaimakis T. Sintering of hydroxyapatite lath-like powders. J Therm Anal Calorim 2006;84:165–74.
[189] Li Z, Wang P, Wu Z. Preparation of nanosized hydroxyapatite particles at low temperatures. J Mater Sci 2005;40:6589–91.
[190] Yarosh E, Dmitrevskii B, Naryzhnyi V, Tsvetkov S. Some characteristics of synthetic hydroxyapatite. Russ J Appl Chem 2001;74:1058–60.
[191] Rodriguez-Lorenzo L, Vallet-Regi M. Controlled crystallization of calcium phosphate apatites. Chem Mater 2000;12:2460–5.

[192] Suvorova E, Buffat P. Electron diffraction and high-resolution transmission electron microscopy in the characterization of calcium phosphate precipitation from aqueous solutions under biomineralization conditions. Eur Cells Mater 2001;1:27–42.
[193] Wang P, Li C, Gong H, Jiang X, Wang H, Li K. Effects of synthesis conditions on the morphology of hydroxyapatite nanoparticles produced by wet chemical process. Powder Technol 2010;203:315–21.
[194] Graham S, Brown PW. Reactions of octacalcium phosphate to form hydroxyapatite. J Cryst Growth 1996;165:106–15.
[195] Pieters IY, De Maeyer EAP, Verbeeck RMH. Influence of Na^+ on the stoichiometry of carbonated hydroxyapatite obtained by the hydrolysis of octacalcium phosphate. Inorg Chem 1998;37:6392–5.
[196] Sturgeon JL, Brown PW. Effects of carbonate on hydroxyapatite formed from $CaHPO_4$ and $Ca_4(PO_4)_2O$. J Mater Sci: Mater Med 2009;20:1787–94.
[197] Park H, Baek D, Park Y, Yoon S, Stevens R. Thermal stability of hydroxyapatite whiskers derived from the hydrolysis of α-TCP. J Mater Sci 2004;39:2531–4.
[198] Sakamoto K, Yamaguchi S, Nakahira A, Kaneno M, Okazaki M, Ichihara J, et al. Shape-controlled synthesis of hydroxyapatite from α-tricalcium bis(orthophosphate) in organic-aqueous binary systems. J Mater Sci 2002;37:1033–41.
[199] Durucan C, Brown P. α-Tricalcium phosphate hydrolysis to hydroxyapatite at and near physiological temperature. J Mater Sci: Mater Med 2000;11:365–71.
[200] Nakahira A, Sakamoto K, Yamaguchi S, Kaneno M, Takeda S, Okazaki M, et al. Novel synthesis method of hydroxyapatite whiskers by hydrolysis of α-tricalcium phosphate in mixtures of water and organic solvent. J Am Ceram Soc 1999;82:2029–32.
[201] Ito H, Oaki Y, Imai H. Selective synthesis of various nanoscale morphologies of hydroxyapatite via an intermediate phase. Cryst Growth Des 2008;8:1055–9.
[202] Shih WJ, Wang MC, Hon MH. Morphology and crystallinity of the nanosized hydroxyapatite synthesized by hydrolysis using cetyltrimethylammonium bromide (CTAB) as a surfactant. J Cryst Growth 2005;275:e2339–44.
[203] Shih WJ, Chen YF, Wang MC, Hon MH. Crystal growth and morphology of the nano-sized hydroxyapatite powders synthesized from $CaHPO_4{\cdot}2H_2O$ and $CaCO_3$ by hydrolysis method. J Cryst Growth 2004;270:211–8.
[204] Morgan H, Wilson R, Elliott J, Dowker S, Anderson P. Preparation and characterisation of monoclinic hydroxyapatite and its precipitated carbonate apatite intermediate. Biomaterials 2000;21:617–27.
[205] Štulajterová R, Medvecký Ľ. Effect of calcium ions on transformation brushite to hydroxyapatite in aqueous solutions. Colloid Surface A 2008;316:104–9.
[206] Fulmer M, Brown P. Hydrolysis of dicalcium phosphate dihydrate to hydroxyapatite. J Mater Sci: Mater Med 1998;9:197–202.
[207] Monma H, Kamiya T. Preparation of hydroxyapatite by the hydrolysis of brushite. J Mater Sci 1987;22:4247–50.
[208] Seo DS, Lee JK. Synthesis of hydroxyapatite whiskers through dissolution–reprecipitation process using EDTA. J Cryst Growth 2008;310:2162–7.
[209] TenHuisen KS, Brown PW. Formation of calcium-deficient hydroxyapatite from α-tricalcium phosphate. Biomaterials 1998;19:2209–17.
[210] Padmanabhan SK, Balakrishnan A, Chu MC, Lee YJ, Kim TN, Cho SJ. Sol–gel synthesis and characterization of hydroxyapatite nanorods. Particuology 2009;7:466–70.
[211] Sanosh K, Chu MC, Balakrishnan A, Lee YJ, Kim T, Cho SJ. Synthesis of nano hydroxyapatite powder that simulate teeth particle morphology and composition. Curr Appl Phys 2009;9:1459–62.
[212] Ramanan SR, Venkatesh R. A study of hydroxyapatite fibers prepared via sol–gel route. Mater Lett 2004;58:3320–3.
[213] Anee T, Ashok M, Palanichamy M, Narayana Kalkura S. A novel technique to synthesize hydroxyapatite at low temperature. Mater Chem Phys 2003;80:725–30.
[214] Bose S, Saha SK. Synthesis of hydroxyapatite nanopowders via sucrose-templated sol–gel method. J Am Ceram Soc 2004;86:1055–7.
[215] Montero M, Sáenz A, Castaño V. Synthesis of nano-hydroxyapatite from silica suspensions through chemical compensation. J Exp Nanosci 2009;4:193–202.
[216] Ruban Kumar A, Kalainathan S. Sol–gel synthesis of nanostructured hydroxyapatite powder in presence of polyethylene glycol. Phys B Condens Matter 2010;405:2799–802.
[217] Sanosh K, Chu MC, Balakrishnan A, Kim T, Cho SJ. Preparation and characterization of nano-hydroxyapatite powder using sol–gel technique. Bull Mater Sci 2009;32:465–70.
[218] Bigi A, Boanini E, Rubini K. Hydroxyapatite gels and nanocrystals prepared through a sol–gel process. J Solid State Chem 2004;177:3092–8.
[219] Kuriakose TA, Kalkura SN, Palanichamy M, Arivuoli D, Dierks K, Bocelli G, et al. Synthesis of stoichiometric nano crystalline hydroxyapatite by ethanol-based sol–gel technique at low temperature. J Cryst Growth 2004;263:517–23.
[220] Bezzi G, Celotti G, Landi E, La Torretta T, Sopyan I, Tampieri A. A novel sol–gel technique for hydroxyapatite preparation. Mater Chem Phys 2003;78:816–24.
[221] Fathi M, Hanifi A, Mortazavi V. Preparation and bioactivity evaluation of bone-like hydroxyapatite nanopowder. J Mater Process Tech 2008;202:536–42.
[222] Eshtiagh-Hosseini H, Housaindokht MR, Chahkandi M. Effects of parameters of sol–gel process on the phase evolution of sol–gel-derived hydroxyapatite. Mater Chem Phys 2007;106:310–6.
[223] Hsieh MF, Perng LH, Chin TS, Perng HG. Phase purity of sol–gel-derived hydroxyapatite ceramic. Biomaterials 2001;22:2601–7.
[224] Jillavenkatesa A, Hoelzer D, Condrate R. An electron microscopy study of the formation of hydroxyapatite through sol–gel processing. J Mater Sci 1999;34:4821–30.
[225] Chen J, Wang Y, Chen X, Ren L, Lai C, He W, et al. A simple sol–gel technique for synthesis of nanostructured hydroxyapatite, tricalcium phosphate and biphasic powders. Mater Lett 2011;65:1923–6.
[226] Montazeri N, Jahandideh R, Biazar E. Synthesis of fluorapatite–hydroxyapatite nanoparticles and toxicity investigations. Int J Nanomedicine 2011;6:197–201.
[227] Ioițescu A, Vlase G, Vlase T, Ilia G, Doca N. Synthesis and characterization of hydroxyapatite obtained from different organic precursors by sol–gel method. J Therm Anal Calorim 2009;96:937–42.
[228] Munguía N, Guzmán Vázquez C, Piña Barba C. Stoichiometric hydroxyapatite obtained by precipitation and sol gel processes. Rev Mex Fis 2005;51:284–93.
[229] Milev A, Kannangara G, Ben-Nissan B. Morphological stability of hydroxyapatite precursor. Mater Lett 2003;57:1960–5.
[230] Liu DM, Yang Q, Troczynski T, Tseng WJ. Structural evolution of sol–gel-derived hydroxyapatite. Biomaterials 2002;23:1679–87.
[231] Hsieh MF, Perng LH, Chin TS. Formation mechanisms of sol–gel-derived hydroxyapatite using different thermal processings. J Sol–Gel Sci Technol 2002;23:205–14.
[232] Liu DM, Troczynski T, Tseng WJ. Water-based sol–gel synthesis of hydroxyapatite: process development. Biomaterials 2001;22:1721–30.
[233] Chai CS, Gross KA, Ben-Nissan B. Critical ageing of hydroxyapatite sol–gel solutions. Biomaterials 1998;19:2291–6.
[234] Rajabi-Zamani A, Behnamghader A, Kazemzadeh A. Synthesis of nanocrystalline carbonated hydroxyapatite powder via nonalkoxide sol–gel method. Mater Sci Eng C 2008;28:1326–9.
[235] Feng W, Mu-Sen L, Yu-Peng L, Yong-Xin Q. A simple sol–gel technique for preparing hydroxyapatite nanopowders. Mater Lett 2005;59:916–9.
[236] Kim IS, Kumta PN. Sol–gel synthesis and characterization of nanostructured hydroxyapatite powder. Mater Sci Eng B 2004;111:232–6.
[237] Cheng K, Weng W, Han G, Du P, Shen G, Yang J, et al. The effect of triethanolamine on the formation of sol–gel derived fluoroapatite/hydroxyapatite solid solution. Mater Chem Phys 2003;78:767–71.
[238] Weng W, Han G, Du P, Shen G. The effect of citric acid addition on the formation of sol–gel derived hydroxyapatite. Mater Chem Phys 2002;74:92–7.
[239] Zhang G, Chen J, Yang S, Yu Q, Wang Z, Zhang Q. Preparation of amino-acid-regulated hydroxyapatite particles by hydrothermal method. Mater Lett 2011;65:572–4.
[240] Jokić B, Mitrić M, Radmilović V, Drmanić S, Petrović R, Janaćković D. Synthesis and characterization of monetite and hydroxyapatite whiskers obtained by a hydrothermal method. Ceram Int 2011;37:167–73.
[241] Cao H, Zhang L, Zheng H, Wang Z. Hydroxyapatite nanocrystals for biomedical applications. J Phys Chem C 2010;114:18352–7.
[242] Zhang H, Darvell BW. Synthesis and characterization of hydroxyapatite whiskers by hydrothermal homogeneous precipitation using acetamide. Acta Biomater 2010;6:3216–22.
[243] Cihlar J, Castkova K. Direct synthesis of nanocrystalline hydroxyapatite by hydrothermal hydrolysis of alkylphosphates. Monatsh Chem 2002;133:761–71.
[244] Ioku K, Yamauchi S, Fujimori H, Goto S, Yoshimura M. Hydrothermal preparation of fibrous apatite and apatite sheet. Solid State Ionics 2002;151:147–50.
[245] Yasukawa A, Matsuura T, Nakajima M, Kandori K, Ishikawa T. Preparation of nonstoichiometric calcium hydroxyapatite using formamide. Mater Res Bull 1999;34:589–601.
[246] Zhu K, Yanagisawa K, Onda A, Kajiyoshi K, Qiu J. Morphology variation of cadmium hydroxyapatite synthesized by high temperature mixing method under hydrothermal conditions. Mater Chem Phys 2009;113:239–43.
[247] Manafi S, Rahimipour M. Synthesis of nanocrystalline hydroxyapatite nanorods via hydrothermal conditions. Chem Eng Technol 2011;34:972–6.
[248] Zhang H, Zhang M. Characterization and thermal behavior of calcium deficient hydroxyapatite whiskers with various Ca/P ratios. Mater Chem Phys 2011;126:642–8.
[249] Guo X, Xiao P, Liu J, Shen Z. Fabrication of nanostructured hydroxyapatite via hydrothermal synthesis and spark plasma sintering. J Am Ceram Soc 2005;88:1026–9.
[250] Neira IS, Guitián F, Taniguchi T, Watanabe T, Yoshimura M. Hydrothermal synthesis of hydroxyapatite whiskers with sharp faceted hexagonal morphology. J Mater Sci 2008;43:2171–8.
[251] Zhang H, Darvell BW. Morphology and structural characteristics of hydroxyapatite whiskers: effect of the initial Ca concentration, Ca/P ratio and pH. Acta Biomater 2011;7:2960–8.
[252] Lee DK, Park JY, Kim MR, Jang DJ. Facile hydrothermal fabrication of hollow hexagonal hydroxyapatite prisms. CrystEngComm 2011;13:5455–9.
[253] Lin K, Liu X, Chang J, Zhu Y. Facile synthesis of hydroxyapatite nanoparticles, nanowires and hollow nano-structured microspheres using similar structured hard-precursors. Nanoscale 2011;3:3052–5.
[254] Tsiourvas D, Tsetsekou A, Kammenou MI, Boukos N. Controlling the formation of hydroxyapatite nanorods with dendrimers. J Am Ceram Soc 2011;94:2023–9.
[255] Xu H, Chen Y, Zhang SF. Synthesis and characterization of microporous hydroxyapatite via hydrothermal method. Synth React Inorg M 2011;41:31–5.

[256] Zhang H, Zhang M. Phase and thermal stability of hydroxyapatite whiskers precipitated using amine additives. Ceram Int 2011;37:279–86.
[257] Du X, Chu Y, Xing S, Dong L. Hydrothermal synthesis of calcium hydroxyapatite nanorods in the presence of PVP. J Mater Sci 2009;44:6273–9.
[258] Kandori K, Takeguchi K, Fukusumi M, Morisada Y. Preparation and characterization of calcium hydroxyapatite and balloon-like calcium phosphate particles from forced hydrolysis of $Ca(OH)_2$ triphosphate solution. Polyhedron 2009;28:3036–42.
[259] Earl J, Wood D, Milne S. Hydrothermal synthesis of hydroxyapatite. Phys: Conf Ser 2006;26:268–71.
[260] Zhang H, Darvell BW. Formation of hydroxyapatite whiskers by hydrothermal homogeneous precipitation using acetamide. J Am Ceram Soc 2011;94:2007–13.
[261] Viswanath B, Ravishankar N. Controlled synthesis of plate-shaped hydroxyapatite and implications for the morphology of the apatite phase in bone. Biomaterials 2008;29:4855–63.
[262] Yoshimura M, Sujaridworakun P, Koh F, Fujiwara T, Pongkao D, Ahniyaz A. Hydrothermal conversion of calcite crystals to hydroxyapatite. Mater Sci Eng C 2004;24:521–5.
[263] Loo SCJ, Siew YE, Ho S, Boey FYC, Ma J. Synthesis and hydrothermal treatment of nanostructured hydroxyapatite of controllable sizes. J Mater Sci: Mater Med 2008;19:1389–97.
[264] Zhu R, Yu R, Yao J, Wang D, Ke J. Morphology control of hydroxyapatite through hydrothermal process. J Alloys Compd 2008;457:555–9.
[265] Sadat-Shojai M, Atai M, Nodehi A, Khanlar LN. Hydroxyapatite nanorods as novel fillers for improving the properties of dental adhesives: synthesis and application. Dent Mater 2010;26:471–82.
[266] Chen JD, Wang YJ, Wei K, Zhang SH, Shi XT. Self-organization of hydroxyapatite nanorods through oriented attachment. Biomaterials 2007;28:2275–80.
[267] Sadat-Shojai M, Khorasani MT, Jamshidi A. Hydrothermal processing of hydroxyapatite nanoparticles – a Taguchi experimental design approach. J Cryst Growth 2012;361:73–84.
[268] Zhang C, Yang J, Quan Z, Yang P, Li C, Hou Z, et al. Hydroxyapatite nano-and microcrystals with multiform morphologies: controllable synthesis and luminescence properties. Cryst Growth Des 2009;9:2725–33.
[269] Zhang H, Zhou K, Li Z, Huang S. Plate-like hydroxyapatite nanoparticles synthesized by the hydrothermal method. J Phys Chem Solids 2009;70:243–8.
[270] Wang A, Yin H, Liu D, Wu H, Wada Y, Ren M, et al. Effects of organic modifiers on the size-controlled synthesis of hydroxyapatite nanorods. Appl Surf Sci 2007;253:3311–6.
[271] Jiang D, Li D, Xie J, Zhu J, Chen M, Lü X, et al. Shape-controlled synthesis of F-substituted hydroxyapatite microcrystals in the presence of Na_2EDTA and citric acid. J Colloid Interface Sci 2010;350:30–8.
[272] Zhang H, Zhou K, Li Z, Huang S, Zhao Y. Morphologies of hydroxyapatite nanoparticles adjusted by organic additives in hydrothermal synthesis. J Cent South Univ Technol 2009;16:871–5.
[273] Lak A, Mazloumi M, Mohajerani M, Kajbafvala A, Zanganeh S, Arami H, et al. Self-assembly of dandelion-like hydroxyapatite nanostructures via hydrothermal method. J Am Ceram Soc 2008;91:3292–7.
[274] Chen H, Sun K, Tang Z, Robert V, Mansfield JF, Czajka-Jakubowska A, et al. Synthesis of fluorapatite nanorods and nanowires by direct precipitation from solution. Cryst Growth Des 2006;6:1504–8.
[275] Arce H, Montero ML, Sáenz A, Castaño VM. Effect of pH and temperature on the formation of hydroxyapatite at low temperatures by decomposition of a Ca–EDTA complex. Polyhedron 2004;23:1897–901.
[276] Aminian A, Solati-Hashjin M, Samadikuchaksaraei A, Bakhshi F, Gorjipour F, Farzadi A, et al. Synthesis of silicon-substituted hydroxyapatite by a hydrothermal method with two different phosphorous sources. Ceram Int 2011;37:1219–29.
[277] Xiao XF, Liu RF, Gao YJ. Hydrothermal preparation of nanocarbonated hydroxyapatite crystallites. Mater Sci Tech 2008;24:1199–203.
[278] Wang A, Yin H, Liu D, Wu H, Ren M, Jiang T, et al. Size-controlled synthesis of hydroxyapatite nanorods in the presence of organic modifiers. Mater Lett 2007;61:2084–8.
[279] Zhou ZH, Zhou PL, Yang SP, Yu XB, Yang LZ. Controllable synthesis of hydroxyapatite nanocrystals via a dendrimer-assisted hydrothermal process. Mater Res Bull 2007;42:1611–8.
[280] Guo X, Xiao P. Effects of solvents on properties of nanocrystalline hydroxyapatite produced from hydrothermal process. J Eur Ceram Soc 2006;26:3383–91.
[281] Mizutani Y, Hattori M, Okuyama M, Kasuga T, Nogami M. Large-sized hydroxyapatite whiskers derived from calcium tripolyphosphate gel. J Eur Ceram Soc 2005;25:3181–5.
[282] Yasukawa A, Yokoyama T, Ishikawa T. Preparation of cadmium hydroxyapatite particles using acetamide. Mater Res Bull 2001;36:775–86.
[283] Li Y, Tjandra W, Tam KC. Synthesis and characterization of nanoporous hydroxyapatite using cationic surfactants as templates. Mater Res Bull 2008;43:2318–26.
[284] Wang X, Zhuang J, Peng Q, Li Y. Liquid–solid–solution synthesis of biomedical hydroxyapatite nanorods. Adv Mater 2006;18:2031–4.
[285] Vázquez-Hernández F, Mendoza-Barrera C, Altuzar V, Meléndez-Lira M, Santana-Aranda M, de la L Olvera M. Synthesis and characterization of hydroxyapatite nanoparticles and their application in protein adsorption. Mater Sci Eng B 2010;174:290–5.
[286] Yan L, Li Y, Deng ZX, Zhuang J, Sun X. Surfactant-assisted hydrothermal synthesis of hydroxyapatite nanorods. Int J Inorg Mater 2001;3:633–7.
[287] Salarian M, Solati-Hashjin M, Shafiei SS, Salarian R, Nemati ZA. Template-directed hydrothermal synthesis of dandelion-like hydroxyapatite in the presence of cetyltrimethylammonium bromide and polyethylene glycol. Ceram Int 2009;35:2563–9.
[288] Zhang F, Zhou ZH, Yang SP, Mao LH, Chen HM, Yu XB. Hydrothermal synthesis of hydroxyapatite nanorods in the presence of anionic starburst dendrimer. Mater Lett 2005;59:1422–5.
[289] Zhu A, Lu Y, Si Y, Dai S. Frabicating hydroxyapatite nanorods using a biomacromolecule template. Appl Surf Sci 2011;257:3174–9.
[290] Murray M, Wang J, Ponton C, Marquis P. An improvement in processing of hydroxyapatite ceramics. J Mater Sci 1995;30:3061–74.
[291] Zhou W, Wang M, Cheung W, Guo B, Jia D. Synthesis of carbonated hydroxyapatite nanospheres through nanoemulsion. J Mater Sci: Mater Med 2008;19:103–10.
[292] Pradeesh T, Sunny M, Varma H, Ramesh P. Preparation of microstructured hydroxyapatite microspheres using oil in water emulsions. Bull Mater Sci 2005;28:383–90.
[293] Wei K, Wang Y, Lai C, Ning C, Wu D, Wu G, et al. Synthesis and characterization of hydroxyapatite nanobelts and nanoparticles. Mater Lett 2005;59:220–5.
[294] Lim G, Wang J, Ng S, Gan L. Formation of nanocrystalline hydroxyapatite in nonionic surfactant emulsions. Langmuir 1999;15:7472–7.
[295] Lim G, Wang J, Ng S, Gan L. Nanosized hydroxyapatite powders from microemulsions and emulsions stabilized by a biodegradable surfactant. J Mater Chem 1999;9:1635–9.
[296] Shum HC, Bandyopadhyay A, Bose S, Weitz DA. Double emulsion droplets as microreactors for synthesis of mesoporous hydroxyapatite. Chem Mater 2009;21:5548–55.
[297] Jarudilokkul S, Tanthapanichakoon W, Boonamnuayvittaya V. Synthesis of hydroxyapatite nanoparticles using an emulsion liquid membrane system. Colloid Surface A 2007;296:149–53.
[298] Ethirajan A, Ziener U, Chuvilin A, Kaiser U, Cölfen H, Landfester K. Biomimetic hydroxyapatite crystallization in gelatin nanoparticles synthesized using a miniemulsion process. Adv Funct Mater 2008;18:2221–7.
[299] Saha SK, Banerjee A, Banerjee S, Bose S. Synthesis of nanocrystalline hydroxyapatite using surfactant template systems: role of templates in controlling morphology. Mater Sci Eng C 2009;29:2294–301.
[300] Li H, Zhu MY, Li LH, Zhou CR. Processing of nanocrystalline hydroxyapatite particles via reverse microemulsions. J Mater Sci 2008;43:384–9.
[301] Ponomareva N, Poprygina T, Karpov S, Lesovoi M, Agapov B. Microemulsion method for producing hydroxyapatite. Russ J Gen Chem 2010;80:905–8.
[302] Chen BH, Chen KI, Ho ML, Chen HN, Chen WC, Wang CK. Synthesis of calcium phosphates and porous hydroxyapatite beads prepared by emulsion method. Mater Chem Phys 2009;113:365–71.
[303] Koumoulidis GC, Katsoulidis AP, Ladavos AK, Pomonis PJ, Trapalis CC, Sdoukos AT, et al. Preparation of hydroxyapatite via microemulsion route. J Colloid Interf Sci 2003;259:254–60.
[304] Sato K, Hotta Y, Nagaoka T, Yasuoka M, Watari K. Agglomeration control of hydroxyapatite nano-crystals grown in phase-separated microenvironments. J Mater Sci 2006;41:5424–8.
[305] Lai C, Wang YJ, Wei K. Nucleation kinetics of calcium phosphate nanoparticles in reverse micelle solution. Colloid Surface A 2008;315:268–74.
[306] Ren W, Li S, Wang Y, Cao X, Chen X. Preparation and characterization of nanosized hydroxyapatite particles in AOT inverse microemulsion. J Wuhan Univ Technol 2004;19:24–9.
[307] Sun Y, Guo G, Wang Z, Guo H. Synthesis of single-crystal HAP nanorods. Ceram Int 2006;32:951–4.
[308] Sadat-Shojai M. Preparation of hydroxyapatite nanoparticles: comparison between hydrothermal and solvo-treatment processes and colloidal stability of produced nanoparticles in a dilute experimental dental adhesive. J Iran Chem Soc 2009;6:386–92.
[309] Banerjee A, Bandyopadhyay A, Bose S. Hydroxyapatite nanopowders: synthesis, densification and cell–materials interaction. Mater Sci Eng C 2007;27:729–35.
[310] Sadasivan S, Khushalani D, Mann S. Synthesis of calcium phosphate nanofilaments in reverse micelles. Chem Mater 2005;17:2765–70.
[311] Guo G, Sun Y, Wang Z, Guo H. Preparation of hydroxyapatite nanoparticles by reverse microemulsion. Ceram Int 2005;31:869–72.
[312] Lai C, Tang SQ, Wang YJ, Wei K. Formation of calcium phosphate nanoparticles in reverse microemulsions. Mater Lett 2005;59:210–4.
[313] Bose S, Saha SK. Synthesis and characterization of hydroxyapatite nanopowders by emulsion technique. Chem Mater 2003;15:4464–9.
[314] Furuzono T, Walsh D, Sato K, Sonoda K, Tanaka J. Effect of reaction temperature on the morphology and size of hydroxyapatite nanoparticles in an emulsion system. J Mater Sci Lett 2001;20:111–4.
[315] Jevtic M, Mitric M, Skapin S, Jancar B, Ignjatovic N, Uskokovic D. Crystal structure of hydroxyapatite nanorods synthesized by sonochemical homogeneous precipitation. Cryst Growth Des 2008;8:2217–22.
[316] Han Y, Wang X, Li S. A simple route to prepare stable hydroxyapatite nanoparticles suspension. J Nanopart Res 2009;11:1235–40.
[317] Kim W, Saito F. Sonochemical synthesis of hydroxyapatite from H_3PO_4 solution with $Ca(OH)_2$. Ultrason Sonochem 2001;8:85–8.

[318] Rouhani P, Taghavinia N, Rouhani S. Rapid growth of hydroxyapatite nanoparticles using ultrasonic irradiation. Ultrason Sonochem 2010;17:853–6.
[319] Giardina MA, Fanovich MA. Synthesis of nanocrystalline hydroxyapatite from $Ca(OH)_2$ and H_3PO_4 assisted by ultrasonic irradiation. Ceram Int 2010;36:1961–9.
[320] Zhang J, Zhan X, Wen X, Song B, Ma L, Peng W. Effects of ultrasonic and dispersants on shape and composition of hydroxyapatite by reflux method. Inorg Mater 2009;45:1362–5.
[321] Kuznetsov A, Fomin A, Veresov A, Putlyaev V, Fadeeva I, Barinov S. Hydroxyapatite of platelet morphology synthesized by ultrasonic precipitation from solution. Russ J Inorg Chem 2008;53:1–5.
[322] Cao L, Zhang C, Huang J. Synthesis of hydroxyapatite nanoparticles in ultrasonic precipitation. Ceram Int 2005;31:1041–4.
[323] Han Y, Li S, Wang X, Bauer I, Yin M. Sonochemical preparation of hydroxyapatite nanoparticles stabilized by glycosaminoglycans. Ultrason Sonochem 2007;14:286–90.
[324] Han Y, Wang X, Li S. Change of phase composition and morphology of sonochemically synthesised hydroxyapatite nanoparticles with glycosaminoglycans during thermal treatment. Adv Appl Ceram 2009;108:400–5.
[325] Ayers RA, Burkes DE, Gottoli G, Yi HC, Zhim F, Yahia LH, et al. Combustion synthesis of porous biomaterials. J Biomed Mater Res 2007;81:634–43.
[326] Sasikumar S, Vijayaraghavan R. Effect of metal-ion-to-fuel ratio on the phase formation of bioceramic phosphates synthesized by self-propagating combustion. Sci Technol Adv Mater 2008;9:035003 [5pp].
[327] Aghayan M, Rodríguez M. Influence of fuels and combustion aids on solution combustion synthesis of Bi-phasic Calcium Phosphates (BCP). Mater Sci Eng C 2012;32:2464–8.
[328] Ghosh SK, Roy SK, Kundu B, Datta S, Basu D. Synthesis of nano-sized hydroxyapatite powders through solution combustion route under different reaction conditions. Mater Sci Eng B 2011;176:14–21.
[329] Sasikumar S, Vijayaraghavan R. Solution combustion synthesis of bioceramic calcium phosphates by single and mixed fuels – a comparative study. Ceram Int 2008;34:1373–9.
[330] Nandi SK, Kundu B, Ghosh SK, De DK, Basu D. Efficacy of nano-hydroxyapatite prepared by an aqueous solution combustion technique in healing bone defects of goat. J Vet Sci 2008;9:183–91.
[331] Pratihar SK, Garg M, Mehra S, Bhattacharyya S. Phase evolution and sintering kinetics of hydroxyapatite synthesized by solution combustion technique. J Mater Sci: Mater Med 2006;17:501–7.
[332] Jagdale PN, Bamane SR. Calcium hydroxyapatite bioceramics and evaluation of their in vitro biocompatibility. RJPBCS 2011;2:180–6.
[333] Sasikumar S, Vijayaraghavan R. Synthesis and characterization of bioceramic calcium phosphates by rapid combustion synthesis. J Mater Sci Technol 2010;26:1114–8.
[334] Tas AC. Combustion synthesis of calcium phosphate bioceramic powders. J Eur Ceram Soc 2000;20:2389–94.
[335] Ghosh SK, Pal S, Roy SK, Pal SK, Basu D. Modelling of flame temperature of solution combustion synthesis of nanocrystalline calcium hydroxyapatite material and its parametric optimization. Bull Mater Sci 2010;33:339–50.
[336] Trommer R, Santos L, Bergmann C. Nanostructured hydroxyapatite powders produced by a flame-based technique. Mater Sci Eng C 2009;29:1770–5.
[337] Ghosh SK, Prakash A, Datta S, Roy SK, Basu D. Effect of fuel characteristics on synthesis of calcium hydroxyapatite by solution combustion route. Bull Mater Sci 2010;33:7–16.
[338] Cho JS, Kang YC. Nano-sized hydroxyapatite powders prepared by flame spray pyrolysis. J Alloys Compd 2008;464:282–7.
[339] Aizawa M, Hanazawa T, Itatani K, Howell F, Kishioka A. Characterization of hydroxyapatite powders prepared by ultrasonic spray-pyrolysis technique. J Mater Sci 1999;34:2865–73.
[340] Itatani K, Tsugawa T, Umeda T, Musha Y, Davies IJ, Koda S. Preparation of submicrometer-sized porous spherical hydroxyapatite agglomerates by ultrasonic spray pyrolysis technique. J Ceram Soc Jpn 2010;118:462–6.
[341] Wakiya N, Yamasaki M, Adachi T, Inukai A, Sakamoto N, Fu D, et al. Preparation of hydroxyapatite–ferrite composite particles by ultrasonic spray pyrolysis. Mater Sci Eng B 2010;173:195–8.
[342] Hwang KS, Jeon KO, Jeon YS, Kim BH. Hydroxyapatite forming ability of electrostatic spray pyrolysis derived calcium phosphate nano powder. J Mater Sci: Mater Med 2007;18:619–22.
[343] Vallet-Regı M, Gutiérrez-Rıos M, Alonso M, De Frutos M, Nicolopoulos S. Hydroxyapatite particles synthesized by pyrolysis of an aerosol. J Solid State Chem 1994;112:58–64.
[344] Aizawa M, Itatani K, Howell F, Kishioka A. Some properties of carbonate-containing hydroxyapatite powder prepared by spray-pyrolysis technique using urea as a foaming agent. J Ceram Soc Japan 1995;103:1214–9.
[345] An GH, Wang HJ, Kim BH, Jeong YG, Choa YH. Fabrication and characterization of a hydroxyapatite nanopowder by ultrasonic spray pyrolysis with salt-assisted decomposition. Mater Sci Eng A 2007;449: 821–4.
[346] Mondal S, Mahata S, Kundu S, Mondal B. Processing of natural resourced hydroxyapatite ceramics from fish scale. Adv Appl Ceram 2010;109:234–9.
[347] Haberko K, Bućko MM, Brzezińska-Miecznik J, Haberko M, Mozgawa W, Panz T, et al. Natural hydroxyapatite – its behaviour during heat treatment. J Eur Ceram Soc 2006;26:537–42.
[348] Barakat NAM, Khil MS, Omran A, Sheikh FA, Kim HY. Extraction of pure natural hydroxyapatite from the bovine bones bio waste by three different methods. J Mater Process Tech 2009;209:3408–15.
[349] Admassu W, Breese T. Feasibility of using natural fishbone apatite as a substitute for hydroxyapatite in remediating aqueous heavy metals. J Hazard Mater 1999;69:187–96.
[350] Lombardi M, Palmero P, Haberko K, Pyda W, Montanaro L. Processing of a natural hydroxyapatite powder: from powder optimization to porous bodies development. J Eur Ceram Soc 2011;31:2513–8.
[351] Sobczak A, Kida A, Kowalski Z, Wzorek Z. Evaluation of the biomedical properties of hydroxyapatite obtained from bone waste. Pol J Chem Technol 2009;11:37–43.
[352] Sobczak A, Kida A, Kowalski Z, Wzorek Z. In vitro tests of dense hydroxyapatite materials. Pol J Chem Technol 2009;11:44–9.
[353] Herliansyah M, Hamdi M, Ide-Ektessabi A, Wildan M, Toque J. The influence of sintering temperature on the properties of compacted bovine hydroxyapatite. Mater Sci Eng C 2009;29:1674–80.
[354] Ooi C, Hamdi M, Ramesh S. Properties of hydroxyapatite produced by annealing of bovine bone. Ceram Int 2007;33:1171–7.
[355] Murugan R, Sampath Kumar T, Panduranga Rao K. Fluorinated bovine hydroxyapatite: preparation and characterization. Mater Lett 2002;57:429–33.
[356] Ozawa M, Suzuki S. Microstructural development of natural hydroxyapatite originated from Fish-bone waste through heat treatment. J Am Ceram Soc 2002;85:1315–7.
[357] Doostmohammadi A, Monshi A, Fathi M, Braissant O. A comparative physico-chemical study of bioactive glass and bone-derived hydroxyapatite. Ceram Int 2011;37:1601–7.
[358] Huang YC, Hsiao PC, Chai HJ. Hydroxyapatite extracted from fish scale: effects on MG63 osteoblast-like cells. Ceram Int 2011;37:1825–31.
[359] Yoganand C, Selvarajan V, Goudouri O, Paraskevopoulos K, Wu J, Xue D. Preparation of bovine hydroxyapatite by transferred arc plasma. Curr Appl Phys 2011;11:702–9.
[360] Coelho T, Nogueira E, Steimacher A, Medina A, Weinand W, Lima W, et al. Characterization of natural nanostructured hydroxyapatite obtained from the bones of Brazilian river fish. J Appl Phys 2006;100:094312.
[361] Ruksudjarit A, Pengpat K, Rujijanagul G, Tunkasiri T. Synthesis and characterization of nanocrystalline hydroxyapatite from natural bovine bone. Curr Appl Phys 2008;8:270–2.
[362] Gergely G, Wéber F, Lukács I, Tóth AL, Horváth ZE, Mihály J, et al. Preparation and characterization of hydroxyapatite from eggshell. Ceram Int 2010;36:803–6.
[363] Gergely G, Wéber F, Lukács I, Illés L, Tóth AL, Horváth ZE, et al. Nano-hydroxyapatite preparation from biogenic raw materials. Cent Eur J Chem 2010;8:375–81.
[364] Zhao H, He W, Wang Y, Zhang X, Li Z, Yan S, et al. Biomineralization of large hydroxyapatite particles using ovalbumin as biosurfactant. Mater Lett 2008;62:3603–5.
[365] Meski S, Ziani S, Khireddine H. Removal of lead ions by hydroxyapatite prepared from the egg shell. J Chem Eng Data 2010;55:3923–8.
[366] Siva Rama Krishna D, Siddharthan A, Seshadri S, Sampath Kumar T. A novel route for synthesis of nanocrystalline hydroxyapatite from eggshell waste. J Mater Sci: Mater Med 2007;18:1735–43.
[367] Jokanović V, Izvonar D, Dramićanin M, Jokanović B, Živojinović V, Marković D, et al. Hydrothermal synthesis and nanostructure of carbonated calcium hydroxyapatite. J Mater Sci: Mater Med 2006;17:539–46.
[368] Lee S, Oh S. Fabrication of calcium phosphate bioceramics by using eggshell and phosphoric acid. Mater Lett 2003;57:4570–4.
[369] Meski S, Ziani S, Khireddine H, Yataghane F, Ferguene N. Elaboration of the hydroxyapatite with different precursors and application for the retention of the lead. Water Sci Technol 2011;63:2087–96.
[370] Boonyang U, Chaopanich P, Wongchaisuwat A, Senthongkaew P, Siripaisarnpipat S. Effect of phosphate precursor on the production of hydroxyapatite from crocodile eggshells. J Biomim Biomater Tissue Eng 2010;5:31–7.
[371] Vecchio KS, Zhang X, Massie JB, Wang M, Kim CW. Conversion of bulk seashells to biocompatible hydroxyapatite for bone implants. Acta Biomater 2007;3:910–8.
[372] Lemos A, Rocha J, Quaresma S, Kannan S, Oktar F, Agathopoulos S, et al. Hydroxyapatite nano-powders produced hydrothermally from nacreous material. J Eur Ceram Soc 2006;26:3639–46.
[373] Guo YP, Yao Y, Ning CQ, Guo YJ, Chu LF. Fabrication of mesoporous carbonated hydroxyapatite microspheres by hydrothermal method. Mater Lett 2011;65:2205–8.
[374] Rodriguez-Lugo V, Hernández JS, Arellano-Jimenez MJ, Hernandez-Tejeda P, Recillas-Gispert S. Characterization of hydroxyapatite by electron microscopy. Microsc Microanal 2005;11:516–23.
[375] Felício-Fernandes G, Laranjeira M. Calcium phosphate biomaterials from marine algae. Hydrothermal synthesis and characterisation. Quim Nova 2000;23:441–6.
[376] Xu Y, Wang D, Yang L, Tang H. Hydrothermal conversion of coral into hydroxyapatite. Mater Charact 2001;47:83–7.
[377] Walsh P, Buchanan F, Dring M, Maggs C, Bell S, Walker G. Low-pressure synthesis and characterisation of hydroxyapatite derived from mineralise red algae. Chem Eng J 2008;137:173–9.

[378] Jinawath S, Polchai D, Yoshimura M. Low-temperature, hydrothermal transformation of aragonite to hydroxyapatite. Mater Sci Eng C 2002;22:35–9.
[379] Turhani D, Cvikl B, Watzinger E, Weißenböck M, Yerit K, Thurnher D, et al. In vitro growth and differentiation of osteoblast-like cells on hydroxyapatite ceramic granule calcified from red algae. J Oral Maxillofac Surg 2005;63:793–9.
[380] Weißenbock M, Stein E, Undt G, Ewers R, Lauer G, Turhani D. Particle size of hydroxyapatite granules calcified from red algae affects the osteogenic potential of human mesenchymal stem cells in vitro. Cells Tissues Organs 2006;182:79–88.
[381] Han Y, Li S, Wang X. A novel thermolysis method of colloidal protein precursors to prepare hydroxyapatite nanocrystals. Cryst Res Technol 2009;44:336–40.
[382] Han Y, Li S, Wang X, Jia L, He J. Preparation of hydroxyapatite rod-like crystals by protein precursor method. Mater Res Bull 2007;42:1169–77.
[383] Zhao H, He W, Wang Y, Zhang X, Li Z, Yan S, et al. Biomimetic synthesis and characterization of hydroxyapatite crystal with low phase transformation temperature. J Chem Eng Data 2008;53:2735–8.
[384] Nayar S, Guha A. Waste utilization for the controlled synthesis of nanosized hydroxyapatite. Mater Sci Eng C 2009;29:1326–9.
[385] Zhang Y, Liu Y, Ji X, Banks CE, Song J. Flower-like agglomerates of hydroxyapatite crystals formed on an egg-shell membrane. Colloid Surface B 2011;82:490–6.
[386] Neelakandeswari N, Sangami G, Dharmaraj N. Preparation and characterization of nanostructured hydroxyapatite using a biomaterial. Synth React Inorg M 2011;41:513–6.
[387] Zhang Y, Liu Y, Ji X. Fabrication of flower-like hydroxyapatite agglomerates with the assistant of bamboo membrane. Mater Lett 2011;65:1982–5.
[388] Wang J, Shaw LL. Synthesis of high purity hydroxyapatite nanopowder via sol–gel combustion process. J Mater Sci: Mater Med 2009;20:1223–7.
[389] Yuan Y, Liu C, Zhang Y, Shan X. Sol–gel auto-combustion synthesis of hydroxyapatite nanotubes array in porous alumina template. Mater Chem Phys 2008;112:275–80.
[390] Han Y, Li S, Wang X, Chen X. Synthesis and sintering of nanocrystalline hydroxyapatite powders by citric acid sol–gel combustion method. Mater Res Bull 2004;39:25–32.
[391] Chen CW, Riman RE, TenHuisen KS, Brown K. Mechanochemical–hydrothermal synthesis of hydroxyapatite from nonionic surfactant emulsion precursors. J Cryst Growth 2004;270:615–23.
[392] Abdel-Aal E, El-Midany A, El-Shall H. Mechanochemical–hydrothermal preparation of nano-crystallite hydroxyapatite using statistical design. Mater Chem Phys 2008;112:202–7.
[393] Tian T, Jiang D, Zhang J, Lin Q. Synthesis of Si-substituted hydroxyapatite by a wet mechanochemical method. Mater Sci Eng C 2008;28:57–63.
[394] Mostafa NY. Characterization, thermal stability and sintering of hydroxyapatite powders prepared by different routes. Mater Chem Phys 2005;94:333–41.
[395] Zhang HG, Zhu Q, Xie ZH. Mechanochemical–hydrothermal synthesis and characterization of fluoridated hydroxyapatite. Mater Res Bull 2005;40:1326–34.
[396] Shu C, Yanwei W, Hong L, Zhengzheng P, Kangde Y. Synthesis of carbonated hydroxyapatite nanofibers by mechanochemical methods. Ceram Int 2005;31:135–8.
[397] Riman RE, Suchanek WL, Byrappa K, Chen CW, Shuk P, Oakes CS. Solution synthesis of hydroxyapatite designer particulates. Solid State Ionics 2002;151:393–402.
[398] Suchanek WL, Shuk P, Byrappa K, Riman RE, TenHuisen KS, Janas VF. Mechanochemical–hydrothermal synthesis of carbonated apatite powders at room temperature. Biomaterials 2002;23:699–710.
[399] Rhee SH. Synthesis of hydroxyapatite via mechanochemical treatment. Biomaterials 2002;23:1147–52.
[400] Shuk P, Suchanek WL, Hao T, Gulliver E, Riman RE, Senna M, et al. Mechanochemical–hydrothermal preparation of crystalline hydroxyapatite powders at room temperature. J Mater Res 2001;16:1231–4.
[401] Nakamura S, Isobe T, Senna M. Hydroxyapatite nano sol prepared via a mechanochemical route. J Nanopart Res 2001;3:57–61.
[402] Liu X, Lin K, Chang J. Modulation of hydroxyapatite crystals formed from α-tricalcium phosphate by surfactant-free hydrothermal exchange. CrystEngComm 2010;13:1959–65.
[403] Parthiban SP, Kim IY, Kikuta K, Ohtsuki C. Effect of ammonium carbonate on formation of calcium-deficient hydroxyapatite through double-step hydrothermal processing. J Mater Sci: Mater Med 2011;22:209–16.
[404] Zhang X, Vecchio KS. Hydrothermal synthesis of hydroxyapatite rods. J Cryst Growth 2007;308:133–40.
[405] Ashok M, Kalkura SN, Sundaram NM, Arivuoli D. Growth and characterization of hydroxyapatite crystals by hydrothermal method. J Mater Sci: Mater Med 2007;18:895–8.
[406] Sinitsyna O, Veresov A, Kovaleva E, Kolen'ko YV, Putlyaev V, Tretyakov YD. Synthesis of hydroxyapatite by hydrolysis of α-$Ca_3(PO_4)_2$. Russ Chem Bull 2005;54:79–86.
[407] Liu J, Ye X, Wang H, Zhu M, Wang B, Yan H. The influence of pH and temperature on the morphology of hydroxyapatite synthesized by hydrothermal method. Ceram Int 2003;29:629–33.
[408] Jinawath S, Pongkao D, Yoshimura M. Hydrothermal synthesis of hydroxyapatite from natural source. J Mater Sci: Mater Med 2002;13:491–4.
[409] Jinawath S, Pongkao D, Suchanek W, Yoshimura M. Hydrothermal synthesis of monetite and hydroxyapatite from monocalcium phosphate monohydrate. Int J Inorg Mater 2001;3:997–1001.
[410] Teraoka K, Ito A, Onuma K, Tateishi T, Tsutsumi S. Hydrothermal growth of hydroxyapatite single crystals under natural convection. J Mater Res 1999;14:2655–61.
[411] Sun Y, Guo G, Tao D, Wang Z. Reverse microemulsion-directed synthesis of hydroxyapatite nanoparticles under hydrothermal conditions. J Phys Chem Solids 2007;68:373–7.
[412] Lin K, Chang J, Cheng R, Ruan M. Hydrothermal microemulsion synthesis of stoichiometric single crystal hydroxyapatite nanorods with mono-dispersion and narrow-size distribution. Mater Lett 2007;61:1683–7.
[413] Wang YJ, Lai C, Wei K, Chen X, Ding Y, Wang ZL. Investigations on the formation mechanism of hydroxyapatite synthesized by the solvothermal method. Nanotechnology 2006;17:4405–12.
[414] Zhang S, Lai C, Wei K, Wang Y. Kinetic studies on the synthesis of hydroxyapatite nanowires by solvothermal methods. Aust J Chem 2007;60:99–104.
[415] Wang YJ, Lai C, Wei K, Tang SQ. Influence of temperature, ripening time, and cosurfactant on solvothermal synthesis of calcium phosphate nanobelts. Mater Lett 2005;59:1098–104.
[416] Cao M, Wang Y, Guo C, Qi Y, Hu C. Preparation of ultrahigh-aspect-ratio hydroxyapatite nanofibers in reverse micelles under hydrothermal conditions. Langmuir 2004;20:4784–6.
[417] Ma MG, Zhu JF. Solvothermal synthesis and characterization of hierarchically nanostructured hydroxyapatite hollow spheres. Eur J Inorg Chem 2009;2009:5522–6.
[418] Chen F, Zhu YJ, Wang KW, Zhao KL. Surfactant-free solvothermal synthesis of hydroxyapatite nanowire/nanotube ordered arrays with biomimetic structures. CrystEngComm 2010;13:1858–63.
[419] Ma MG, Zhu YJ, Chang J. Solvothermal preparation of hydroxyapatite microtubes in water/N,N-dimethylformamide mixed solvents. Mater Lett 2008;62:1642–5.
[420] Vani R, Raja SB, Sridevi T, Savithri K, Devaraj SN, Girija E, et al. Surfactant free rapid synthesis of hydroxyapatite nanorods by a microwave irradiation method for the treatment of bone infection. Nanotechnology 2011;22:285701 [10pp].
[421] Rameshbabu N, Rao KP, Kumar TSS. Acclerated microwave processing of nanocrystalline hydroxyapatite. J Mater Sci 2005;40:6319–23.
[422] Torrent-Burgués J, Gómez-Morales J, López-Macipe A, Rodríguez-Clemente R. Continuous precipitation of hydroxyapatite from Ca/citrate/phosphate solutions using microwave heating. Cryst Res Technol 1999;34:757–62.
[423] Fang Y, Agrawal DK, Roy DM, Roy R. Fabrication of porous hydroxyapatite ceramics by microwave processing. J Mater Res 1992;7:490–4.
[424] Fang Y, Agrawal DK, Roy DM, Roy R. Microwave sintering of hydroxyapatite ceramics. J Mater Res 1994;9:180–7.
[425] Ruban Kumar A, Kalainathan S, Saral AM. Microwave assisted synthesis of hydroxyapatite nano strips. Cryst Res Technol 2010;45:776–8.
[426] Teoreanu I, Preda M, Melinescu A. Synthesis and characterization of hydroxyapatite by microwave heating using $CaSO_4{\cdot}2H_2O$ and $Ca(OH)_2$ as calcium source. J Mater Sci: Mater Med 2008;19:517–23.
[427] Manjubala I, Sivakumar M. In-situ synthesis of biphasic calcium phosphate ceramics using microwave irradiation. Mater Chem Phys 2001;71:272–8.
[428] Sarig S, Kahana F. Rapid formation of nanocrystalline apatite. J Cryst Growth 2002;237:55–9.
[429] Siddharthan A, Seshadri S, Kumar TSS. Microwave accelerated synthesis of nanosized calcium deficient hydroxyapatite. J Mater Sci: Mater Med 2004;15:1279–84.
[430] Katsuki H, Furuta S, Komarneni S. Microwave- vs. conventional-hydrothermal synthesis of hydroxyapatite crystals from gypsum. J Am Ceram Soc 1999;82:2257–9.
[431] Kalita SJ, Verma S. Nanocrystalline hydroxyapatite bioceramic using microwave radiation: synthesis and characterization. Mater Sci Eng C 2010;30:295–303.
[432] Komarneni S, Katsuki H. Nanophase materials by a novel microwave-hydrothermal process. Pure Appl Chem 2002;74:1537–44.
[433] Zyman Z, Goncharenko A, Rokhmistrov D, Epple M. Nanocrystalline calcium-deficient hydroxyapatite prepared by a microwave-assisted solvent-free reaction. Mat-wiss uWerkstofftech 2011;42:154–7.
[434] Cao JM, Feng J, Deng SG, Chang X, Wang J, Liu JS, et al. Microwave-assisted solid-state synthesis of hydroxyapatite nanorods at room temperature. J Mater Sci 2005;40:6311–3.
[435] Parhi P, Ramanan A, Ray AR. A convenient route for the synthesis of hydroxyapatite through a novel microwave-mediated metathesis reaction. Mater Lett 2004;58:3610–2.
[436] Park Y, Ryu S, Yoon S, Stevens R, Park H. Preparation of whisker-shaped hydroxyapatite/β-tricalcium phosphate composite. Mater Chem Phys 2008;109:440–7.
[437] Yoon S, Park Y, Park S, Stevens R, Park H. Synthesis of hydroxyapatite whiskers by hydrolysis of α-tricalcium phosphate using microwave heating. Mater Chem Phys 2005;91:48–53.
[438] Poinern GEJ, Ghosh MK, Ng YJ, Issa TB, Anand S, Singh P. Defluoridation behavior of nanostructured hydroxyapatite synthesized through an ultrasonic and microwave combined technique. J Hazard Mater 2011;185:29–37.

[439] Jalota S, Tas AC, Bhaduri SB. Microwave-assisted synthesis of calcium phosphate nanowhiskers. J Mater Res 2004;19:1876–81.
[440] Jalota S, Bhaduri SB, Tas AC. In vitro testing of calcium phosphate (HA, TCP, and biphasic HA-TCP) whiskers. J Biomed Mater Res 2006;78:481–90.
[441] Liu J, Li K, Wang H, Zhu M, Yan H. Rapid formation of hydroxyapatite nanostructures by microwave irradiation. Chem Phys Lett 2004;396: 429–32.
[442] Liu J, Li K, Wang H, Zhu M, Xu H, Yan H. Self-assembly of hydroxyapatite nanostructures by microwave irradiation. Nanotechnology 2004;16:82–7.
[443] Lak A, Mazloumi M, Mohajerani MS, Zanganeh S, Shayegh MR, Kajbafvala A, et al. Rapid formation of mono-dispersed hydroxyapatite nanorods with narrow-size distribution via microwave irradiation. J Am Ceram Soc 2008;91:3580–4.
[444] Pon-On W, Meejoo S, Tang I. Formation of hydroxyapatite crystallites using organic template of polyvinyl alcohol (PVA) and sodium dodecyl sulfate (SDS). Mater Chem Phys 2008;112:453–60.
[445] Meejoo S, Maneeprakorn W, Winotai P. Phase and thermal stability of nanocrystalline hydroxyapatite prepared via microwave heating. Thermochim Acta 2006;447:115–20.
[446] Yang Z, Jiang Y, Wang YJ, Ma LY, Li F. Preparation and thermal stability analysis of hydroxyapatite derived from the precipitation process and microwave irradiation method. Mater Lett 2004;58:3586–90.
[447] Elkady M, Mahmoud M, Abd-El-Rahman H. Kinetic approach for cadmium sorption using microwave synthesized nano-hydroxyapatite. J Non-Cryst Solids 2011;357:1118–29.
[448] Sampath Kumar T, Manjubala I, Gunasekaran J. Synthesis of carbonated calcium phosphate ceramics using microwave irradiation. Biomaterials 2000;21:1623–9.
[449] Arami H, Mohajerani M, Mazloumi M, Khalifehzadeh R, Lak A, Sadrnezhaad S. Rapid formation of hydroxyapatite nanostrips via microwave irradiation. J Alloys Compd 2009;469:391–4.
[450] Siddharthan A, Seshadri S, Kumar T. Influence of microwave power on nanosized hydroxyapatite particles. Scr Mater 2006;55:175–8.
[451] Wang KW, Zhu YJ, Chen F, Cheng GF, Huang YH. Microwave-assisted synthesis of hydroxyapatite hollow microspheres in aqueous solution. Mater Lett 2011;65:2361–3.
[452] Lee BT, Youn MH, Paul RK, Lee KH, Song HY. In situ synthesis of spherical BCP nanopowders by microwave assisted process. Mater Chem Phys 2007;104:249–53.
[453] Wang YZ, Fu Y. Microwave-hydrothermal synthesis and characterization of hydroxyapatite nanocrystallites. Mater Lett 2011;65:3388–90.
[454] Han JK, Song HY, Saito F, Lee BT. Synthesis of high purity nano-sized hydroxyapatite powder by microwave-hydrothermal method. Mater Chem Phys 2006;99:235–9.